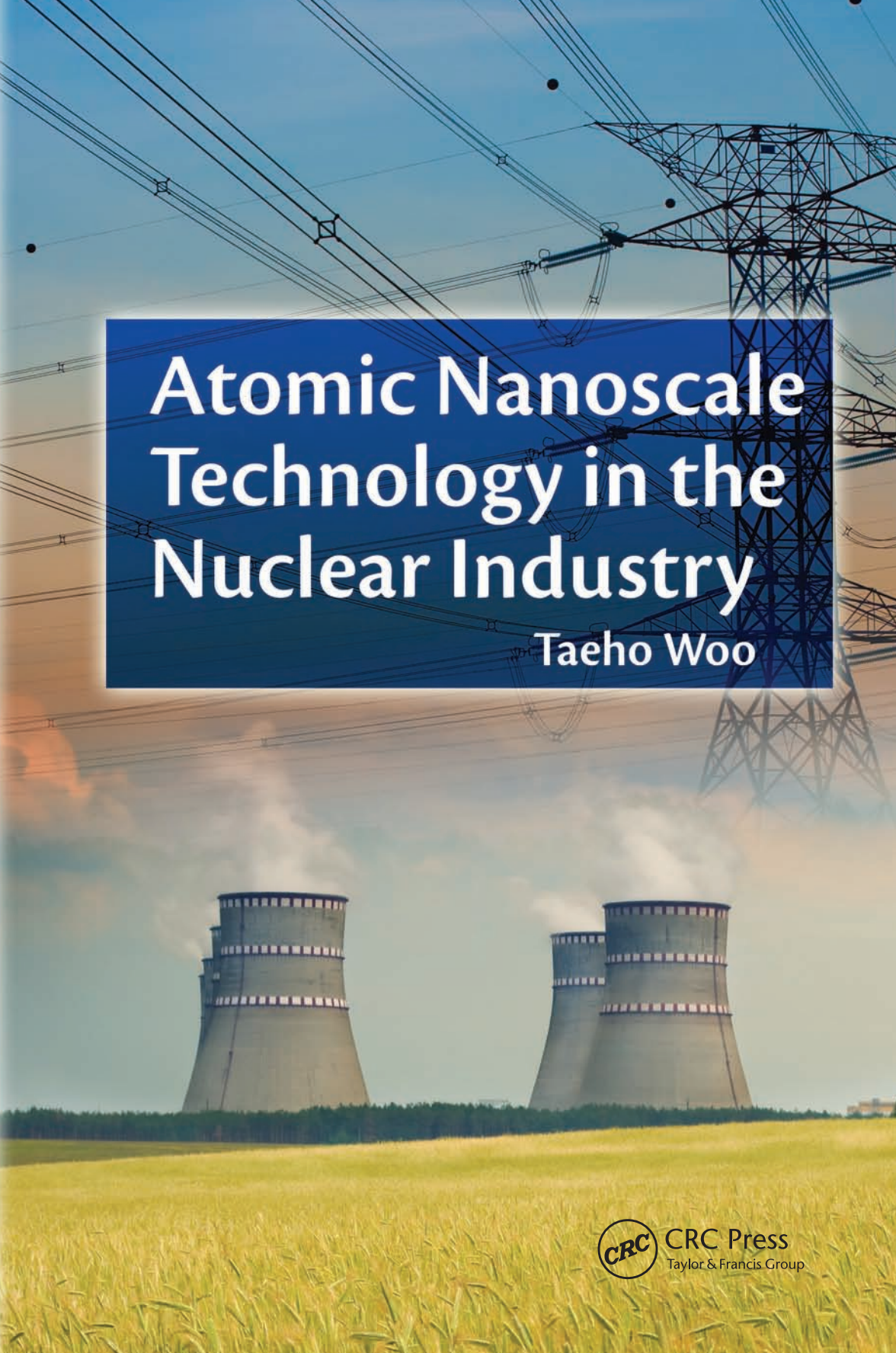
Atomic Nanoscale Technology in the Nuclear Industry
Taeho Woo
CRC
CRC Press
Taylor & Francis Group

# Atomic Nanoscale Technology in the Nuclear Industry

Taeho Woo

CRC Press
Taylor & Francis Group
Boca Raton London New York

CRC Press is an imprint of the
Taylor & Francis Group, an **informa** business

CRC Press
Taylor & Francis Group
6000 Broken Sound Parkway NW, Suite 300
Boca Raton, FL 33487-2742


Version Date: 20111107

International Standard Book Number-13: 978-1-4398-8159-0 (eBook - PDF)

# *Contents*

## Section III Atomic Nanoscale Material Management

# *Preface*

New kinds of industrial challenges have been introduced in the nuclear industry, especially in nanoscale methods. The object of this growth focuses on conventional critical matter like nuclear waste treatment. Multidisciplinary cooperation has created new possibilities with respect to economics as well as safety in the global nuclear market.

This book focuses on the wide range of nanoscale technology in the atomic power industry. Using the Monte Carlo and solid-state measurement methods, advanced studies have been performed. These areas are very important in the nuclear industry. This technology could expand reliability enhancement in a variety of applications. Therefore, this book deals with nanoscale treatment in the nuclear industry, where economic and safety improvements could be attained.

The nuclear power plant (NPP) has had a critical impact in the industry as a source of energy production. Several countries rely on atomic power for generation of a large portion of their electricity. In France, over 80% of electricity is produced using nuclear power. However, the political situation has blocked construction of new NPPs, especially in the United Stated during last 30 years. The recent NPP accident in Japan has created a dark cloud on research and development (R&D) in the atomic sciences. Therefore, alternative technologies are needed to overcome the current unclear situation. There are several important advances like medical physics in the nuclear technology field. This trend is accompanied by similar twenty-first-century trends in information technology (IT), biotechnology (BT), and nanotechnology (NT). This book focuses on NT as it relates to atomic technology.

Some challenges in power engineering, biotechnology, and materials are covered in this book. Nuclear waste treatment is reconsidered as nanoscopic treatment instead of according to the diffusion concept of radioactive materials, which is the conventional method of nuclear waste management. Cancer in humans is treated with ion beams, where nanoscale behavior is very important in order to decrease radiation damage to the body. The molecular lattice of the designed structure could produce the nuclear reaction with excess energy. These two cases are in the chapters entitled "Lattice Squeezed Nuclear Reaction (LSNR) of a Power Cell for Nanoscopic Investigations Using Ion Beam Injections" and "Measurement Profiles of Nanoscale Ion Beam for Optimized Radiation Energy Losses," which are fundamentally different from the classical atomic technology of the twentieth century.

In the future, advanced possibilities can be imagined like nanoscale operation management in NPPs where the behavior of nuclear fuel is controlled by deterministic nanoscale operations, which are different from the conventional probability-based transport equations for neutron movement. In addition,

thermohydraulics by nanofluids, which are combinations of nanoparticles in the normal coolant, such as light water, are under investigation.

This book is just a basic step in multicombinational research. We should see great research output of the atomic technology fields in the twenty-first century, which will contribute to the welfare of humankind and build a better world.

**Taeho Woo**
*Seoul, Korea*

# *Author*

**Taeho Woo** has worked in a number of areas in nuclear technology for industrial applications. His research fields range from basic nuclear physics to engineering applications. He launched the field of *atomic multinology* (see "Management of Energy Policy in Atomic-Multinology (AM) Using the System Dynamics (SD) Method," *Annals of Nuclear Energy* 37 (2010): 707–714), which includes the application of information technology (IT), biotechnology (BT), and nanotechnology (NT) in the nuclear industry. *Atomic Nanoscale Technology in the Nuclear Industry* introduces products in atomic multinology. This could provide tremendous synergy and profitable creations for nuclear power economics using IT, BT, and NT.

Taeho Woo received his PhD and MSE in nuclear engineering from Seoul National University, South Korea, and his BS in nuclear engineering from Kyung Hee University, South Korea. He also earned an MS in nuclear engineering and radiological sciences from the University of Michigan at Ann Arbor. He has focused on the most important factors in the industry—safety and economics using IT, BT, and NT. His work is currently in the initial stages but could be valuable for research and development activities in the future.

# *Contributors*

**Hyosung Cho**
Department of Radiological Science
College of Health Science
Yonsei University
Gangwondo, Republic of South Korea

**Yunil Kim**
Korea Institute of Nuclear Safety
Daejeon, Republic of South Korea

**Soonho Lee**
SK Engineering & Construction Co., Ltd.
Seoul, Republic of South Korea

**Sangwoo Noh**
Department of Nuclear Engineering
Seoul National University
Seoul, Republic of South Korea

**Taeho Woo**
Seoul National University
Seoul, Republic of South Korea

# 1

# *Introduction*

**Taeho Woo**

**CONTENTS**



## 1.1 Background

Nanoscale technology is applied in the nuclear industry from power production to financial and safeguard management including risk analysis. A new kind of nonlinear algorithm is introduced that can be used in determining the radiation dispersion for the Chernobyl accident as well as in risk management. This involves statistical manipulations of the nuclear interactions. Even the hardware for the electronics in radiation measurement is classified in the nanotechnology (NT) field in atomic technology. Table 1.1 classifies the content in this book by section and topic. Figure 1.1 shows the configurations of the topics in atomic nanoscale technology.

## 1.2 Basic Theory

The fundamental equations are described. The mechanics of the governing equations are momentum, continuity, and energy. These equations are used in thermodynamics science and engineering applications. The conventional equations in solving these design problems are imported into nanoscale science and engineering. It, however, is an important point to find the applicable characteristics in the real applications. It is also necessary to modify the suitable apparatus to fit a situation.

For the momentum equation and continuity equation, the Navier-Stokes equations are below. For the case of an incompressible Newtonian fluid,

**TABLE 1.1**

Classification of Contents

| Section Title | Topic | Chapter Title |
|---|---|---|
| Atomic nanoscale power | Nuclear waste treatment | Nanoscopic treatment of nuclear waste forms using ion beam injection in a drum-type container treatment |
| | Nuclear power cell | Lattice squeezed nuclear reaction (LSNR) of power cell for nanoscopic investigations using ion beam injections |
| | Lunar nuclear base | Safety assessment study in nanoscopic circumstances for an accidental cooling loop failure (ACLF) in a lunar nuclear power reactor (LNPR) |
| | Space nuclear power | Analysis of characteristics of nuclear spacecraft in a nanogravity environment for deep space exploration |
| Atomic nanoscale biotechnology | Radiation diagnostics | Light collection enhancement analysis for digital x-ray detector using $Gd_2O_2S$:Tb and CsI:Tl phosphors in nanoscale treatment |
| | Radiation therapy by ion beam | Measurement profiles of nanoscale ion beam for optimized radiation energy losses |
| | Radiation therapy by isotope | Brachytherapy for nanoscale cancer therapy using radioisotopes |
| Atomic nanoscale material management | Economic management | Analysis for nanotechnology financial progression in the energy industry using systems thinking decision making |
| | Safeguard management | Safeguard assessment in nanoscale nuclear material in nuclear power plants (NPPs) operations using analytic hierarchy process (AHP) and production function |
| | | Investigation of safeguards management for operation security of nanoscale nuclear material in nuclear power plants using game theory |

$$\rho\left(\frac{\partial v}{\partial t} + v\cdot \quad v\right) = - \quad p + \mu \quad {}^2v + f \tag{1.1}$$

For Cartesian coordinates, the momentum equation is, with $u$, $v$, $w$:

$$\begin{aligned}
\rho\left(\frac{\partial u}{\partial t} + u\frac{\partial u}{\partial x} + v\frac{\partial u}{\partial y} + w\frac{\partial u}{\partial z}\right) &= -\frac{\partial p}{\partial x} + \mu\left(\frac{\partial^2 u}{\partial x^2} + v\frac{\partial^2 u}{\partial y^2} + w\frac{\partial^2 u}{\partial z^2}\right) + \rho g_x \\
\rho\left(\frac{\partial v}{\partial t} + u\frac{\partial v}{\partial x} + v\frac{\partial v}{\partial y} + w\frac{\partial v}{\partial z}\right) &= -\frac{\partial p}{\partial y} + \mu\left(\frac{\partial^2 v}{\partial x^2} + v\frac{\partial^2 v}{\partial y^2} + w\frac{\partial^2 v}{\partial z^2}\right) + \rho g_y \\
\rho\left(\frac{\partial w}{\partial t} + u\frac{\partial w}{\partial x} + v\frac{\partial w}{\partial y} + w\frac{\partial w}{\partial z}\right) &= -\frac{\partial p}{\partial z} + \mu\left(\frac{\partial^2 w}{\partial x^2} + v\frac{\partial^2 w}{\partial y^2} + w\frac{\partial^2 w}{\partial z^2}\right) + \rho g_z
\end{aligned} \tag{1.2}$$

and the continuity equation is

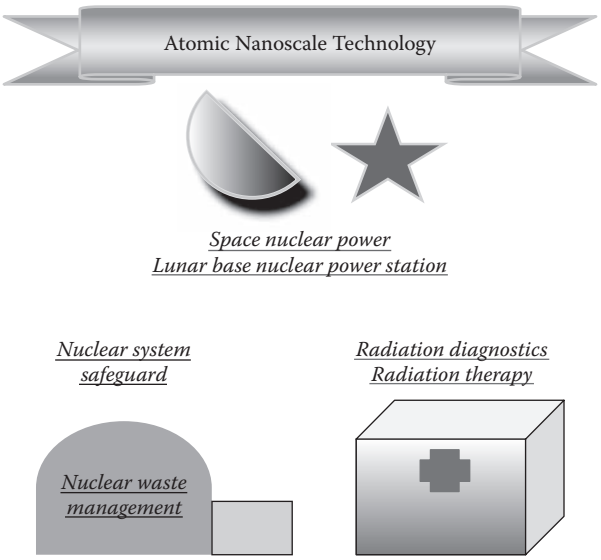


**FIGURE 1.1**
Configurations of the topics in atomic nanoscale technology.

$$\frac{\partial u}{\partial x}+\frac{\partial v}{\partial y}+\frac{\partial w}{\partial z}=0 \tag{1.3}$$

For cylindrical coordinates, the momentum equation is, with $r$, $\theta$, $z$:

$$\begin{aligned}
&\rho\left(\frac{\partial u_r}{\partial t}+u_r\frac{\partial u_r}{\partial r}+\frac{u_\theta}{r}\frac{\partial u_r}{\partial \theta}+u_z\frac{\partial u_r}{\partial z}-\frac{u_\theta^2}{r}\right)\\
&\quad=-\frac{\partial p}{\partial r}+\mu\left(\frac{1}{r}\frac{\partial}{\partial r}\left(r\frac{\partial u_r}{\partial r}\right)+\frac{1}{r^2}\frac{\partial^2 u_r}{\partial \theta^2}+\frac{\partial^2 u_r}{\partial z^2}-\frac{u_r}{r^2}-\frac{2}{r^2}\frac{\partial u_\theta}{\partial \theta}\right)+\rho g_r\\
&\rho\left(\frac{\partial u_\theta}{\partial t}+u_r\frac{\partial u_\theta}{\partial r}+\frac{u_\theta}{r}\frac{\partial u_\theta}{\partial \theta}+u_z\frac{\partial u_\theta}{\partial z}+\frac{u_r u_\theta}{r}\right)\\
&\quad=-\frac{1}{r}\frac{\partial p}{\partial \theta}+\mu\left(\frac{1}{r}\frac{\partial}{\partial r}\left(r\frac{\partial u_\theta}{\partial r}\right)+\frac{1}{r^2}\frac{\partial^2 u_\theta}{\partial \theta^2}+\frac{\partial^2 u_\theta}{\partial z^2}+\frac{2}{r^2}\frac{\partial u_r}{\partial \theta}-\frac{u_\theta}{r^2}\right)+\rho g_\theta\\
&\rho\left(\frac{\partial u_z}{\partial t}+u_r\frac{\partial u_z}{\partial r}+\frac{u_\theta}{r}\frac{\partial u_z}{\partial \theta}+u_z\frac{\partial u_z}{\partial z}\right)\\
&\quad=-\frac{\partial p}{\partial z}+\mu\left(\frac{1}{r}\frac{\partial}{\partial r}\left(r\frac{\partial u_z}{\partial r}\right)+\frac{1}{r^2}\frac{\partial^2 u_z}{\partial \theta^2}+\frac{\partial^2 u_z}{\partial z^2}\right)+\rho g_z
\end{aligned} \tag{1.4}$$

The continuity equation is

$$\frac{1}{r}\frac{\partial}{\partial x}(ru_r)+\frac{1}{r}\frac{\partial u_\theta}{\partial \theta}+\frac{\partial u_z}{\partial z}=0 \tag{1.5}$$

For spherical coordinates the momentum equation is, with $r$, $\theta$, $\phi$ ($\phi$ = colatitudes):

$$\begin{aligned}
&\rho\left(\frac{\partial u_r}{\partial t}+u_r\frac{\partial u_r}{\partial r}+\frac{u_\theta}{r\sin(\ )}\frac{\partial u_r}{\partial \theta}+\frac{u}{r}\frac{\partial u_r}{\partial}-\frac{u_\theta^2+u^2}{r}\right)\\
&\quad=-\frac{\partial p}{\partial r}+\rho g_r+\mu\left[\frac{1}{r^2}\frac{\partial}{\partial r}\left(r^2\frac{\partial u_r}{\partial r}\right)+\frac{1}{r^2\sin(\ )^2}\frac{\partial^2 u_r}{\partial \theta^2}\right.\\
&\qquad\left.+\frac{1}{r^2\sin(\ )}\frac{\partial}{\partial}\left(\sin(\ )\frac{\partial u_r}{\partial}\right)-2\frac{u_r+\dfrac{\partial u}{\partial}+u\ \cot(\ )}{r^2}-\frac{2}{r^2\sin(\ )}\frac{\partial u_\theta}{\partial \theta}\right]\\
&\rho\left(\frac{\partial u_\theta}{\partial t}+u_r\frac{\partial u_\theta}{\partial r}+\frac{u_\theta}{r\sin(\ )}\frac{\partial u_\theta}{\partial \theta}+\frac{u}{r}\frac{\partial u_\theta}{\partial}-\frac{u_r u_\theta+u_\theta u\ \cot(\ )}{r}\right)\\
&\quad=-\frac{1}{r\sin(\ )}\frac{\partial p}{\partial \theta}+\rho g_\theta+\mu\left[\frac{1}{r^2}\frac{\partial}{\partial r}\left(r^2\frac{\partial u_\theta}{\partial r}\right)\right.\\
&\qquad\left.+\frac{1}{r^2\sin(\ )^2}\frac{\partial^2 u_\theta}{\partial \theta^2}+\frac{1}{r^2\sin(\ )}\frac{\partial}{\partial}\left(\sin(\ )\frac{\partial u_\theta}{\partial}\right)+\frac{2\dfrac{\partial u_r}{\partial \theta}+2\cos(\ )\dfrac{\partial u}{\partial \theta}+u_\theta}{r^2\sin(\ )^2}\right]\\
&\rho\left(\frac{\partial u}{\partial t}+u_r\frac{\partial u}{\partial r}+\frac{u_\theta}{r\sin(\ )}\frac{\partial u}{\partial \theta}+\frac{u}{r}\frac{\partial u}{\partial}-\frac{u_r u\ -u_\theta^2\cot(\ )}{r}\right)\\
&\quad=-\frac{1}{r}\frac{\partial p}{\partial}+\rho g\ +\mu\left[\frac{1}{r^2}\frac{\partial}{\partial r}\left(r^2\frac{\partial u}{\partial r}\right)+\frac{1}{r^2\sin(\ )^2}\frac{\partial^2 u}{\partial \theta^2}\right.\\
&\qquad\left.+\frac{1}{r^2\sin(\ )}\frac{\partial}{\partial}\left(\sin(\ )\frac{\partial u}{\partial}\right)+\frac{2}{r^2}\frac{\partial u_r}{\partial}-\frac{u\ +2\cos(\ )\dfrac{\partial u_\theta}{\partial \theta}}{r^2\sin(\ )^2}\right]
\end{aligned} \tag{1.6}$$

and the continuity equation is

$$\frac{1}{r^2}\frac{\partial}{\partial r}(r^2u_r)+\frac{1}{r\sin(\ )}\frac{\partial u_\theta}{\partial \theta}+\frac{1}{r\sin(\ )}\frac{\partial}{\partial}(r\sin(\ )u\ )=0 \tag{1.7}$$

The energy equation is as follows:

$$\frac{\partial}{\partial t}(\rho E) + \quad \cdot(\vec{v}(\rho E + P)) = \quad \cdot(k_{eff} \quad T) + S_h \tag{1.8}$$

## 1.3 Methods

Atomic nanoscale technology is basically incorporated with the Monte Carlo (MC) method (Lewis and Miller 1984; Manno 1999; Palisade 2011; Rubinstein 2008; Sobol 1994; Woller 1996) and the solid-state material measurement studies (Ashby and Jones 2005; Central Facility for Electron Microscopy 1995; Evans Analytical Group, LLC 2011; Grosso and Parravicini 2000; Hook and Hall 1991; IBM Research 1998; Kittel 1986; Marder 2000; Materials Research Laboratory 2007; Material Science and Engineering Department 2011; NanoScience Instruments, Inc. 2011; Nobelprize.org 2011; Sander 2009; SilliconFarEast 2005; UKSAF [UK Surface Analysis Forum] 2006; The Thomas Group 2011). It is useful to account for any quantitative analysis and decision making using the MC technique, which is used by professionals in such widely disparate fields as manufacturing, engineering, finance, project management, energy, research and development, insurance, oil–gas, transportation, and the environment. The MC method can give the decision maker many possible results and the probabilities for any choice of action. The decision-making analysis could involve a variety of cases that happen every day. The MC method was developed with the invention of the atomic bomb. MC simulation has been used to model many applications since its introduction in World War II. The name *Monte Carlo* is taken from the Monaco resort town renowned for its casinos.

Although it is generally referred to as the MC method or simulation, it is a stochastic technique, meaning that it is based on the use of random numbers and probability statistics to investigate problems. It can be applied in a variety of fields, from physics to management problems, which is one of its very important characteristics. Random number generation is used for specified cases in various problems. Customarily, scientific experiments and social matters are compared with theoretical simulations by the MC method. This gives the reader higher reliability of the modeling. For example, the matter of atomic interactions is a large system that can be sampled in a number of random configurations, and that data can be used to describe the system as a whole.

There are some simulation codes for the MC. Monte Carlo N-Particle Transport (MCNP) and Monte Carlo N-Particle eXpanded (MCNPX) are famous simulation code systems developed at the Los Alamos National Laboratory (LANL) for simulating nuclear processes. In addition, the Electron

Gamma Shower (EGS) computer system for the transport of electrons and photons was developed at Stanford University (EGSnrc 2011). Also, there are several applications for business and finance. The System dDynamics (SD) is a methodology and computer simulation modeling technique for framing, understanding, and discussing complex issues and problems (Forrester 1961). (See Table 1.2.)

For the experiment, it is necessary to make use of modern nanostructural and nanochemical analysis techniques including scanning electron microscopy (SEM, TEM, and LEEM), surface microanalysis (SIMS, AES, and XPS), scanning probe microscopy (AFM, STM), x-ray scattering in all modes, and ion-beam spectroscopes (RBS and NRA). The following are descriptions of these analysis techniques:

- Scanning electron microscope (SEM): The SEM is a microscope that uses electrons rather than light to form an image. Many advantageous analyses are possible that are not possible with a light microscope. The SEM has a large depth of field, which allows a large amount of the sample to be in focus at one time. High-resolution images can be produced by SEM, which means that closely spaced features can be examined at high magnification because the sample is conductive.
- Transmission electron microscopy (TEM): The TEM is like a slide projector that projects a beam of light through (transmits) a slide. As the light passes through, it is affected by the structures and objects on the slide. Only a certain part of the light beam is transmitted through certain parts of the slide. A transmitted beam is then projected onto the viewing screen, forming an enlarged image of the slide.
- Low-energy electron microscopy (LEEM): LEEM was developed in 1985 by Ernst Bauer and Wolfgang Telieps, more than twenty years after its invention by E. Bauer in 1962. The first LEEM was installed at the University of Clausthal in Germany. Then, Dr. Ruud Tromp and Dr. Marc Reuter initiated the development of a new one at IBM. It started operation in 1991 and was later sold worldwide. Several kinds of designs have been developed using new theoretical concepts for the correction of the imaging errors of magnetic lenses, magnetic deflectors, and analyzers, including the energy filtered by LEEM for chemical analysis, the spin polarized LEEM (SP-LEEM) for magnetic imaging, the baby LEEM approach, and the SMART project. IBM built the first LEEM that included a 90° beam deflector in 1998.
- Secondary ion mass spectroscopy (SIMS): SIMS operates on the principle that bombardment of a material with a beam of ions with high energy (1–30 keV) results in the ejection or sputtering of atoms from

the material. The secondary ions are ejected as a small percentage. Information on the sample composition is obtained by the collection of these sputtered secondary ions, and their analysis by mass-to-charge spectrometry gives information on the composition of the sample. This is done by the locally destructive technique of analyzing material removed from the sample by sputtering.

- AES (Auger Electron Spectroscopy): The sample is irradiated by a primary electron beam with an energy range of 2 to 10 keV. This results in the emission of Auger electrons that can be detected and analyzed. Auger point analysis and scanning analysis can be done with a spatial resolution down to 250 nm.
- X-ray photoelectron spectroscopy (XPS): XPS is a quantitative spectroscopic technique that measures the elemental composition, empirical formula, chemical state, and electronic state of the elements that exist within a material. The kinetic energy and number of electrons that escape from the top 1 to 10 nm of the material by irradiating x-ray beam are shown as the XPS spectra. Ultrahigh vacuum (UHV) conditions are necessary.
- Atomic force microscopy (AFM): This is a very high-resolution type of scanning probe microscopy, with demonstrated resolution on the order of fractions of a nanometer, more than 1,000 times better than the optical diffraction limit. The precursor to the AFM was developed by Gerd Binnig and Heinrich Rohrer in the early 1980s at IBM Research-Zurich, a development that earned them the Nobel Prize for Physics in 1986. The first commercial AFM was developed in 1989. This is one of the foremost tools for imaging, measuring, and manipulating matter at the nanoscale. The information is collected by "feeling" the surface with a mechanical probe. Piezoelectric elements facilitate tiny, but accurate and precise movements on (electronic) command, enabling very precise scanning. Electric potentials can also be scanned using conducting cantilevers in some variations. The currents can even be passed through the tip to probe the electrical conductivity or transport of the underlying surface in newer more advanced versions, but this is much more challenging and few groups have reported reliable data.
- Scanning tunneling microscope (STM): This is an instrument for imaging surfaces at the atomic level. In 1981, the newer more advanced versions were made by Gerd Binnig and Heinrich Rohrer (at IBM Zürich), who received the Nobel Prize in Physics in 1986. Good STM resolution is considered to be 0.1 nm lateral resolution and 0.01 nm depth resolution. Usually, STM can be used not only in ultrahigh vacuum but also in air, water, and various other liquid or gas ambients, and at temperatures ranging from near zero kelvin to a few hundred degrees Celsius.

**TABLE 1.2**

Classification of Monte Carlo Codes

| Code Name | Application |
|---|---|
| Abalone | Molecular dynamics, visualization |
| ACEMD | Molecular dynamics |
| AMBER | Molecular dynamics |
| BOSS | Biochemical and organic simulation system |
| BRAHMS | Molecular dynamics |
| CASTEP | Density-functional theory |
| CCP5 | Program library, various |
| CHARMM | Chemistry at Harvard molecular mechanics |
| CPMD | Molecular dynamics |
| Dalton | Computational chemistry |
| DiMol2D | Molecular dynamics |
| DL_MESO | Dissipative particle dynamics |
| DL_POLY | Molecular dynamics |
| DYNAMO | Molecular dynamics |
| EGO VIII | Molecular dynamics |
| ENCAD | Molecular dynamics |
| ESPResSo | Molecular dynamics |
| FOCUS | Molecular dynamics |
| Gaussian | Electronic, computational chemistry |
| gdpc | Molecular dynamics visualization |
| GROMACS | Molecular dynamics |
| GROMOS | Molecular dynamics |
| HOOMD | Molecular dynamics |
| IMD | Molecular dynamics |
| Jmol | Visualization |
| QMGA | Visualization |
| RasMol | Visualization |
| RedMD | Molecular dynamics |
| SageMD | Simulation, front and back end |
| SIESTA | Molecular dynamics |
| SMMP | Monte Carlo simulation |
| SYBYL | Various |
| Tesla Bio Workbench | GPU computing |
| TINKER | Software tools for molecular design |
| UHBD | Brownian dynamics |
| VASP | Molecular dynamics |
| VMD | Visualization, molecular dynamics visualization in 3 dimensions |
| WIEN2K | Electronic structure calculation in solids |
| XCrysDen | Visualization, crystalline and molecular structure visualization |
| X-PLOR | Computational structural biology |
| YASARA | Fee and commercial |
| YASP | Molecular dynamics |

- Rutherford backscattering spectrometry (RBS): Lord Ernest Rutherford presented the concept of atoms having nuclei in 1911. RBS measures the number and energy of ions in a beam that backscatter after colliding with atoms in the near-surface region of a sample at which the beam has been targeted.
- Neutron reflection analysis (NRA): NRA makes use of the knowledge that the reflection of neutrons (neutron reflectometry) at a surface is very similar to the phenomenon of the reflection of light (optical reflectometry) demonstrated by Fermi. There is a light of strong interference depending on the wavelength of the light, its state of polarization, the thickness of the layer, and the refractive indices of the media involved.

There are nanoscopic simulation codes for molecular behavior in solid-state materials, which are listed in Table 1.2 (Gunsteren and Mark 1988).

Additionally, Towhee is a Monte Carlo molecular simulation code originally designed for the prediction of fluid-phase equilibrium using atom-based force fields and the Gibbs ensemble, with particular attention paid to algorithms addressing molecule conformation sampling (Sourceforge 1988). The code has subsequently been extended to several ensembles, many different force fields, and solid (or at least porous) phases. Furthermore, the Stopping and Range of Ions in Matter (SRIM) is a collection of software packages that calculate many features of the transport of ions in matter (Ziegler et al. 2008).

## References

Ashby, M. F., and D. R. H. Jones. 2005. Engineering materials 1. In *An introduction to properties, applications and design*. Amsterdam: Elsevier Butterworth-Heinemann.

Central Facility for Electron Microscopy. 1995. Transmission electron microscope (TEM). University of Nebraska, Lincoln, http://www.unl.edu/CMRAcfem/temoptic.htm.

EGSnrc. 2011. Institute for National Measurement Standards, National Research Council of Canada.

Evans Analytical Group, LLC. 2011. RBS Theory Tutorial, http://www.eaglabs.com/training/tutorials/rbs_theory_tutorial/.

Forrester, J. W. 1961. *Industrial dynamics*. Cambridge, MA: MIT Press.

Grosso, G., and G. P. Parravicini. 2000. *Solid state physics*. San Diego, CA: Academic Press

Gunsteren, W. F. V., and A. E. Mark. 1998. Validation of molecular dynamics simulation. *Journal of Chemical Physics* 108: 6109–6116.

Hook, J. R., and H. E. Hall. 1991. *Solid state physics*. London: Wiley.

IBM Research. 1998. Low energy electron microscopy, http://www.research.ibm.com/leem/.

Kittel, C. 1986. *Introduction to solid state physics*. New York: Wiley.
Lewis, E. E. and W. F. Miller, Jr. 1984. *Computational methods of neutron transport*. New York: Wiley.
Manno, István, 1999. *Introduction to the Monte-Carlo method*. Budapest: Akadémiai Kiadó.
Marder, M. P. 2000. *Condensed matter physics*. New York: Wiley.
Materials Research Laboratory. 2007. University of Illinois, Urbana-Champaign, http://mrl.illinois.edu/facilities.html.
Material Science and Engineering Department. 2011. What is the S.E.M.?, http://mse.iastate.edu/microscopy/whatsem.html.
NanoScience Instruments, Inc. 2011. Atomic force microscopy, http://www.nanoscience.com/education/afm.html.
Nobelprize.org. 2011. The scanning tunneling microscope, http://nobelprize.or g/educational/physics/microscopes/scanning/index.html.
Palisade. 2011. Monte Carlo Simulation, Palisade Corporation, http://www.palisade.com/risk/monte_carlo_simulation.asp.
Rubinstein, Reuven Y. 2008. *Simulation and the Monte Carlo method*. Hoboken, NJ: Wiley.
Sander, L. M. 2009. *Advanced condensed matter physics*. Cambridge, UK: Cambridge University Press.
SilliconFarEast. 2005. Secondary ion mass spectroscopy (SIMS), http://www.siliconfareast.com/SIMS.htm.
Sobol, I. M. 1994. *A primer for the Monte Carlo method*. Boca Raton, FL: CRC Press.
Sourceforge. 1988. MCCCS (The Monte Carlo for Complex Chemical Systems) Towhee, http://towhee.sourceforge.net/.
The Thomas Group. 2011. Neutron reflectometry/neutron reflection, http://rkt.chem.ox.ac.uk/techniques/nrmain.html.
UKSAF (UK Surface Analysis Forum). 2006. XPS—X-ray photoelectron spectroscopy or ESCA—Electron spectroscopy for chemical analysis, http://www.uksaf.org/tech/xps.html.
Woller, J. 1996. The basics of Monte Carlo simulations, University of Nebraska, Lincoln, http://www.chem.un l.edu/zeng/joy/mclab/ mcintro.html.
Ziegler, J. F., J. P. Biersack, and M. D. Ziegler. 2008. SRIM—The stopping and range of ions in matter. SRIM Co.

# Section I

# Atomic Nanoscale Power

# 2

# *Nanoscopic Nuclear Waste Treatment Using Ion Beam Injection in a Drum-Type Container*

**Taeho Woo**

**CONTENTS**



## 2.1 Introduction

Nuclear spent fuel waste management using ion beam injection has been investigated. Ion beam injection can make the form of the container for the nuclear waste safer for the proposed radiation. The investigation is performed at the nanoscale level. The computer simulation can predict the reliability of the industrial application in several outputs such as ion distribution, range, ionization, phonons, recoiled energy, and whether there will be a damage event. Currently, it is very difficult to find a nuclear waste repository site for permanent waste disposal in some countries including the United States. Therefore, it is important to make a strong container material for nuclear waste radiation shielding for the interim period until a repository can be selected and agreed upon by the community and the government. Nuclear waste containers should provide protective barriers against physical and chemical stresses during transportation, interim storage, and disposal. In the case of high-level waste (HLW), separated casks are used for transportation, and special emphasis is given to the disposal containers to ensure long-term isolation of the waste. The key performance parameter is the resistance to environmental attack (chemical performance). Mechanical performances, thermal/neutronic performance, compatibility with other materials, fabricability, and previous experience, as well as cost, are also taken into account (McCright 1991).

High-level waste of nuclear spent fuels should be especially considered for realistic treatment. Nanoscopic manipulation shows the deterministic analysis in the radiation–material interaction compared to the numerical study where the radioactive diffusion was emphasized. G. F. Thomas studied the diffusion from a finite cylindrical waste form where the usefulness of disposal was emphasized (Thomas 1987). In this work, there were no small-scale investigations of waste particle behaviors. G. D. Sizgek reported an investigation of a thermal model in which the analyses were performed for an *in-floor* type HLW repository in granitic rock. The results showed that decreasing the spacing between the canisters had a more pronounced effect on the temperature field than decreasing the spacing between the tunnels (Sizgek 2005). In addition, J. Andersson showed that the performance of a deep repository for nuclear waste relies heavily on its potential to retain radionuclides at the source (Andersson et al. 1998). Although there was a geological viewpoint study, it was difficult to determine the small-scale movement of the scenarios.

Therefore, in this paper, irradiation-induced nuclear waste material is studied in the nanoscale. The material science and geological aspects are considered for the materials of interest, which are used for the nuclear waste forms. The HLW has been treated as a long-term confinement process in the nuclear waste repository, because reprocessing of nuclear waste has been prohibited in many countries. Even the United States needs a strong, long-term method of treating HLW so that the environment can be protected from hazardous materials. The Yucca Mountain project could provide this kind of protection if the reliability of the HLW treatment is increased by enhanced storage technology. Construction of this project has been blocked due to several legal disputes.

Section 2.2 explains the method of the study. The results of the simulation are shown in Section 2.3, and Section 2.4 describes the study conclusions.

## 2.2 Method

In radioactive waste management, geological investigation of potential nuclear waste sites must be studied realistically. There are several issues involved in the nuclear repository. One of most critical matters is that nuclear waste storage must be guaranteed to be *absolutely* reliable for a very long time. A given site must be confirmed to provide at least 1,000 years of safe storage. The wastes are fixed in a glass matrix or synthetic rock (Lindblom and Gnirk 1982). In HLW, the immobilization requires the formation of an insoluble, solid waste form that will remain stable for many thousands of years. Generally, borosilicate glass has been chosen as the medium for dealing with HLW. The stability of ancient glass for thousands of years highlights

the suitability of borosilicate glass as a matrix material (EPA 1992). This type of process is referred to as *vitrification*. Nuclear waste is combined with glass-forming chemicals, melted, and formed as molten glass in a stainless container and allowed to cool as a solid matrix. The containers are then welded closed and are ready for storage and final disposal.

Classical nuclear waste research has focused on simulations of unwanted release scenarios using variables like the geometry of the waste source, the groundwater, and so on. This kind of research, however, couldn't account for real situations that may happen in microscopic or nanoscopic scale fields. If full research in these fields is not done, the nuclear release oriented diffusion aspect of the research is not complete.

Transuranic (TRU) waste is studied with respect to the alpha-emitting radionuclides of sufficiently long life of atomic number 92 and concentrations greater than 100 nanocuries, except $^{289}$Pu and $^{241}$Pu and their daughter products (sometimes these are considered as TRU waste by local requirements) (Saling and Fentiman 2002). Treatment of TRU waste can be realized with a long-term safety guarantee because the nanoscale behavior is monitored by simulations. This is done in a manner similar to molecular simulation in multiscale aspects. Therefore, if all of these investigations are accomplished, the waste site selection problem could be solved by the residents' understanding of this new reliable research trend. The Stopping Range of Ions in Matter (SRIM) 2008 code is used for these simulations (Ziegler 1985). This is a group of programs that can calculate the stopping and range of ions from 10 eV to 2 GeV/amu in quantum mechanical matter including solid and liquid states for ion–atom collisions.

In this study, four kinds of materials were investigated: sheet silicate (mica) compositions, zeolite compositions, smectite compositions, and crystalline silicotitanate, which have been studied by Dr. Ewing (Wang et al. 1998). These materials are candidates for HLW forms for several reasons. In the case of sheet silicate (mica) compositions, this includes the immobilization of the radionuclides by sorption, precipitation or coprecipitation, or the migration of the alkaline front in the argillaceous matrix (European Commission 2005). Zeolite compositions have a microporous ability to capture some ions while allowing others to pass freely, and allow many fission products to be efficiently removed from nuclear waste and permanently trapped (Dyer and Abou-Jamous 2007). For smectite compositions, artificially prepared smectitic clays, like those proposed for embedding canisters with highly radioactive waste, have a higher conductivity than natural clays with the same smectite content because the microstructural homogeneity of the artificial clays is not as good. The anion diffusive transport capacity of smectite-rich clays with high density is much lower than that of clays with low density in contrast to the cation diffusive capacity. This is explained by using quantitative microstructural data (Pusch 1997). Crystalline silicotitanate has been developed for radioactive waste treatment in a collaborative effort between the Sandia National Laboratory and Texas A&M University. The materials

demonstrated high Cs distribution coefficients in acidic, alkaline, and neutral solution despite the presence of a high concentration of completive ions such as $Na^+$ and $K^+$ (Yu et al. 2002).

The alpha particle is the injected ion in the simulation (Saling and Fentiman 2002). In the simulation, 10,000 ions are injected into the four targets. The ion beam energy is 2 MeV. For susceptibility, it is suggested that following equation be used (Andersson 1998):

$$\text{dpa} = \left(1 \times 10^{-16}\right) N_d \cdot D_c / \rho_n \tag{2.1}$$

where
$N_d$ = Target displacement (displacement/ion/Å).
$D_c$ = Critical dose (ions/cm$^2$).
$\rho_n$ = Atomic density of the target material (atoms/Å$^3$).

This is used for the calculation of $D_c$ (critical dose, ions/cm$^2$), which is related to the susceptibility of the waste form.

## 2.3 Results

The critical doses are the main results of the simulation and are shown in Table 2.1, which is obtained using Equation (2.1). The nontronite of smectite has the highest value. The highest deposition is around 300 nm. Figure 2.1 shows the Z-axis view of $He^{+2}$ ion injection for muscovite and the simplified configuration of the nuclear waste drum (A = crystalline silicotitanate layer, B = concrete layer). For the ion beam distribution, the highest point for the critical dose is at 300 nm. Crystalline silicotitanate has a higher value for stopping power of most regions among the four forms in Figure 2.2. According to Figure 2.3, the energy loss of stopping power changes in 204 nm for nontronite and crystalline silicotitanate. The nontronite has the lowest energy loss in 300 and 400 nm. After calculating the comparisons between the two

**TABLE 2.1**
Critical Dose

| Waste Form | Critical Dose (ions/cm$^2$) : $D_c$ |
|---|---|
| Sheet silicate (mica) : muscovite | $18.4438 \times 10^{-4}$ |
| Zeolite : analcim | $146.9250 \times 10^{-4}$ |
| Smectite : nontronite | $217.5820 \times 10^{-4}$ |
| Crystalline : silicotitanate | $28.8761 \times 10^{-4}$ |

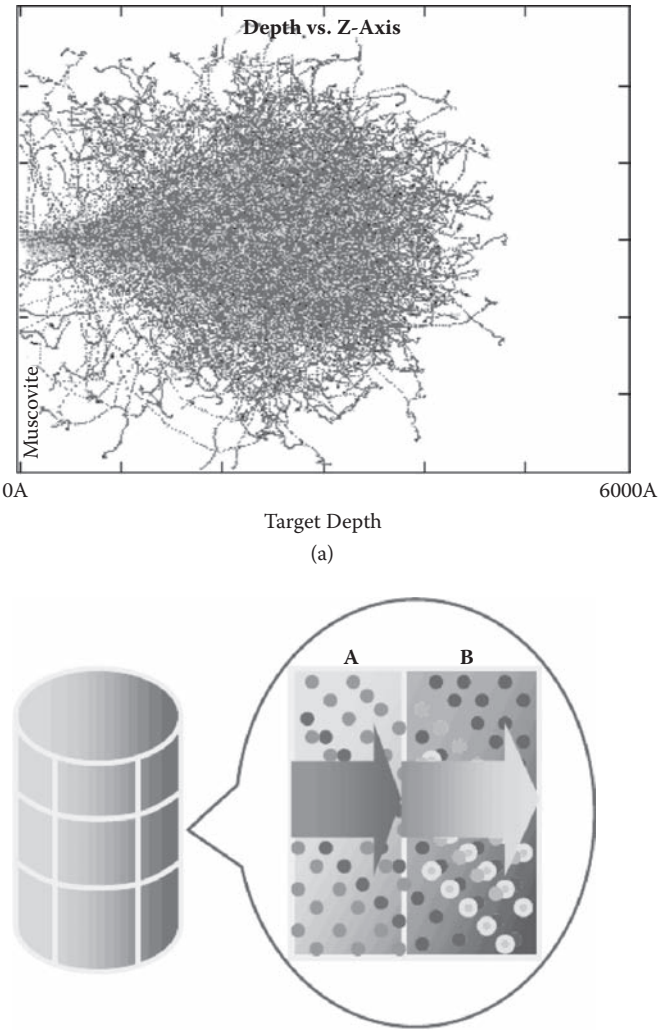


**FIGURE 2.1**
(a) Z-axis view of $He^{+2}$ ion injection for muscovite, and (b) simplified molecular configuration of nuclear waste drum. A = crystalline silicotitanate layer, B = concrete layer.

materials, the nontronite shows the highest stopping power after the point of 204 nm.

Considering dynamic analysis, it is important that the stability of the material used to safeguard against radioactivity be effective for several thousand years. However, it is impossible to experiment based on time. The comparisons among the four candidate forms in this paper could

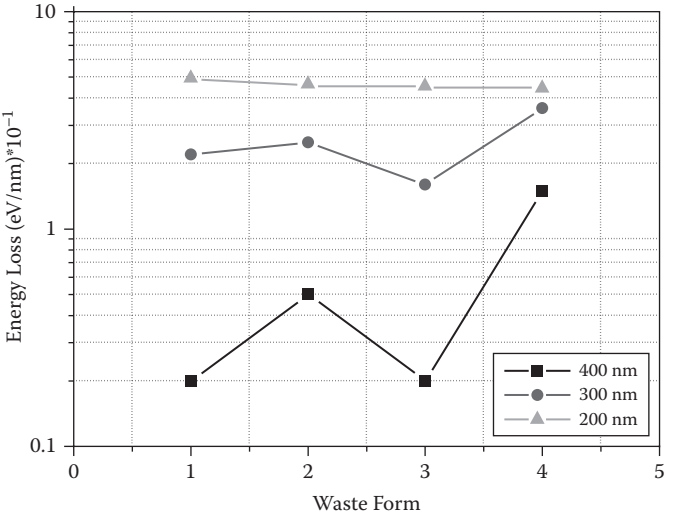


**FIGURE 2.2**
Stopping power. 1 = muscovite, 2 = analcime, 3 = nontronite, 4 = crystalline silicotitanate.

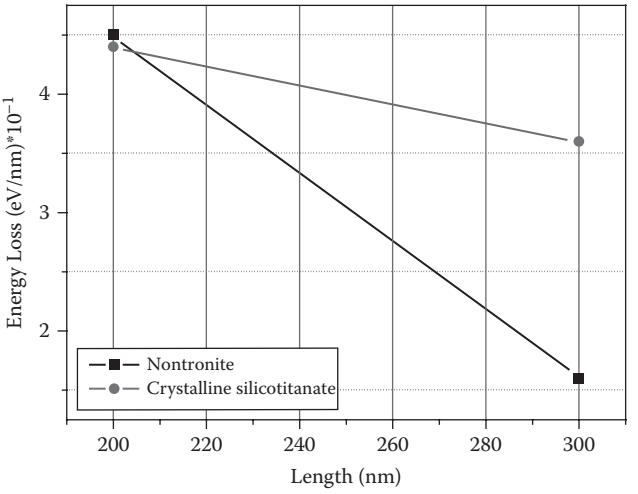


**FIGURE 2.3**
Stopping power change of nontronite and crystalline silicotitanate.

result in strength that can withstand radioactive hazard characteristics. Figure 2.4 shows the relative values for muscovite at the critical dose. The other three values are divided by the value of muscovite. So, muscovite has a value of 1.0. The higher value means the form can resist radiation at the higher critical dose.

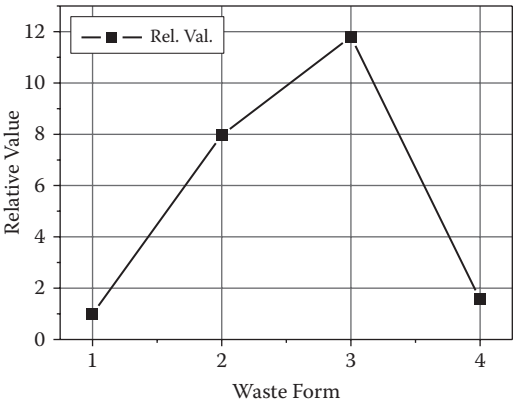


**FIGURE 2.4**
Relative values for sheet silicate at critical dose. 1 = muscovite, 2 = analcim, 3 = nontronite, 4 = crystalline silicotitanate.

## 2.4 Conclusions

It is important to consider the stopping power that causes the displacement in the target material. Therefore, the higher displacement by the stopping power is very important in the nuclear waste form. The possible $He^{+2}$ of the nuclear waste material can be stopped more effectively in the higher displacement. Otherwise, the highest critical dose shows the lowest energy loss of the lowest displacement in nontronite. The conclusions of this simulation are as follows:

- Several characteristics of irradiated material are analyzed for nuclear waste forms.
- The experimental study should be accompanied by this theoretical simulation research.
- The two factors of critical dose and energy loss are examined for the suitable waste forms.
- A realistic application is required for nuclear waste treatment.

A nuclear waste drum of 200 liters is suggested. Two layers of HLW treatment are proposed. The inner layer is crystalline silicotitanate or its compound and the outer layer is a conventional material such as metal or concrete. This layer is reduced using a higher stopping material like crystalline silicotitanate, considering the alpha particle shielding. Alpha particles are serious factors in health concerns associated with nuclear waste, because they are most destructive if the source is ingested or inhaled. Considering

other radiations, the phenomena of the radiation–material interactions are related to the characteristics of the radiation. In the case of beta rays, the damage from this type of radiation could be blocked near the surface of the waste form due to the short-range characteristics of beta particles. The gamma interactions with the materials show the three kinds of photoelectron effects, Compton scattering, and pair production. The neutron case is very serious because of the possibility of new fission if there is some fissile material in the HLW.

The nuclear waste business is very important due to the danger and the strategic concerns. It is necessary to develop more reasonable and safe methods for nuclear waste confinement. Micro- and nanoscale investigation is a new frontier for this research. Advanced small-scale technology should be developed for this waste issue as well as new materials. For future work, it is proposed that the sensitive multi-acquisition radiation technique (SMART) be developed for selecting a nuclear waste confinement using high-resolution examination such as high-resolution transmission electron microscopy (HRTEM). The micro- and nanoscale investigation is a fine frontier for nuclear waste research.

## References

Andersson, J., P. Robinson, and M. Impey. 1998. Implications of rock structure on the performance in the near field of a nuclear waste repository. *Engineering Geology* 49(3–4):195–200.

Dyer, A., and J. K. Abou-Jamous. 1997. Zeolites for nuclear waste treatment: Co, Ni and Zn uptake into synthetic faujasite X. *J. Radioana. Nuc. Che.* 224(1–2): 59–66.

Environmental Protection Agency (EPA). 1992. *EPA handbook: Vitrification technologies for hazardous and radioactive waste*, EPA/625/R-92/002.

European Commission. 2005. *Effect of cement on clay barrier performance—Phase II*, Final Report, Directorate-General for Research Euratom.

Lindblom, U., and P. Gnirk. 1982. *Nuclear waste disposal, Can we rely on bedrock?* New York: Pergamon Press.

McCright et al. 1991. Candidate container materials for Yucca Mountain Waste package design, *Proc. Nuclear Waste Packaging Focus Conf.* La Grange Park, IL: American Nuclear Society.

Pusch, R. 1997. Transport phenomena in smectite clay explained by considering microstructural features. *Engineering Geology* 54 (1–2):167–172.

Saling, J. H., and A. W. Fentiman. 2002. *Radioactive Waste Management*, 2nd ed. Boca Raton, FL: Taylor & Francis.

Sizgek, G. D. 2005. Three-dimensional thermal analysis of in-floor type nuclear waste repository for a ceramic waste form. *Nuclear Engineering and Design* 235(1):101–109.

Thomas, G. F. 1987. Diffusional release of a single component material from a finite cylindrical waste form. *Annals of Nuclear Energy* 14(6):283–294.

Yu, B., J. Chen, and C. Song. 2002. Crystalline silicotitanate: A new type of ion exchanger for Cs removal from liquid waste. *J. Mater. Sci. Technol.* 18(3):206–210.

Wang, S. X., L. M. Wang, and R. C. Ewing. 1998. Ion irradiation-induced amorphization of $CaAl_2O_4$. *Nuclear Instruments and Methods in Physics Research B* 141:509–513.

Ziegler, J. F., J. P. Biersack, and U. Littmark. 1985. *The stopping and range of ions in solids*. New York: Pergamon Press.

# 3

# *Lattice Squeezed Nuclear Reaction (LSNR) of a Power Cell for Nanoscopic Investigations Using Ion Beam Injections*

**Taeho Woo and Sangwoo Noh**

**CONTENTS**



## 3.1 Introduction

This chapter proposes a hypothetical lattice squeezed nuclear reaction (LSNR). The conventional low-energy nuclear reaction (LENR) is studied from the lattice viewpoint, which can make possible a nuclear reaction in room temperature conditions as a nontheoretical scenario. The object is to find the possibility of the LENR in the designed method. The indirect examinations could lead to novel nuclear reactions.

Following the announcement of Pons and Fleischmann in 1989, room-temperature nuclear reaction has been investigated (Fleischmann and Pons 1989). The most important characteristics of the LENR were to determine excess heat production (De Ninno et al. 2008). Using computer simulation, one can predict the reliability of an industrial application based on several outputs such as ion distribution, range, ionization, phonons, recoiled energy, and potential damage events.

Historically, accelerator-driven nuclear transduction was performed by Cockcroft and Walton in the 1930s (Cockcroft and Walton 1932). In the experiment, the proton was collided with lithium and then two helium atoms were produced, which is similar to nuclear waste transmutation.

On the other hand, the lattice of the atomic structure can make enough space to press the deuteron or proton to produce a nuclear reaction with abundant excess heat. The most important idea is to make the lattice structure in the form of a sandwich. There were several previous works for this trend (Chicea 2003, Iwamura et al. 2002). Especially after publication by Dr. Iwamura (Iwamura et al. 2002), several characteristics were examined for industrial applications. The LENR aspect is suggested using this method in this study. If the technology is formulated theoretically and experimentally, the power cell could be manufactured.

The injected ion is incorporated with the vacancy and the vacancy energy was obtained by Brooks' method (Brooks 1955) using Equation (3.1).

$$E_o = 4\pi r_o^2 \gamma_o \left[ \frac{1}{1 + \gamma_o / (2Gr_o)} \right] \tag{3.1}$$

In this equation, $G$ and $\Upsilon_o$ are the shear modules and surface energy per unit area of the surrounding material, and $r_o$ is the radius of the atom. This can be used to calculate the vacancy formation energies of bulk materials. As a result, the vacancy formation energy in the nanoparticle is obtained (Qi et al. 2003). It could be used to determine the vacancy formation energy in the nanoparticle injection, which collides with the three layer materials.

In this chapter, the Stopping and Range of Ions in Matter (SRIM) 2008 code shows several variables for energy production in thin film layers. A much more reasonable study has been done for the LENR. The displacement of lay ions could be a place for the LENR and makes the energy production. Quantum mechanical scenario is assumed. Section 3.2 explains the method of the study. The calculation for the modeling is shown in Section 3.3. Section 3.4 describes the results of the study, and some conclusions are offered in Section 3.5.

## 3.2 Method

For the higher possibility of the nuclear reactions, LENR, which is called *room-temperature nuclear reaction* or *catalysis nuclear fusion*, has been investigated in a lattice of several atomic layers. It is suggested that a private company might develop this concept for commercialization, although the concept of the reaction has not yet been manifested theoretically (Wired.com 2007). Funds have been invested in this research field as a result of worldwide interest in nanotechnology. The U.S. government has also started to recognize the possibilities of the LENR concept, as can be seen if one searches the Grants.gov website.

In LENR, Mitsubishi Heavy Industries, Ltd. in Japan has created a new kind of nuclear transmutation system (Iwamura et al. 2002, 2003). This chapter shows the reliability of the reaction system through simple computer simulation using SRIM 2008 (Biersack and Ziegler 1982; Ziegler 1988; Ziegler et al. 2009). The displacement can create a possible place for the reaction of the deuteron (or proton) and the substrates of interest. The gas is injected into the substrates. Some elements could be produced in the other side of the layers. These could be the products for nuclear reactions because these atoms are different from the input atoms.

Table 3.1 shows the characteristics where all layers are of the face-centered cubic (fcc) structure, except the body-centered cubic (bcc) structure of cesium and the hexagonal close-packed (hcp) structure of graphite. Figure 3.1 shows the layers of the substrates, which are composed of Cs-coated thin film Pd (400 Å), one of three elements (graphite, Ca, or Ni) (1000 Å), and bulked Pd (0.1 mm). In the case of deuteron, the gas is injected into the surface of the substrates, so there are many chances for interaction between deuterons and the substrate materials.

**TABLE 3.1**

Characteristics of Element Lattice

| Element | Structure |
|---|---|
| Cs | BCC |
| Pd | FCC |
| Graphite | HCP |
| Ca | FCC |
| Ni | FCC |

*Note:* BCC = body-centered cubic, FCC = face-centered cubic, HCP = hexagonal close-packed.

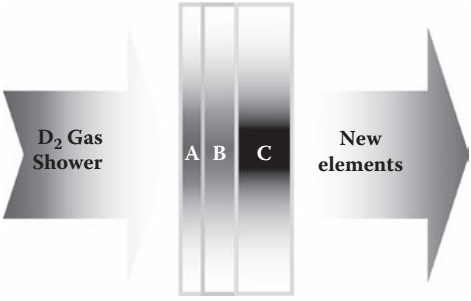


**FIGURE 3.1**
Simplified configuration of a power-cell system. A = Cs + Pd (400 Å), B = graphite, Ca, or Ni (1000 Å), C = Pd (0.1 mm).

Although it is possible to create a nuclear transmutation of the ion beam injections, it is difficult to find theoretical explanations for the reaction. In considering the several kinds of lattice characteristics, it is reasonable to guess the effect of the space in unnatural conditions like vacuum suction in lower energy rather than the conventional very hot nuclear reaction or accelerator-driven transmutation. The second layer condition is another effect for the room temperature reaction, where the sandwich arrangement is simulated. This material could be transmuted to another material or allow a nuclear transmutation reaction.

## 3.3 Calculation

The SRIM 2008 code is a well-known simulation package that is used in this type of research (Biersack and Ziegler 1982; Ziegler 1988), and consists of a group of programs. The programs can calculate the stopping and range of ions from 10 eV × (amu)$^{-1}$ to 2 GeV × (amu) $^{-1}$ in quantum mechanical matters including solid and liquid states in ion–atom collisions. The Coulomb collision screens the atoms and ions and has been improved compared to the previous codes: SRIM 2000 and TRIM 96 (Transport of Ions in Matter; this is the former name of the SRIM code system). There are some enhanced points where minor bugs have been removed, and the method has been modified for heavy ions. Furthermore, the nuclear stopping power for specific atoms is introduced. The irradiation effects are instantaneous, and more complex methods must be developed for experiments involving real situations.

In the simulation, the small energy ion is injected into several layers of the atomic structures. Therefore, an ion beam is used for the simulation. For the experiment, a system could be suggested using different types of molecular structures. However, fundamentally the lattice shape is the main factor in the room-temperature nuclear reaction.

## 3.4 Results

Table 3.2 shows the results of the simulations. The most probable points are obtained by the energy. The lowest values shown are 10 keV. The most probable point increases as the energy increases. As the energy increases, the vacancies are also increased. In addition, the change rate is not increased in graphite and Ca at the 10 keV energy value.

Figure 3.2 shows the production of the displacement, which is assumed for the reaction. The distributions in the edge between Pd + Cs and one of

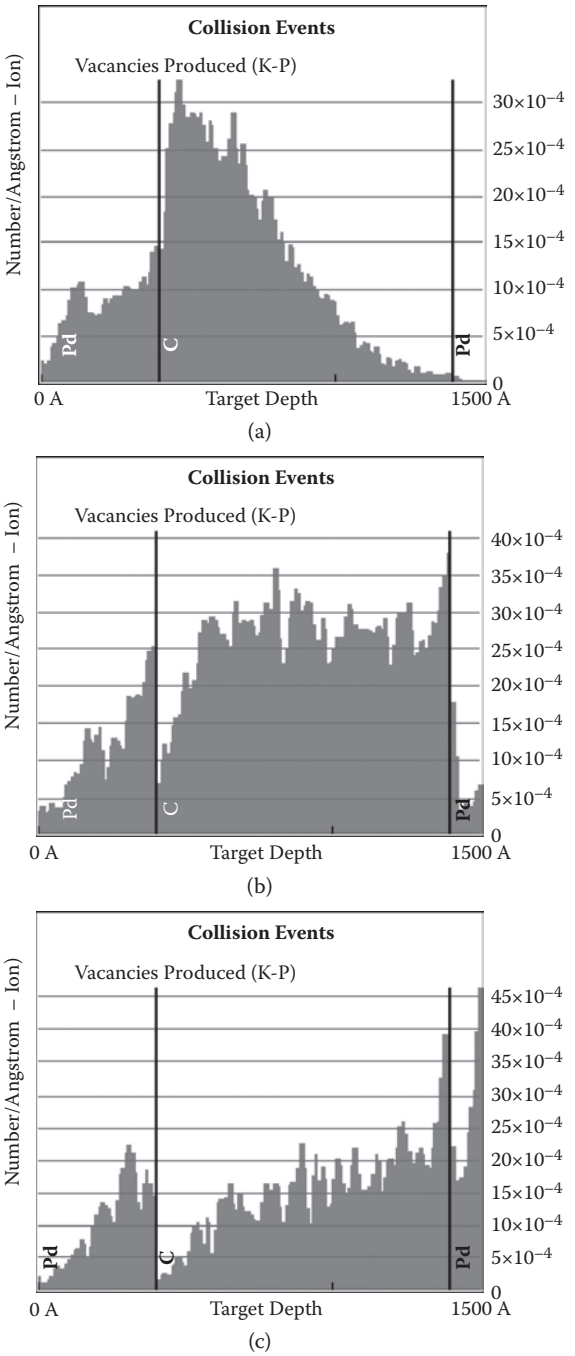


**FIGURE 3.2**
Trend of collision events using SRIM 2008. (a) 5 keV, (b) 10 keV, (c) 20 keV.

**TABLE 3.2**

Results of Simulations

| Layer | Ion Beam Energy (keV) | Vacancy at Most Probable Point ($\times 10^{-4}$) | Most Probable Point per D+ Collision (Å) |
|---|---|---|---|
| Graphite | 5 | 32.5 | **71** |
| | 10 | 38.0 | 1,000 |
| | 20 | 39.4 | 1,000 |
| Ca | 5 | 10.1 | **156** |
| | 10 | 20.7 | 1,000 |
| | 20 | 17.5 | 1,000 |
| Ni | 5 | 36.7 | **71** |
| | 10 | 53.3 | 214 |
| | 20 | 45.0 | 1000 |

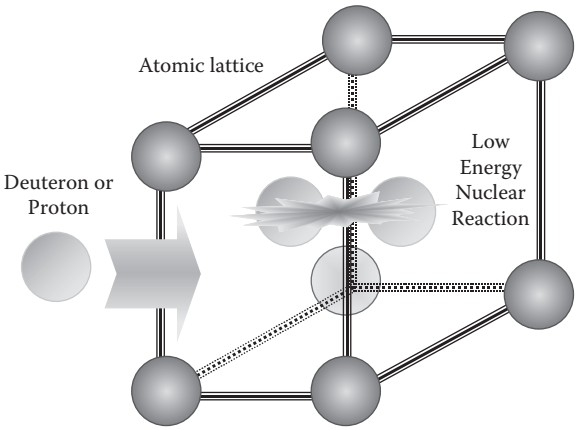


**FIGURE 3.3**
Configuration of the behavior in the lattice.

three layers (graphite, CA, or Ni) show the peak values that will make the vacancies. It is strange that there is another peak in the edge between one of three layers and Pd layers. Following this phenomenon, it is assumed the lattice of the layer plays a major role in the peak vacancy. Figure 3.3 shows the configuration for the reaction of LSNR. Figure 3.4 shows the simplified proposed package of the power cell, where the vacuum generator is attached. This is a prototype of the power cell, which will be changed for commercial purposes. In this process, the proton–proton chain reaction is proposed. Namely, the reaction in Equation (3.2) will occur, which was introduced by Bethe (1939).

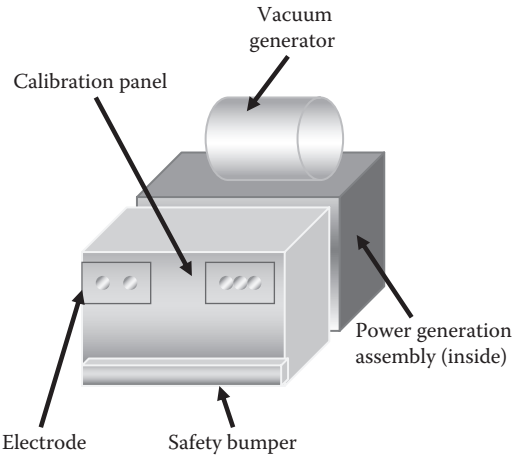


**FIGURE 3.4**
Simplified proposed package of the power cell.

$$
\begin{aligned}
{}_1H + {}_1H &\rightarrow {}_1D + e^+ + \nu_e + 0.42\ \text{MeV} \\
e^+ + e^- &\rightarrow 2\gamma + 1.02\ \text{MeV}
\end{aligned}
\tag{3.2}
$$

Consequently, these photons can generate the electrons by the photocathode in the package of the power cell. Regarding the theory of Bethe, there are some analyses for the table-top facility instead of analyzing star or solar conditions. Zhou et al. showed the selective resonant tunneling model as compared with Bethe's early model for solar energy calculation. They are similar in considering the resonance effect, the weak interaction, the assumption for nuclear potential, and the Coulomb barrier in order to obtain the correct result for the energy density of the sun. However, the selectivity of resonant tunneling is new in the present selective resonant model (Zhou et al. 2003; Li et al. 2004). In addition, Chen explained how two principles of the selective resonant tunneling model are recapitulated and applied to the case of tritium production. The model can semiquantitatively explain tritium production in a condensed matter nuclear reaction with no neutron and gamma radiation. A similar model may produce excess heat with no commensurate neutron and gamma radiation. Some experiments are suggested to test our explanation (Chen and Li 2002). Also, Jiang et al. (2008) said the mantle $^3$He and $^3$H might have originated from natural nuclear fusion (d–d and d–p reaction, or other reactions) in deep Earth. Encouraged by this new idea, they tried to re-create nuclear fusion at low temperatures in the laboratory. The paper described charged particles emitted from the deuterium-loaded titanium foil and powder at low temperature. Although the counts were very low (about 0.13 counts/h), fortunately, broad and narrow peaks

were observed for the deuterium-loaded titanium foil and TiD-Mo sample, respectively. The charged particle was identified as a proton having energy of about 2.8 MeV after exiting the sample. They suggested that the proton might originate from the d–d reaction in the samples. Then the d–d reaction rate was calculated to be $1.4 \times 10^{-24}$ fusion/d-d·sec for the deuterium-loaded titanium foil sample. On the other hand, no charged particles were observed above the background level for the deuterium-loaded titanium powder sample. Therefore, this work provided a positive result of nuclear fusion for the metal foil samples, but a negative result for the powder samples. The negative result of the deuterium-loaded titanium powder sample suggested that the reaction yield might be correlated with deuterium density, or it might be correlated with microscopic variations in the deuterium-loaded titanium materials. The negative result also indicated that the d–d reaction catalyzed by $\mu$-meson from a cosmic ray can be excluded in this experiment. The work might be helpful to further study on the physical mechanism of nuclear fusion in deuterium (hydrogen)-loaded metals and also helpful to the study of the origin of $^3$He in the deep Earth (Jiang, 2008).

## 3.5 Conclusions

In the lattice pressed LSNR, the multiple-layer system is an important factor. That is to say, while palladium–platinum is the best couple for the reaction in LENR (Chubb 2002), several layers should be in a sandwich format between the palladium layers. In the study, the most probable energy of the injection ion is around 10 keV, which shows the reduction of work energy in the room temperature reaction. It is thought that the lattice of the element is the important characteristic of molecular structure where the possible nuclear reaction could occur at the lower energy.

It has been considered that the lattice of the molecular structure could squeeze the protons or deuterons, which might create a nuclear reaction. One of the empirical scenarios is performed in the LSNR. This reaction depends on the energy of the injected deuterium gas. By assuming a kind of nuclear reaction, the excess heat could be produced by the nuclear reaction in a vacancy of the molecular lattice. Therefore, the energy of injection ions and the compound of the substrate are important factors in explaining the vacuum-assisted LSNR.

Using several injection molecules other than the deuteron gas, one can determine the vacancy numbers in the energy (by injection gas or most probable point) and the distance from the barrier. So, the formulization will be made by the energy, vacancy, and distance from the barrier. One can examine the excess heat and electron generation from the reactions, which is the main factor in the LSNR and power cell manufacturing.

## References

Bethe, H. 1939. Energy production in stars. *Physical Review* 55:103, 434.

Biersack, J. P., and Z. F. Ziegler. 1982. The calculation of ion ranges in solids with analytic solutions. In *Ion Implantation Techniques*, 157–176. Berlin: Springer Verlag.

Brooks, H. 1955. *Impurities and Imperfection*. Cleveland, OH: American Society for Metals.

Chen, S., and X. Z. Li. 2002. Tritium production and selective resonant tunneling model. In *Proceedings of the 9th International Conference on Cold Fusion, Condensed Matter Nuclear Science*. Beijing: Tsinghua University Press.

Chicea, D. 2003. Comment on carbon production in deuterium-metal systems. Paper presented at the 10th International Conference on Cold Fusion, Cambridge, MA.

Chubb, T. A. 2002. Comments on search for $^{3}$He and $^{4}$He in Arata-style palladium cathodes I: A negative result and search for $^{3}$He and $^{4}$He in Arata-style palladium cathodes II: Evidence for tritium production, *Fusi. Sci. Tech.* 41: 151.

Cockcroft, J. D., and E. T. S. Walton. 1932. Experiments with high velocity ions. *Proc. R. Soc. London A*137, 229.

De Ninno, A., E. Del Giudice, and A. Frattolillo. 2008. Excess heat and calorimetric calculation evidence of coherent nuclear reactions in condensed matter at room temperature. In *Low-Energy Nuclear Reactions Sourcebook*. New York: Oxford University Press, pp. 127–152.

Fleischmann, M., and S. Pons. 1989. Electrochemically induced nuclear fusion of deuterium. *J. of Elec. Chem.* 261(2): 301–308.

Iwamura, Y., T. Itoh, M. Sakano, S. Sakai, and S. Kuribayashi. 2003. Low energy nuclear transmutation in condensed matter induced by D2 gas permeation through Pd complexes: Correlation between deuterium flux and nuclear products. Paper presented at the 10th International Conference on Cold Fusion, Cambridge, MA.

Iwamura, Y., M. Sakano, and T. Itoh, 2002. Elemental analysis of Pd complexes: Effects of D2 gas permeation. *Jpn. J. Appl. Phys.* 41:4642–4650.

Jiang, S., J. Li, M. He, S. Wu, J. Wang, H. Zhang, S. Yao, Y. Zhao, and C. Wang. 2008. New results of charged particle released from deuterium-loaded metal at low temperature. Paper presented at the ICCF-14 International Conference on Condensed Matter Nuclear Science. Washington, DC.

Li, X. Z., B. Liu, Q. M. Wei, S. X. Zheng, D. X. Cao. 2004. A Chinese view on summary of condensed matter nuclear science. *J. Fus. Eng.* 23(3):217–221.

Qi, W. H., M. P. Wang. 2003. Size dependence of vacancy formation energy of metallic Nanoparticles, *Physica B* 334:432–435.

Wired.com. 2007. Cold-fusion graybeards keep the research coming. http://www.wired.com/sci ence/discoveries/news/20 07/08/cold_fusion.

Zhou, Z., X. Li, and B. Liu. 2003. Bethe's calculation for solar energy and selective resonant tunneling. Paper presented at the 10th International Conference on Cold Fusion. Cambridge, MA.

Ziegler, Z. F., ed. 1988. *Ion Implantation Science and Technology*, 2nd ed. Boston: Academic Press, Inc.

Ziegler, Z. F. Biersack, J. P., Littmark, U. 2009. *The Stopping and Range of Ions in Solids*. New York: Pergamon Press.

# 4

# *Safety Assessment Study in Nanoscopic Circumstances for an Accidental Cooling Loop Failure (ACLF) in a Lunar Nuclear Power Reactor (LNPR)*

**Taeho Woo and Yunil Kim**

**CONTENTS**



## 4.1 Introduction

A possible lunar base power is investigated using nuclear energy. Nuclear fission is a conceptual design for nuclear power plants (NPPs) in a very low gravity situation. The National Aeronautics and Space Administration (NASA) has developed a lunar nuclear power reactor (LNPR) concept for the manned lunar base, which could be realized in near future. The transient thermal system is investigated using analytic techniques with respect to safety. Conventional methods have focused on functional characteristics such as power efficiency. In this chapter, the reliability of the system is examined using a nonlinear algorithm due to the uncertainty of the lunar environment.

A fission surface power system on the Moon has the possibility of producing 40 kilowatts of electric power, which can supply about eight houses on Earth (NASA 2009). Figure 4.1 shows NASA's conceptual design of a fission surface power system (NASA 2010). Figure 4.2 shows a front view of a fission surface power system construction that is based on the NASA design (Coulter 2010). Figure 4.3 shows the LNPR. In addition, Figure 4.4 shows the

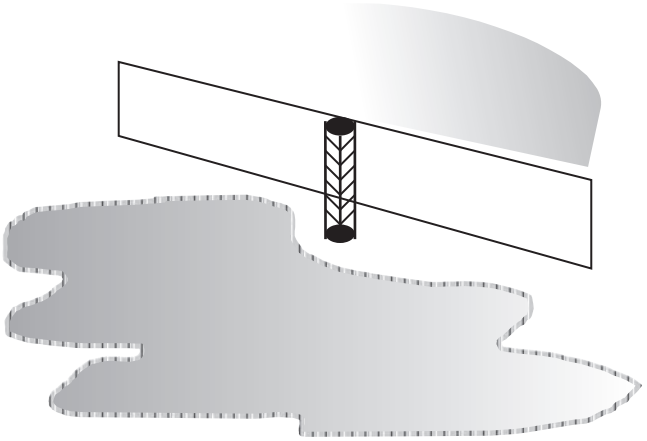

**FIGURE 4.1**
Conceptual design of a fission surface power system.

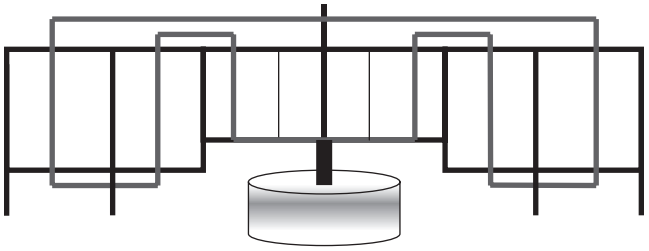

**FIGURE 4.2**
Front view of a fission surface power system.

simplified configuration of the LNPR. The event flow of an accidental cooling loop failure (ACLF) is shown in Figure 4.5. The cooling matter is the regolith, which is lunar highland soil. Table 4.1 shows a comparison of lunar highland soil and Earth soil (Prado 2009). The temperature of the Moon is changed by the Sun's angle of the solar light to the exposed lunar surface. The effective heat sink temperature is examined for the horizontal and vertical radiator located at the lunar equator (Ewert 1993), which is in Figure 4.6. The heat transfer of the cooling is done by the radiation on the Moon. The surface temperature rises up to equilibrium with incoming solar radiation because there is no atmosphere and the surface is rock material of low conductivity and relatively low heat capacity. The Stefan–Boltzmann equation sets the numbers that govern solar radiation:

$$I = \varepsilon\sigma T^4 \tag{4.1}$$

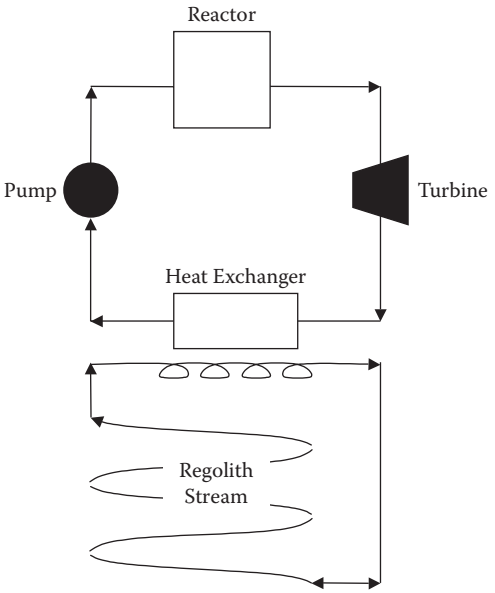


**FIGURE 4.3**
Lunar nuclear power reactor (LNPR).

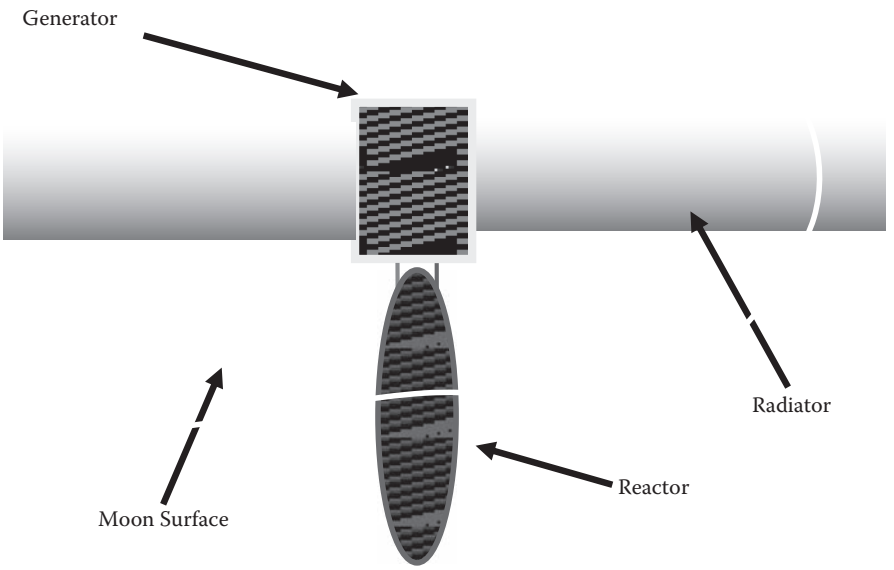


**FIGURE 4.4**
Simplified configuration of a lunar nuclear power reactor (LNPR).

| Initiating Event | Response to Initiating Event | | | | Sequence Number | Event Sequence Frequency (Rx-yr) | Remarks |
|---|---|---|---|---|---|---|---|
| Accident of cooling loop failure (ACLF) | Core Trip | Criticality stabilization | Geological stabilization | Long term cooling | | | |

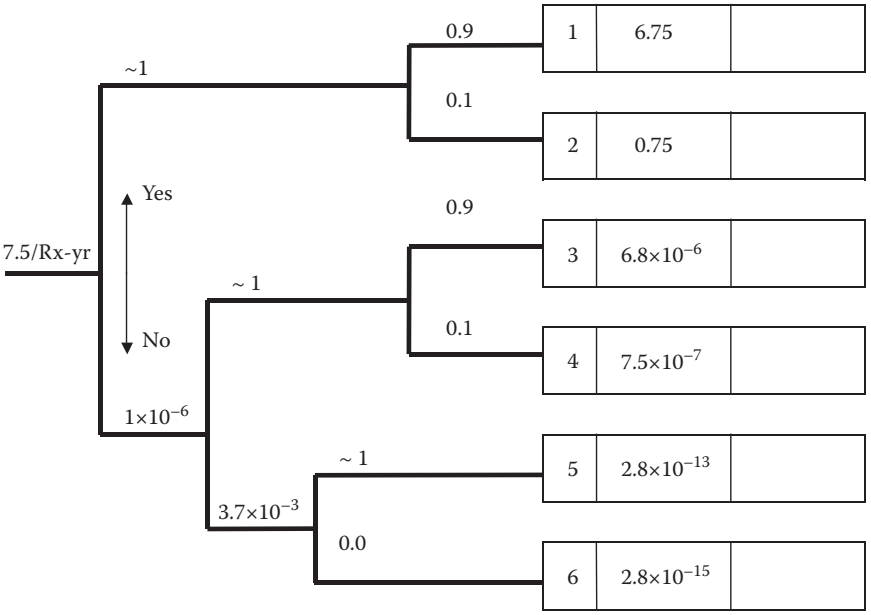


**FIGURE 4.5**
Event flow of an accidental cooling loop failure (ACLF).

where, $I$ is the absorbed solar energy per unit area. $T$ is the absolute surface temperature (Kelvin), ε is the emissivity, and σ is Stefan's constant, $5.67 \times 10^8$ in metric units.

There has been some research into space risk assessment. Everline and Paulos (2006) studied multiple event risks in aerospace applications. Fragola et al. (1995) investigated the space station in a long-term facility assessment. For space power using nuclear energy, the Cassini spacecraft mission to Saturn and its moon, Titan, carried three radioisotopic thermoelectric generators (RTGs) and 32.8 kg of $^{238}$Pu fuel, which provided total electrical power of 870 $W_e$. High-efficiency thin film silicon solar cell arrays can produce 676 $W_e$/kg and triple-junction InGaAs solar cell arrays can produce 360 $W_e$/kg at geosynchronous orbit (Fatemi 1999). There was a safety assessment of the Cassini mission where two kinds of probabilistic analyses were compared (Swaminathan 1997). Schmitt investigated the private enterprise to lunar base activation. The commercial applications are silicon-containing components,

**TABLE 4.1**

Comparison of Lunar High Land Soil and Earth Soil in ppm

| Element | Lunar Highland | Earth |
|---|---|---|
| Oxygen | 446,000 | 466,000 |
| Silicon | 210,000 | 277,000 |
| Aluminum | 133,000 | 81,300 |
| Iron | 48,700 | 50,000 |
| Calcium | 106,800 | 36,300 |
| Sodium | 3,100 | 28,300 |
| Potassium | 800 | 25,900 |
| Magnesium | 45,500 | 20,900 |
| Titanium | 3,100 | 4,400 |
| Hydrogen | 56 | 1,400 |
| Phosphorus | 500 | 1,050 |
| Manganese | 675 | 950 |
| Carbon | 100 | 200 |
| Chlorine | 17 | 130 |
| Chromium | 850 | 100 |

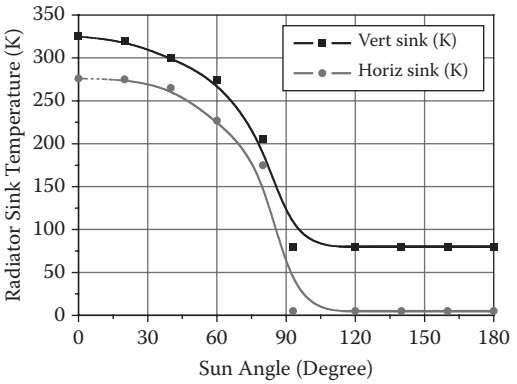


**FIGURE 4.6**
Effective heat sink temperature of the horizontal and vertical radiators located at the lunar equator.

which can be converted into solar photovoltaic cells, and solar wind $^{3}H$, which can fuel fusion power plants (Schmitt 2003). However, there were no safety considerations for the reactor systems in this research. Research was limited to power generation. Bodkin et al. (2006) reported on the support systems of the lunar base. This was controlled by the environmental control and life support system (ECLSS). The importance of the system was the operation of the pressure and air mixture ratio. This kind of central control

system supplies the basic matter to build the LNPR. The thermohydraulic two-phase system in space has been devised by Park and Sunada (2008). The vapor compressor-driven hybrid two-phase loop was developed for high-temperature application. The evaporator used passive capillary pumping to feed a well-balanced liquid for thin film boiling heat transfer, which improves the high heat flux capability. Several results were demonstrated in the small-scale prototype. This was the fundamental thermal behavior that was incorporated with heat transfer. It is suggested that the safety aspects of system operations need improvement. For the dynamic risk assessment, Siu (1994) and Belhadj and Aldemir (1996) performed computational simulations on the system safety.

The simulations using system dynamics (SD) are constructed for time-dependent quantification of management for the safety assessment. Section 4.3 explains the method of the study. The calculation for the modeling is shown in Section 4.4. Section 4.5 describes the results of the study. There are some conclusions in Section 4.6.

## 4.2 Method

System dynamics was created by Dr. J. Forrest at the Massachusetts Institute of Technology (MIT) for quantification of systematic situations. Applications for nonlinear characteristics of social and economical systems have been studied. Quantification is accomplished by testing and modeling the complex features in the dynamic scenarios in the areas of interest. Feedback on the event and the time step are particular characteristics of SD, where the event flows are expressed in a nonlinear algorithm. Quantification is done by Monte Carlo simulations of the defined algorithm.

M. Radzicki described SD, which is a powerful methodology and computer simulation modeling technique for understanding, framing, and discussing complex issues and problems (Radzicki and Taylor 1971). It is designed for managers to improve their understanding of complex issues, and is applicable in all kinds of policy and design areas. SD can be used to investigate how and why complex real-world systems behave the way they do during a specified time period. Improved understanding can lead to implementation of more effective policies. The most important thing is the dynamic behavior of a system, where the operator tries to identify patterns of behavior exhibited by particular system variables, and then builds a model based on the characteristics of those patterns. In SD modeling, single- and double-arrow lines are used for the purpose. Lines are used for the event flows and time flows. The dynamic behavior of a system is manipulated by SD using its key physical and information flows, stocks,

and feedback structures for SD. Several characteristics of SD are explained in the following text.

- *Nonlinearity:* A large part of SD modeling process involves the application of common sense to dynamic problems. Such behaviors usually indicate a nonlinearity of the events. This is seen as single- and double-arrow lines in the modeling. The arrow line shows the event flow without any restriction.
- *Stock flow:* The principle of accumulation is affected by dynamic behavior, which means that all kinds of dynamic behaviors could happen when flows accumulate in stocks. Both informational and noninformational objects can move through flows and accumulations in stocks.
- *Feedback:* The effect of feedback loops is shown by the stocks and flows in real-world systems. The feedback loops are often joined together by nonlinear couplings where any object can cause counterintuitive behavior.
- *Time Paths:* The dynamic behavior of systems is quantified, where the operator tries to identify the patterns of behavior exhibited by certain system variables, and then builds a model with the characteristics of those patterns.

There are special expressions for these characteristics in SD modeling. Especially in the Vensim code, technical methods are shown as single- and double-arrow lines as follows:

- Single-arrow line: This line shows the flow of the event. It is the sequence of the scenarios as well as the dynamic behavior. So, the direction of the line gives the event flow and event feedback.
- Double-arrow line: The dynamic behavior is increased in SD modeling for the principle of accumulation. All kinds of dynamic behaviors can happen when flows accumulate in stocks, which are seen in Figure 4.7 as EXAMPLE for accumulation and INPUT–OUTPUT for flows. This is like a bathtub where a flow can be thought of as a faucet and pipe assembly that fills or drains the

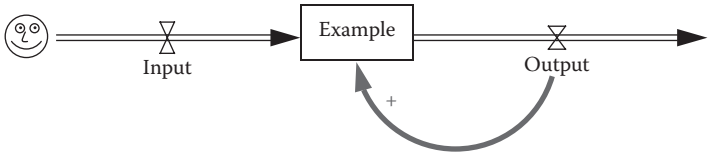


**FIGURE 4.7**
Stock flow and feedback.

stock. This is the simplest dynamic system in the stock-flow structure. Both informational and noninformational objects can move through flows and accumulation in stocks in SD. It is thought that the feedback loops are often joined together by nonlinear couplings where any object can cause counterintuitive behavior, which is seen as the backward loop in Figure 4.7. A plus sign signifies an addition to the EXAMPLE feedback value, OUTPUT. If it is a minus sign, the feedback value, OUTPUT, is subtracted from the EXAMPLE value.

There are some publications available that cover the transition of time (Forrester 1961, 1968, 1969, 1971). There are also some papers available that relate to decision making (Forrester 1975, Kampmann 1996, Liehr et al. 2001). The dynamic simulation methods using SD are commercial software packages such as Vensim (2011), Powersim (2011), and ITHINK (2011), which are used for quantifications. For this study, Vensim was used for the simulations.

## 4.3 Calculation

The object of the study is to determine the possibility of success of an event that is initiated by the accident of interest. The characteristics of SD show the relative value of the possibility of the event. Figure 4.8 shows the fundamental algorithm of problem solving using SD. There is the parallel configuration between the real world and the systems thinking world, which shows the characteristics of the construction in the modeling. *Systems thinking* is any problem-solving process that views "problems" as parts of an overall system, rather than reacting to outcomes or events and potentially contributing to further development of the undesired issue or problem. Therefore, SD is the dynamic algorithm of systems thinking. In SD, the simulation is quantified in the time step, which is the time cycle of the quantification. The dynamic simulation is performed by presetting the time interval. As seen in Figure 4.6, the lunar surface temperature changes very frequently due to the solar altitude, which is written as the radiator sink temperature. Therefore, it is necessary to analyze the event scenario by the cyclic variation method, which is like SD.

Figure 4.9 shows the main algorithm of the scenario, which is modified from Figure 4.5. Conventional tree-type analysis requires that the event tree and fault tree be separate. In SD, the event flow, however, can be expressed with the event tree and fault tree simultaneously. There are three figures for the subscenarios of Figure 4.9. The Figure 4.10 shows the scenario for an ACLF. Figure 4.11 is the scenario for criticality stabilization. Figure 4.12 gives the scenario for geological stabilization. Each figure shows the combination

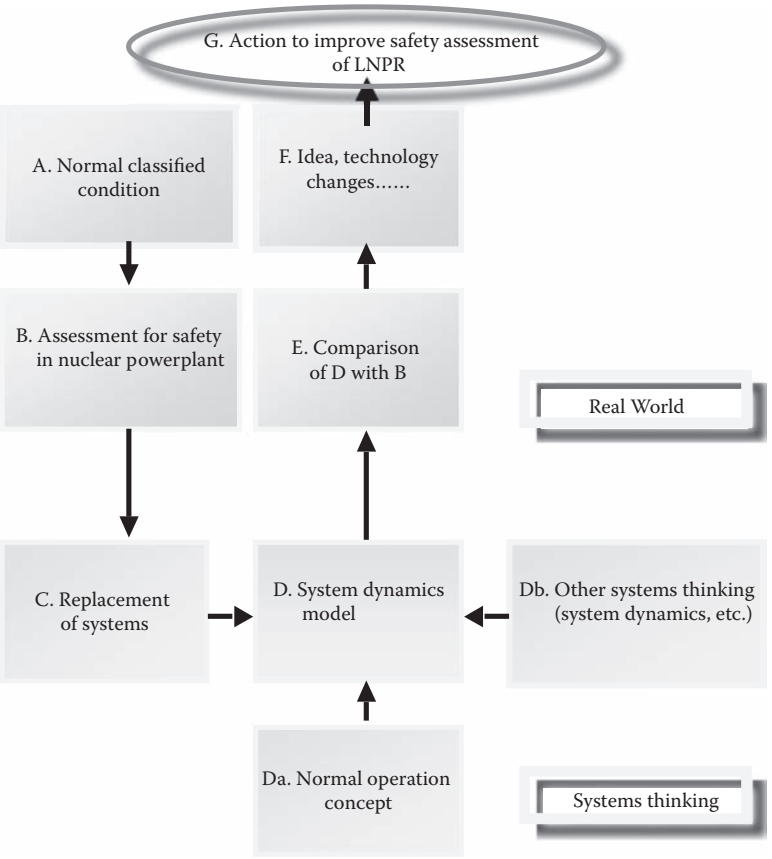


**FIGURE 4.8**
Real world versus systems thinking world.

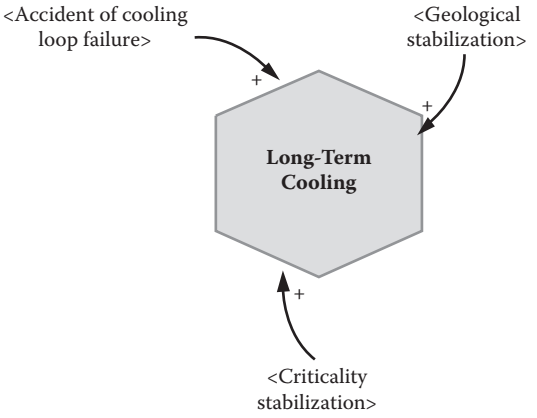


**FIGURE 4.9**
System dynamics (SD) algorithm for long-term cooling.

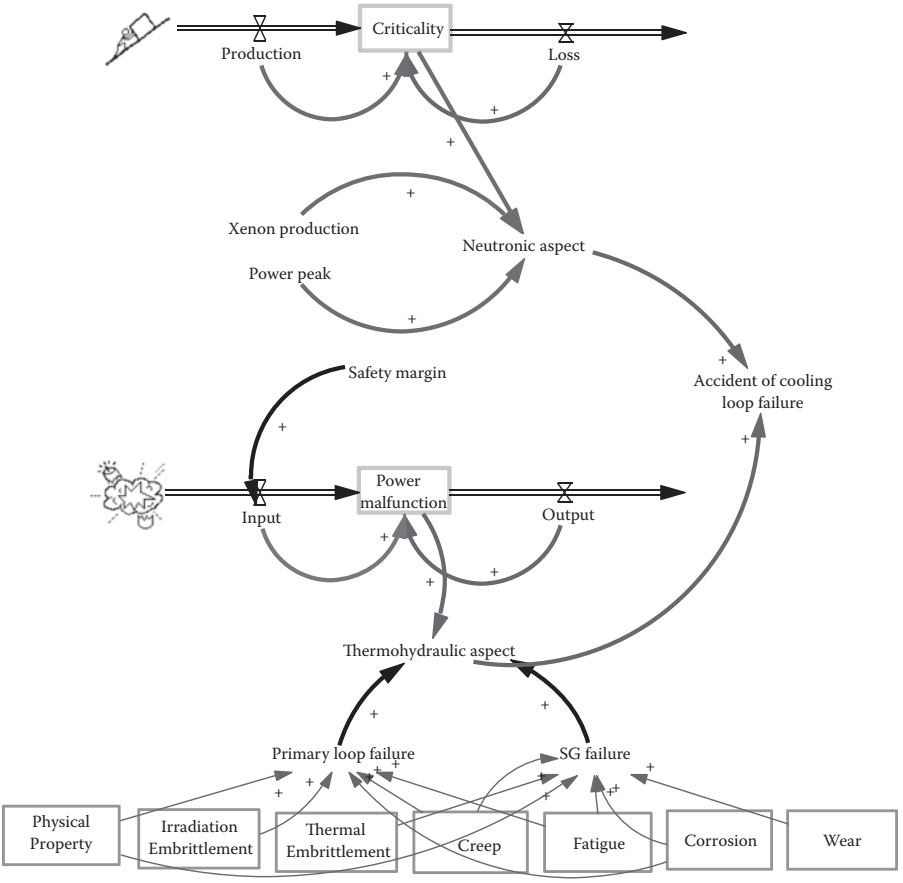


**FIGURE 4.10**
Accidental cooling loop failure.

of the event flows by the feedback and time delay, which are combined with the time step. The geological stabilizations are especially stressed by the low-gravity, nonatmosphere environment. The detailed explanations are shown in the captions of each figure. The chance value is given in Table 4.2 where the values of the basic elements are given. For example, the physical property has accumulation values with the initial value of 1. The time step leads to the accumulated value. The time step and accumulation value are the same as 0.25; that is, the 0.25 is accumulated in every time step for the case of physical property. In irradiation embrittlement, the value is the summation of 1.1 in every time step with the initial value of 0. In xenon production, when the random number is lower than 0.5, the chance value is 0. If it is higher than 0.5, the value is 1.

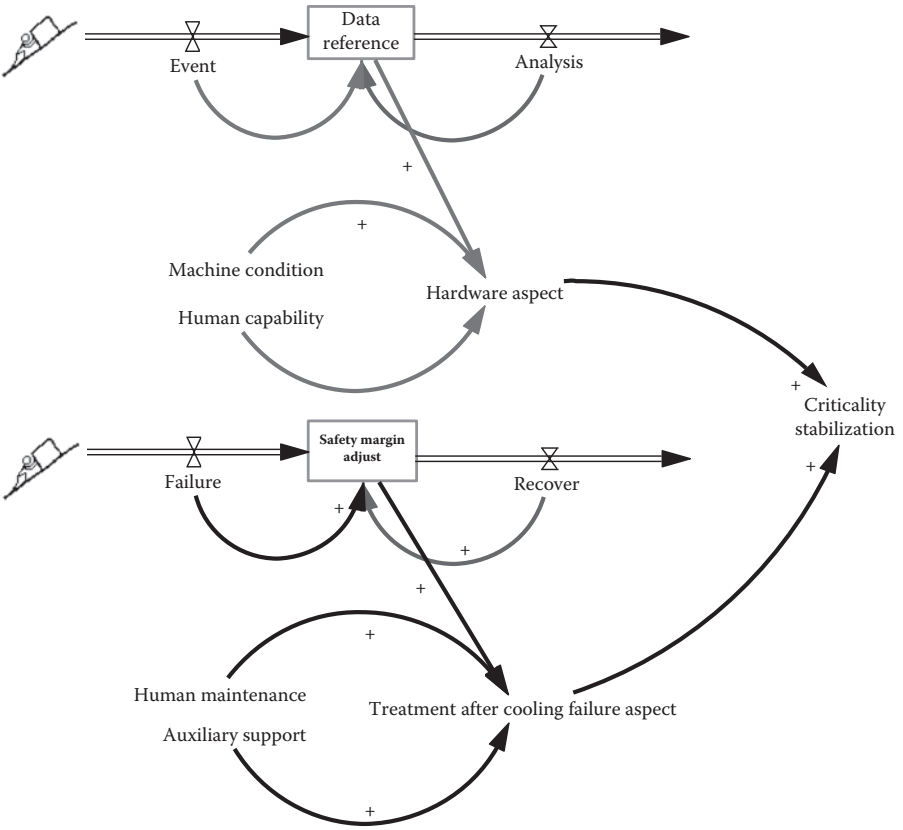


**FIGURE 4.11**
Criticality stabilization.

## 4.4 Results

The result of the dynamic simulation is obtained as the relative value. The reactor is assumed to start in 2020 as part of a possible plan to construct a lunar base. The primary system of the LNPR is a pressurized water reactor (PWR) with the current commercial power utility technology. There is another option where the reactor primary loop is a gas-cooled reactor, but this is not commercialized yet and is one of the generation 4 reactor concepts. This reactor is assumed to produce 40 kilowatts of electric power.

In the simulation, the time period is 30 years, from 2020 to 2050. The time step is 0.25 month, which is one week; that is, the simulation cycle is 0.25 month. The quantification is repeated every week. In Figure 4.13, the possible performance of the long-term cooling increases to 28.4763 in 2049. This is

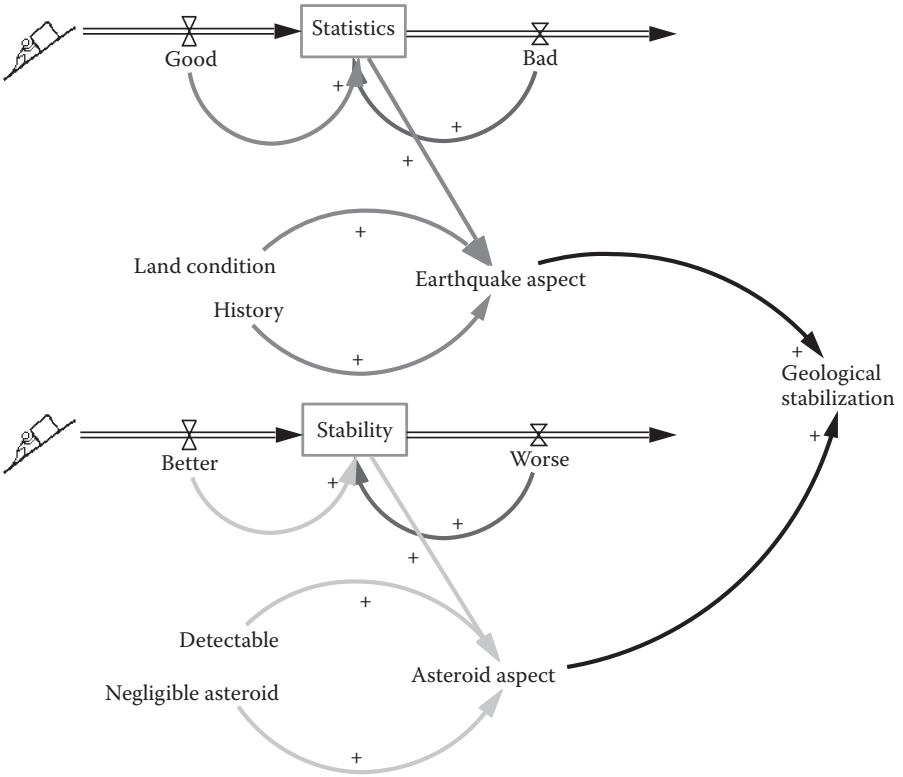


**FIGURE 4.12**
Geological stabilization.

12.54 times higher than the value of 2.27 in 2023. The simulations concerning an ACLF, criticality stabilization, and geological stabilization using the time step of 0.25 month are shown in Figures 4.14–4.16. The higher values are in the middle part of the criticality stabilization. Although the time step is changed in Figure 4.17, the trend is similar to the case of the 0.25 time step. The values increase slightly. In the case of the time step of 0.01562 month, the highest value is as 31.3025 in 2049.

## 4.5 Conclusions

A dynamic simulation is performed for an ACLF in the LNPR. The safety assessment is newly modified using nonlinear SD. The time step is utilized for the examination of the frequent variation cycles. Tree-type quantification is substituted by the nonlinear event flow–oriented method. The dynamical

**TABLE 4.2**

Values of Basic Elements

| Classification | | Chance Value |
|---|---|---|
| Accidental cooling loop failure | Physical property | 1, 1 |
| | Irradiation embrittlement | 0, 1.1 |
| | Thermal embrittlement | 1, 2 |
| | Creep | 3, 1 |
| | Fatigue | 1, 3 |
| | Corrosion | 2, 1 |
| | Wear | 1, 2 |
| | Xenon production | Random < 0.5 [0, 1] |
| | Power peak | Random < 0.5 [0, 1] |
| | Production | Random < 0.3 [0, 1] |
| | Loss | Random < 0.5 [0, 1] |
| | Safety margin | 0.7 |
| | Input | Random < Safety margin [0, 1] |
| | Output | Random < 0.5 [0, 1] |
| Criticality stabilization | Machine condition | Random < 0.5 [0, 1] |
| | Human capability | Random < 0.5 [0, 1] |
| | Event | Random < 0.3 [0, 1] |
| | Analysis | Random < 0.5 [0, 1] |
| | Human maintenance | Random < 0.5 [0, 1] |
| | Auxiliary support | Random < 0.5 [0, 1] |
| | Failure | Random < 0.3 [0, 1] |
| | Recover | Random < 0.5 [0, 1] |
| Geological stabilization | Land condition | Random < 0.5 [0, 1] |
| | History | Random < 0.5 [0, 1] |
| | Good | Random < 0.3 [0, 1] |
| | Bad | Random < 0.5 [0, 1] |
| | Detectable | Random < 0.5 [0, 1] |
| | Negligible asteroid | Random < 0.5 [0, 1] |
| | Better | Random < 0.3 [0, 1] |
| | Worse | Random < 0.5 [0, 1] |

flow of the event is connected by the loop. The situation is changed by the loop connections between the events. The complex Markov chain algorithm could be modified in considering the past event result. This is effected just by the loop. The past event could be related to future events as well as present events. The time flow of the Moon could be different from that of the Earth because the temperature variation and the low gravity require different procedures for maintenance in case of a possible accident. In other words, the time step can change the event scenario. For example, a one-hour task could be changed to a two-hour task by modifying the time step. So, the time step in the accident analysis is very useful in a difficult situation like an operation

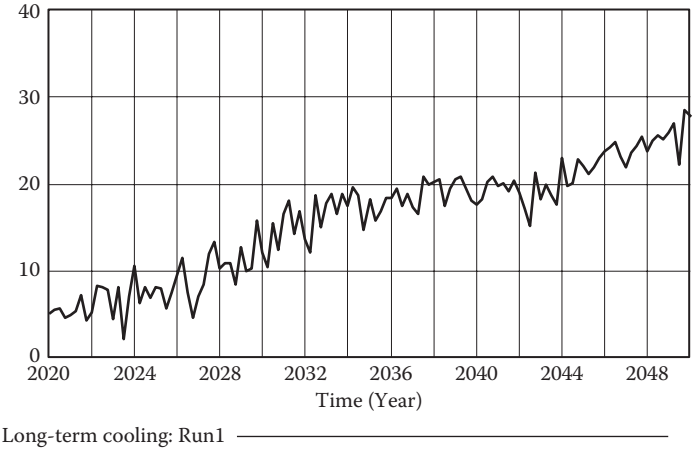


**FIGURE 4.13**
Simulation of long-term cooling ($t$ = 0.25 month).

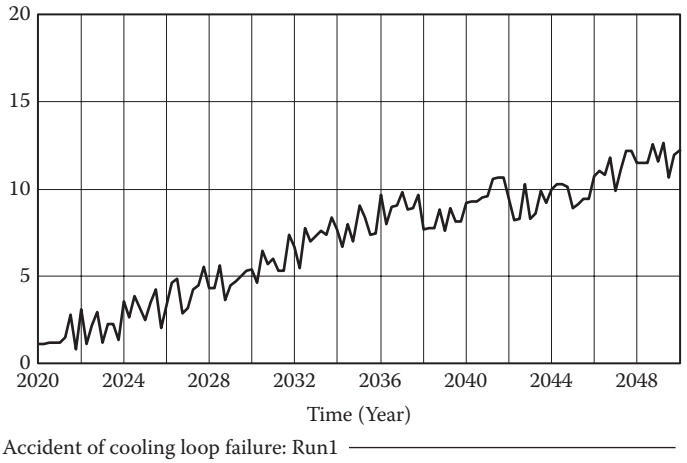


**FIGURE 4.14**
Simulation of an accidental cooling loop failure ($t$ = 0.25 month).

on the lunar surface. These versatile scenarios can be constructed using this loop. There are some particular meanings of the study as follows:

- The nonlinear expression of the ACLF in the LNPR is performed using SD.
- Time steps are used to express the frequent variation of the lunar surface temperature, which is a very harsh environmental condition.

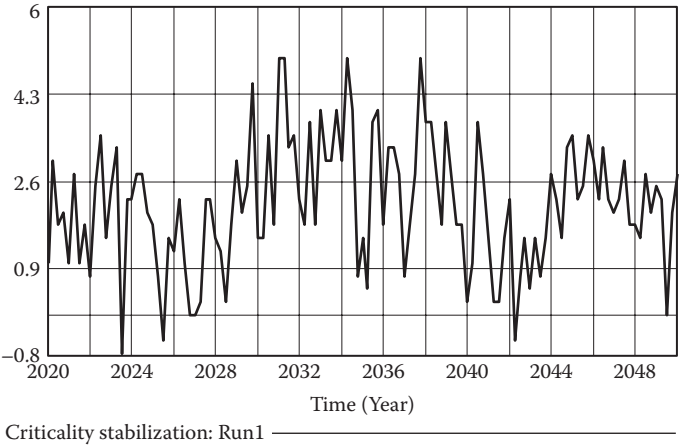


**FIGURE 4.15**
Simulation of criticality stabilization ($t$ = 0.25 month).

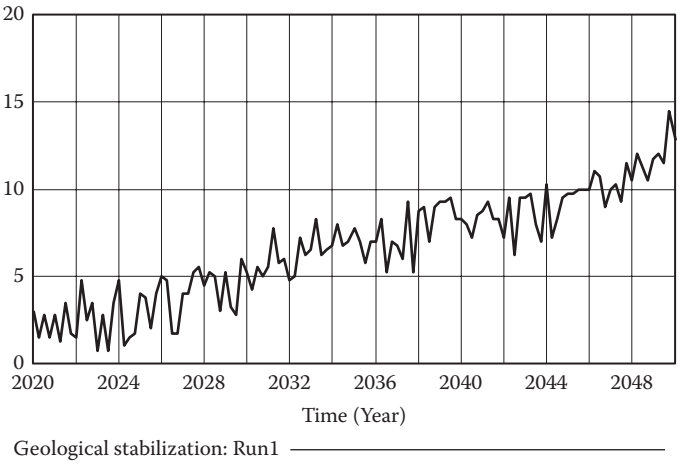


**FIGURE 4.16**
Simulation of geological stabilization ($t$ = 0.25 month).

- The possibility of success increases as the time period increases.
- This reactor can be applied to other planets like Mars.
- The analysis of the events involves an imaginary situation in the lunar colony.
- Other physical behavior of the solid-state material could create other safety factors in the system.

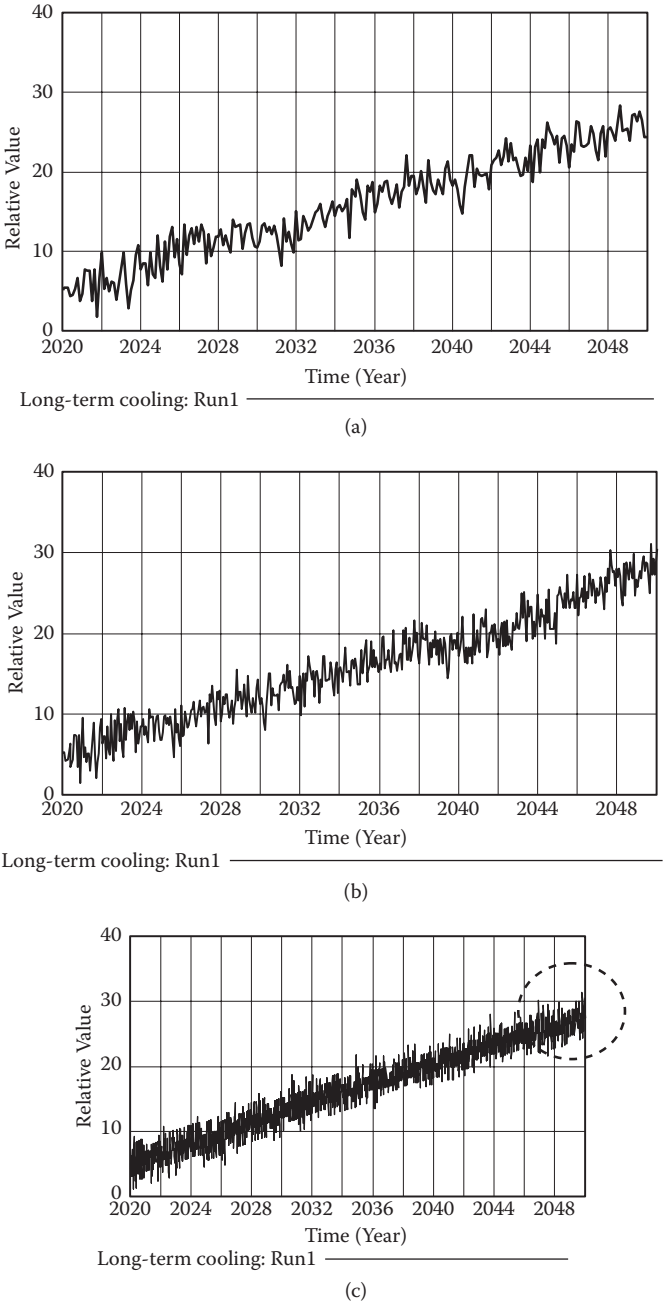


**FIGURE 4.17**
Simulation of long-term cooling, (a) $t$ = 0.125 month, (b) $t$ = 0.0625 month, (c) $t$ = 0.01562 month.

The characteristics of SD using feedback and accumulation can successfully express the uncertainty in space, which is extremely different from Earth conditions, because of very low gravity and nonatmospheric situations. That is, feedback and accumulation of information allow much more reliable decision making, especially in space where information on events is very limited. Real-time simulation is possible with the time step, and cannot be done by conventional methods.

For future work, it is necessary to analyze the reactor core and the turbine in space. Although there is no completed master LNPR plant, this study can address the safety considerations of possible future NPP on the Moon. In addition, other facilities such as buildings on the Moon could be modeled using SD management. A lunar city can be assessed for safety in several facilities like the project in Boston that was performed a half-century ago (Forrester 1969). Fundamentally, the form of the power plant is similar to those on Earth. The general air filtering plants are examples of assessments for a new city on the Moon.

## References

Belhadj, M., and T. Aldemir. 1996. Some computational improvements in process system reliability and safety analysis using dynamic methodologies. *Rel. Eng. Sys. Saf.* 52:339–347.

Bodkin, D., P. Escalera, and K. J. Bocam. 2006. A human lunar surface base and infrastructure solution, AIAA 206-7336. Paper presented at Space 2006, September 19, San Jose, CA.

Coulter, Dauna. 2010. Nuclear power on the Moon. Cosmos, http://www.cosmosmagazine.com/features/online/2760/nuclear-power-moon.

Everline, C-J., and T. Paulos. 2006. Comparison of techniques for modeling accident progression in dynamic aerospace applications with and without repair. *Rel. Eng. Sys. Saf.* 91:370–377.

Ewert, M. 1993. Investigation of lunar base thermal control system options. Paper presented at the 23rd International Conference on Environmental Systems, Colorado Springs, CO, Paper 932112.

Fatemi, N. S., H. E. Polland, H. Q. Hou, and P. R. Sharps. 1999. Solar array trades between very high-efficiency multi-junction and Si space solar cells. Paper presented at the IEEE Photovoltaic Specialist Conference, Anchorage, AK, September 15–20.

Forrester, J. W. 1961. *Industrial dynamics*. Cambridge, MA: Productivity Press.

Forrester, J. W. 1968. *Principles of systems*, 2nd ed. Waltham, MA: Pegasus Communications.

Forrester, J. W. 1969. *Urban dynamics*. Waltham, MA: Pegasus Communications.

Forrester, J. W. 1971. *World dynamics*. Cambridge, MA: Wright-Allen Press.

Forrester, J. W. 1975. *Collected papers of Jay W. Forrester.* Waltham, MA: Pegasus Communications.

Fragola, J. R., and R. H. McFadden. 1995. External maintenance rate prediction and design concepts for high reliability and availability on space station Freedom. *Rel. Eng. Sys. Saf.* 49:255–273.

ITHINK Software. 2011. ISEE Systems, Inc.

Kampmann, C. E. 1996. Feedback loop gains and system behavior. In *Proceedings of the 1996 International System Dynamics Conference Boston*, 260–263. Albany, NY: System Dynamics Society.

Liehr, M., A. Grobler, M. Klein, and P. M. Milling. 2001. Cycles in the sky: Understanding and managing business cycles in the airline market, *System Dynamics Review* 17(4):311–332.

Vensim. 2011. Ventana System, Inc.

NASA (National Aeronautics and Space Administration). 2009. NASA developing fission surface power technology. News and Event Features. http://www.nasa.gov/hom/hqnews/2008/sep/HQ_08-227_Moon_Power.html

NASA (National Aeronautics and Space Administration). 2010. Glenn Research Center, http://www.nasa.gov/centers/glen n/images/content/2726 77main_FSP_HR.jpg

Park, C., and E. Sunada. 2008. Vapor compression hybrid two-phase loop technology to lunar surface applications. Paper presented at Space Technology and Application International Forum-STAIF 2008, Albuquerque, NM.

PowerSim. 2011. Powersim Software.

Prado, M. 2009. Introduction to PERMANENT, http://www.permanent.com/intro.htm

Radzicki, M., and R. Taylor. 1997. U.S. Department of Energy's introduction to system dynamics: A systems approach to understanding complex policy issues 1. http://www.systemdynamics.org/DL-IntroSysDyn/inside.htm

Schmitt, H. 2003. Private enterprise approach to lunar base activation. *Adv. Space Res* 31:2441–2447.

Siu, N. 1994. Risk assessment for dynamic systems: An overview. *Rel. Eng. Sys. Saf.* 43:43–73.

Swaminathan, S., J. Y. Van Halle, C. Smidts, et al. 1997. The Cassini Mission probabilistic risk analysis: Comparison of two probabilistic dynamic methodologies. *Rel. Eng. Sys. Saf.* 58:1–14.

# 5

# *Analysis for Characteristics of Nuclear Spacecraft in a Nanogravity Environment for Deep Space Exploration*[*]

**Taeho Woo and Soonho Lee**

**CONTENTS**



## 5.1 Introduction

Nuclear energy for space craft is studied for deep space travel. Solar energy produces limitations with respect to power production as one moves farther from the Sun so it is necessary to make as much powerful energy as a spacecraft can produce without external energy sources. Safety procedures are important for nuclear spacecraft missions, which is a critical issue in commercial nuclear power plants (NPPs) (IAEA [International Atomic Energy Agency] 2010). There are two kinds of energy sources in deep space beyond the orbit of Mars. The safety analysis for the Cassini mission is seen in Figure 5.1. Similar analyses were used in Galileo and Ulysses missions (NASA [National Aeronautics and Space Administration] 1997). There are several missions to Jupiter shown in Table 5.1.

The radioisotope thermoelectric generator (RTG) is a kind of nuclear electrical generator that obtains its power from radioactive decay. The heat released by the decay of a suitable radioactive material is converted into electricity by the Seebeck effect using an array of thermocouples, which

[*] With permission of the American Society of Civil Engineers.

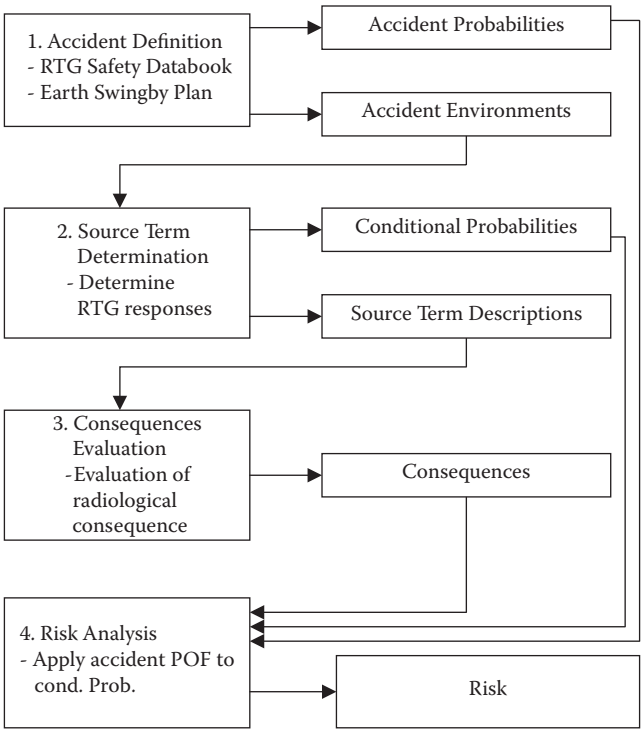


**FIGURE 5.1**
Nuclear launch safety risk analysis process.

**TABLE 5.1**

Missions to Jupiter

| Spacecraft | Power | Launch Date |
|---|---|---|
| Pioneer 10 | 165.0 W (4 SNAP, 19 RTGs) | 1972-03-02 |
| Pioneer 11 | 165.0 W (4 SNAP, 19 RTGs) | 1972-04-06 |
| Voyager 1 | 420.0 W (3 RTGs) | 1977-09-05 |
| Voyager 2 | 420.0 W (3 RTGs) | 1977-08-02 |
| Ulysses | 285.0 W (3 RTGs) | 1990-10-06 |
| Cassini | 640.0 W (3 RTGs) | 1997-10-15 |
| New Horizons | 220.0 W (RTG) | 2006-01-19 |

*Note:* SNAP = Systems Nuclear Auxiliary Power Program; RTG = radioisotope thermoelectric generator.

converts temperature differences directly into electricity (Angelo 1985). The first RTG launched by the United States was the Systems Nuclear Auxiliary Power Program (SNAP) 3 in 1961 aboard the Navy Transit 4A spacecraft. The normal application of RTGs on spacecraft is as a power source. RTGs were used in Pioneer 10, Pioneer 11, Voyager 1, Voyager 2, Galileo, Ulysses,

Cassini, and New Horizons missions. In addition, RTGs were used to power the two Viking landers and for the scientific experiments left on the Moon by the crews of Apollo 12 through 17. RTGs were also used for the Nimbus, Transit, and LES satellites.

A photovoltaic battery is a solid-state device that converts the energy of sunlight directly into electricity by the photovoltaic effect (Tsokos 2008). Assemblies of cells are used to make solar modules and solar panels that produce solar energy. The photovoltaic effect was first recognized in 1839 by French physicist A. E. Becquerel. It was not until 1883, however, that the first photovoltaic cell was built by C. Fritts, who coated the semiconductor selenium with an extremely thin layer of gold to form junctions. The device was only 1% efficient. In 1888, Russian physicist Aleksandr Stoletov built the first photoelectric cell. Russell Ohl patented the modern junction semiconductor solar cell in 1946, which was discovered as he worked on the series of advances that would lead to the transistor.

Spacecraft can be powered by energy stored in a battery or fuel cell and released as the craft travels, or it can be generated as the journey progresses (Patel 2004). There are several ways to store and make energy. The batteries store energy made on Earth and release it as electricity. Additionally, the solar panels convert light from the Sun into electricity. RTGs utilize radioactive materials, encased in a sealed shell to generate heat as they decay into nonradioactive materials. Finally, fuel cells are somewhat like batteries, storing power in the form of separated oxygen and hydrogen. A thin membrane between the two elements harnesses the energy released when the oxygen and hydrogen combine to form water.

System dynamics (SD) is used to quantify the dynamic scenario for a nonlinear algorithm that can be applied in the nuclear industry. Dr. Jay Forrester at Massachusetts Institute of Technology (MIT) created SD to evaluate the nonlinear characteristics of social and economical systems. SD can test the dynamic scenarios of complex systems. SD has been used to quantify organizations over time (Forrester 1961, 1968, 1969, 1971). In addition, there are some papers related to decision making using SD (Eberlein 1989; Forrester 1975; Kampmann 1996; Liehr et al. 2001; Mojtahedzadeh 1997; Schmidt and Gary 2002).

A study by Nathan et al. (cited in Minami and Madnick 2009) discussed the results of several simulations; these suggested that high-level decisions that balance mission rate and operations tempo with troop availability, careful management of the work–rest cycle for deployed troops, and improvement of the processes for evaluating the lessons learned from accidents would lead to a reduction in combat vehicle accidents. In addition, a model, extracted from a larger study, is used to evaluate the effect of road conditions on accident development (Sheldon 2006).

Section 5.2 explains the economic aspect of the study. The calculation for the safety aspect is shown in Section 5.3. Section 5.4 describes results of the study, and some conclusions are discussed in Section 5.5.

## 5.2 Economic Aspect

The specific power conversion efficiency is obtained by the following equations. The photovoltaic-battery system and the RTG system are compared. The power required for the spacecraft is 5 kWe. The spacecraft orbit around the planet is at an altitude that produces a 50/50 light–shadow cycle. The maximum depth of discharge to the secondary battery is 30%.

$$I_R = \frac{R_e^2}{R^2} I_e$$

where

$I_R$ is the solar insolation at R.
$I_e$ is the solar insolation on Earth, 1353 watt/m$^2$.
$R_e$ is the distance from the Sun to the Earth, 1 AU.
$R$ is the distance to the spacecraft.

Insolation is a measure of solar radiation energy incident on a surface. It is the amount of solar energy received on a given area, and may be expressed in W/m$^2$ or over time measured in kilowatt hours per square meter (kW·h/m$^2$). The cell conversion efficiency for the solar concentrator is

$$\eta = \frac{250 \text{ watt/kg}}{1353 \text{ watt}/m^2} \times 0.853 \text{ kg}/m^2 = 0.16$$

The specific power for a location is

$$P_o = \frac{0.16 \times I_R}{0.853 \text{ kg}/m^2}$$

The solar power is (Angelo 1985, Wertz 1999):

$$P_{SA} = \frac{\frac{P_e T_e}{X_e} + \frac{P_d T_d}{X_d}}{T_d}$$

$$= \frac{\frac{(5 \text{ kW}_e)(20 \text{ min})}{0.65} + \frac{(5 \text{ kW}_e)(20 \text{ min})}{0.85}}{20 \text{ min}}$$

$$= 14.932 \text{ kW}_e$$

where

$P_{SA}$ is the solar panel power during daylight period.
$P_e$ is the power requirement during eclipse, 5 $kW_e$.
$P_d$ is the power requirement during daylight, 5 $kW_e$.
$T_e$ is the period of eclipse, 20 min.
$T_d$ is the period of daylight, 20 min.
$X_e$ is the power transfer efficiency during eclipse, 0.65.
$X_d$ is the power transfer efficiency during daylight, 0.85.

So, the solar cell mass is

$$\frac{P_{SA}}{P_o} = \frac{14.932\ \text{kW}_e}{\dfrac{0.16 \times I_R}{0.853\ \text{kg}/m^2}} = \frac{14.932\,\text{kW}_e \times 0.853\ \text{kg}/m^2}{0.16 \times \dfrac{R_e^2}{R^2} \times I_e}$$

$$= \frac{14.932\ \text{kW}_e \times 0.853\ \text{kg}/m^2}{0.16 \times \dfrac{(1AU)^2}{R^2} \times (1353\ \text{w}/m^2)}$$

$$= 58.837\ \text{kg}\ R^2$$

The battery mass is

$$\frac{1\ \text{kg}}{(150\text{W} - \text{hr}) \times 33\%} \times 0.5\ \text{hr} \times 5\ \text{kW}_e = 50.51\ \text{kg}$$

The total mass is

$$58.837\ \text{kg}\ R^2 + 50.51\ \text{kg}$$

This is shown in Figure 5.2. The specific mass of the general purpose heat source (GPHS) is as follows, where it is assumed that the electricity is 250 watts and the mass is 54.0 kg. Each GPHS RTG has a mass of about 57 kg and generates about 300 watts of electrical power at the start of a mission (from about 4,400 watts of thermal energy) from about 7.8 kg of plutonium-238 ($^{238}$Pu)-based fuel (Bennett 2006):

$$m_{GPHS} = \frac{P_{GPHS}}{S_{RTG}} = \frac{5\ \text{kW}_e}{250\ \text{watt}/54.0\ \text{kg}}$$

$$= 1080.0\ \text{kg}$$

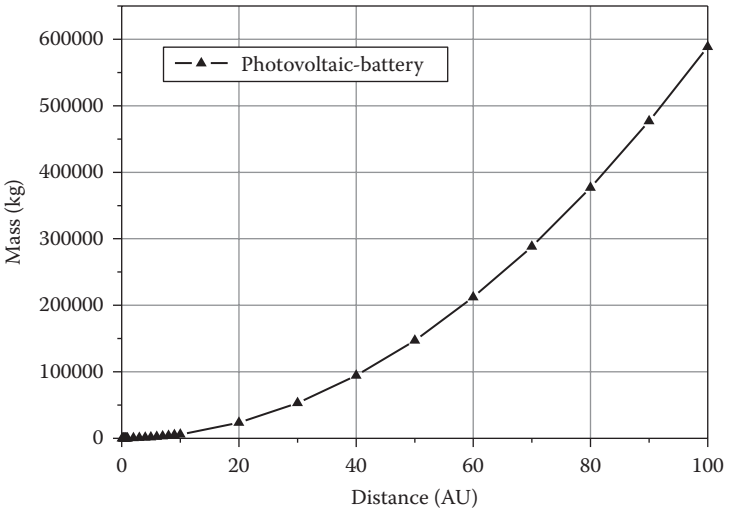


**FIGURE 5.2**
Photovoltaic battery mass versus orbital position.

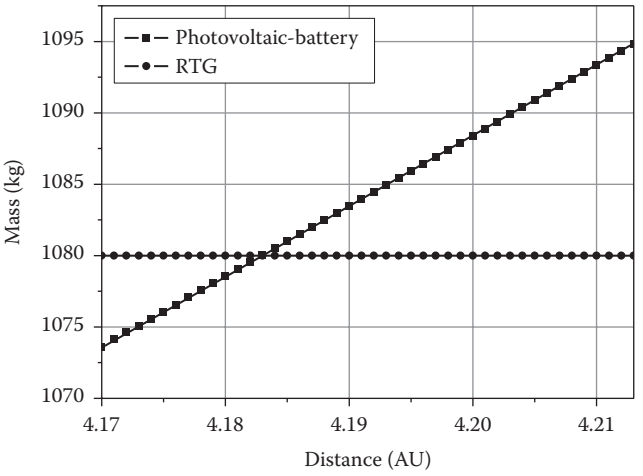


**FIGURE 5.3**
Photovoltaic battery and RTG masses versus orbital position.

This is shown is Figure 5.3. The breakeven orbital location for the two systems is 4.183 AU. This is different from the previous study result of 3 AU (Tsokos 2008).

## 5.3 Safety Aspect

In space travel, the SD method is used for simulations due to its capabilities of analytic estimation and quantification. The matter incorporated with the technological implication has been investigated by SD for a variety of factors. In addition, the tools show the dynamic decision-making abilities in complex matters. The Vensim package used for the simulation was developed in Ventana Systems, Inc.

SD is described as a powerful computer simulation modeling technique for understanding, framing, and discussing complex issues and problems (Radzicki and Taylor 1997). SD can help managers improve their understanding of industrial processes, and is currently used in many kinds of policy analysis and design. SD shows the basic building blocks that can construct models of how and why complex real-world systems behave the way they do during a specified time period. The object is to leverage this added understanding to design and implement more effective policies. The most important aspect of SD modeling involves the dynamic behavior of systems, where the operator tries to identify the patterns of behavior exhibited by certain system variables, and then builds a model with the characteristics of those patterns. The model can be used as a laboratory for testing policies aimed at altering a system's behavior in desired ways. The SD model uses single and double arrow lines to indicate event and time flows. Understanding the dynamic behavior of a system using SD involves its key physical and information flows, stocks, and feedback structures. Some characteristics of SD are as follows:

Single arrow line: Indicates the flow of the event and shows the sequence of the scenarios as well as their dynamic behavior. The direction of line gives the event flow and event feedback.

Double arrow line: There is the principle of accumulation which is to be raised by dynamic behavior in the SD modeling. This means that all kinds of dynamic behaviors can be happening when flows accumulate in stocks. This is seen in Figure 5.4 as EXAMPLE for accumulation and INPUT/OUTPUT for flows. This is like a bathtub where the flow can be thought of a faucet and pipe assembly that fills or drains the stock. It should be considered as the simplest dynamic system in the stock-flow structure. In SD, both informational

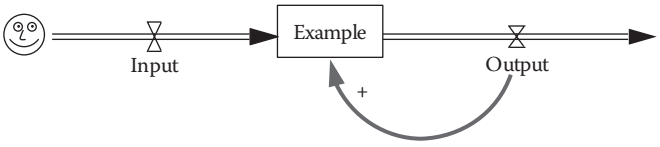


**FIGURE 5.4**
Stock flow and feedback.

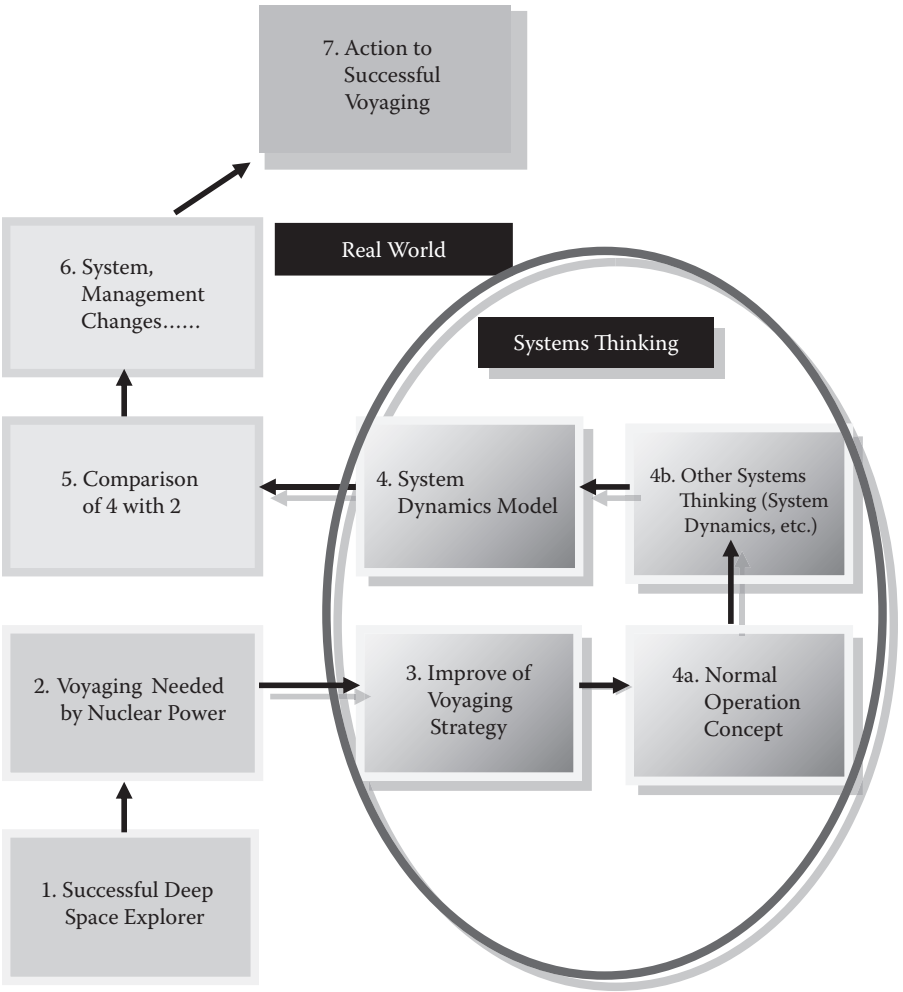


**FIGURE 5.5**
Real world versus systems-thinking world.

and noninformational objects can move through flows and accumulate in stocks. The feedback loops are often joined together by nonlinear couplings where any object can cause counterintuitive behavior. This is seen as the loop in Figure 5.4. A plus sign signifies an addition to the EXAMPLE feedback value, OUTPUT. With a minus sign, the feedback value, OUTPUT, is subtracted from the EXAMPLE value.

The model in Figure 5.5 reflects the real-world situation in the systems-thinking world framework. Systems thinking is a problem-solving process that views problems as parts of an overall system that can potentially contribute to further development of an undesired issue or problem. The

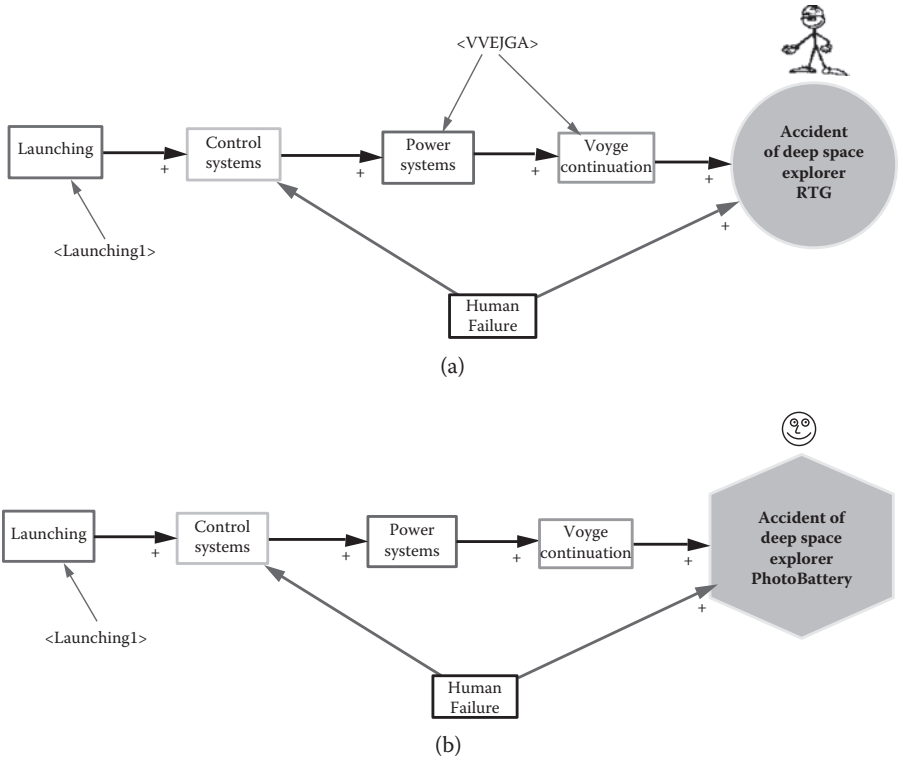


**FIGURE 5.6**
Deep space explorer accident. (a) RTG system and (b) photovoltaic battery system.

configuration of the deep space explorer accident is shown in Figure 5.6. The main object is to find the failure frequency of an expected accident during space travel. The failure probabilities during launch for an RTG system and a photovoltaic battery system are shown in Table 5.2. The data in Table 5.3 are from HNUS 1997 (HNUS [Halliburton NUS] 1997, Section 4.1) and LMM&S 1997 (LMM&S [Lockheed Martin Missiles & Space] 1997) and provide more information on the accident case descriptions. Only accidents that threaten the RTGs or radioisotope heater units (RHUs) with a potential for release of $PuO_2$ are included. Prelaunch value is slightly changed from $6.7 \times 10^{-5}$ to $6.5 \times 10^{-5}$ due to operator's judgment. Venus–Venus–Earth–Jupiter Gravity Assist (VVEJGA) is involved in spacecraft operations, where the gravity is of a nanoscale environment. Harland (2002) explains the process as one in which an insignificant mass approaches a significant mass "from behind" and "steals" some of its orbital momentum. The significant mass of a planet loses a very small proportion of its orbital momentum to the insignificant mass—the space probe, in this case. However, due to the space probe's small mass, this momentum transfer gives it a relatively large momentum increase

**TABLE 5.2**

Launch Accidents

| Segment | Probability |
|---|---|
| Prelaunch | $6.5 \times 10^{-5}$ |
| Early launch | $6.2 \times 10^{-3}$ |
| Late launch | $2.1 \times 10^{-2}$ |
| VVEJGA | $8.0 \times 10^{-7}$ |

*Note:* VVEJGA = Venus–Venus–Earth–Jupiter Gravity Assist trajectory.

**TABLE 5.3**

Failure Frequency (Number per Year)

| Case | Frequency (0th yr) | Frequency (50th yr) |
|---|---|---|
| RTG | $1.822 \times 10^{-6}$ | $2.868 \times 10^{-6}$ |
| Photovoltaic battery | $2.003 \times 10^{-5}$ | $1.160 \times 10^{-4}$ |

in proportion to its initial momentum, speeding its travel through outer space. Thus, this factor significantly affects the RTG system speed compared to the photovoltaic battery system, because of the radioactive hazard or damage to the planets, including the Earth. This is shown in the event flows in Figure 5.6(a). The time period is 50 years of total dynamic simulations.

## 5.4 Results

The problem is to explain several economic and safety aspects. The reason why these characteristics are examined is that these two factors are not proportionally important in nuclear power generation. There are several assumptions that are described in the solar power equation (Angelo 1985; Wertz 1999). The procedures are performed by the aspects of economic and safety. The results are obtained as break-even orbital locations for the two systems.

With respect to the economic aspect, the simplified assumption is that the same power exists (5 kWe) during eclipse and daytime. With respect to the safety aspect, the calculation methods are explained using SD. For example, in Figure 5.6(a), from launch, the line shows the sequence of the scenarios as well as the dynamic behavior. Figure 5.7 shows the events of Launch 1 (see Figure 5.6). The values are obtained using the four rules of arithmetic addition, subtraction, multiplication, and division with the operator's judgments as the event sequence progresses and are described by the lines. Each probability of the accident is decided by the several data judgments including

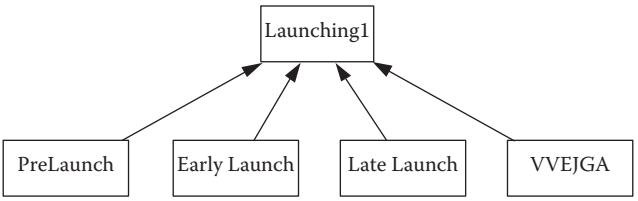


**FIGURE 5.7**
Launching 1 event.

Table 5.3. The results in Figure 5.8 were generated by the calculations for all steps from Figure 5.6 and Table 5.3.

The break-even orbital location for the two systems is 4.183 AU, where the heavier mass of the system is changed to the photovoltaic battery system. Therefore, in the journey beyond the Mars orbit, the RTG system has the priority. This means nuclear power is more economical for deep space travel. As far as safety is concerned, the SD method is used because it is appropriate for a nonlinear scenario such as space travel. There are two kinds of the results in Figure 5.8. Figure 5.8(a) shows the RTG system case and Figure 5.8(b) shows the photovoltaic battery system. The maximum value is seen in year 50, as shown in Table 5.3. The initial difference between the two failure frequencies is just 10%. The last difference is 97.5%, which means that the failure frequency increases as time passes.

## 5.5 Conclusions

The comparisons of two kinds of deep space explorer craft success rates were investigated. The failure frequency of the RTG is less than that of the photovoltaic battery system. The assumptions are that the distance of travel is decided by the following calculations:

- The optimized battery mass and RTG mass for the space travel is obtained.
- The suitable breakeven distance is decided for the proposed spacecraft case.
- The space nuclear power is calculated for the trip out of Mars orbit (about 2.67 AU).

A solar-powered mission to Jupiter planned by NASA is called Juno. Juno's trajectory will use a gravity-assist speed boost from Earth that will be accomplished through an Earth flyby two years after its launch on August 5, 2011 (NASA 2011). The distance is from 4.950 AU in perihelion to 5.458 AU

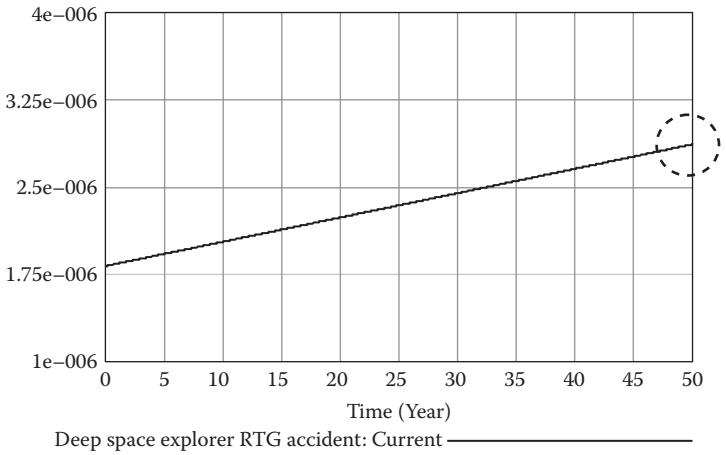


(a)

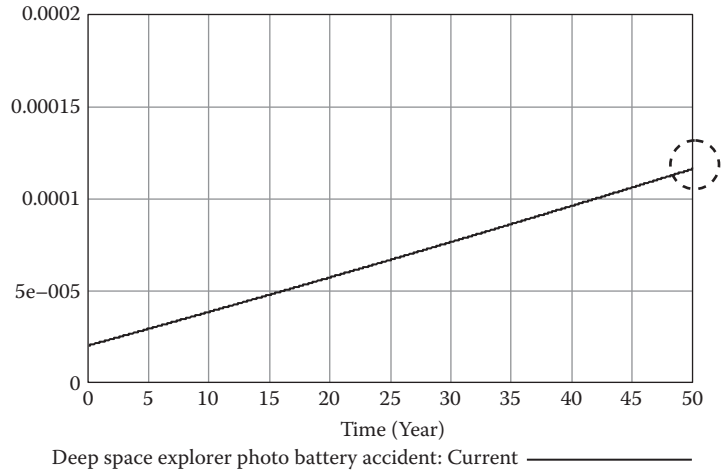


(b)

**FIGURE 5.8**
Deep space explorer accident quantification: (a) RTG system and (b) photovoltaic battery system.

in aphelion, and this can serve as an approximate example of the modeling in this chapter.

The performance of nuclear spacecraft was investigated with respect to safety. The summarized points resulting from this modeling are as follows:

- Dynamic management has been performed in the nuclear spacecraft.
- Nonlinear investigation using SD is effective to analyze the safety of travel.

- The time step algorithm, SD, is applied to the space travel decision-making case.
- Uncertainty could be applied to the dynamics quantification in a low-gravity environment.
- Very tractable quantification is obtained by a computer package.

Further study of nuclear power in space travel is necessary. Human space travel could be used to study the biological aspect, which is not considered in this study. Human aging is also a very important factor. In future study, human biology should be considered.

## Acknowledgment

The author thanks Dr. S. M. Kwak of Systemix, Co. for research discussions.

## References

Angelo, J. 1985. *Space nuclear power*. Malabar, FL: Orbit Books.

Bennett, G. L. 2006. Space nuclear power: Opening the final frontier. Paper presented at the 4th International Energy Conversion Engineering Conference and Exhibit (IECEC), June 26–29, 2006, San Diego, CA, http://www.fas.org/nuke/space/bennett0706.pdf

Eberlein, R. L. 1989. Simplification and understanding of models. *System Dynamics Review* 5(1):51–68.

Forrester, J. W. 1961. *Industrial dynamics*. Cambridge, MA: Productivity Press.

Forrester, J. W. 1968. *Principles of systems*, 2nd ed. Waltham, MA: Pegasus Communications.

Forrester, J. W. 1969. *Urban dynamics*. Waltham, MA: Pegasus Communications.

Forrester, J. W. 1971. *World dynamics*. Cambridge, MA: Wright-Allen Press.

Forrester, J. W. 1975. *Collected papers of Jay W. Forrester.* Waltham, MA: Pegasus Communications.

Halliburton NUS (HNUS). 1997. *Nuclear safety analyses for the Cassini mission environmental impact statement process*. HNUS-97-0010. Halliburton NUS Corporation. Gaithersburg, MD.

Harland, D. M. 2002. *Mission to Saturn: Cassini and the Huygens probe*. London: Springer-Verlag.

IAEA (International Atomic Energy Agency). 2010. *The Power Reactor Information System (PRIS) and its extension to non-electrical applications, decommissioning and delayed projects information*, Technical Reports Series No. 428, http://www-pub.iaea.org/mtcd/publications/pdf/trs428_web.pdf

Kampmann. C. E. 1996. Feedback loop gains and system behavior. In Proceedings of the 1996 International System Dynamics Conference Boston. Cambridge, MA: System Dynamics Society.

Liehr, M., A. Grobler, M. Klein, and P. M. Milling. 2001. Cycles in the sky: Understanding and managing business cycles in the airline market. *System Dynamics Review* 17(4):311–332.

Lockheed Martin Missiles & Space (LMM&S). *GPHS-RTGs in support of the Cassini Mission*, Safety Analysis Report, CRDL C.3, LMM&S, Valley Forge Operations, Philadelphia, PA.

Minami, N. A., and S. Madnick. 2009. Dynamic analysis of combat vehicle accidents. *System Dynamics Review* 25(2):79–100.

Mojtahedzadeh, M. T. 1997. A path taken: Computer-assisted heuristics for understanding dynamic systems. PhD dissertation, Rockefeller College of Public Affairs and Policy, State University of New York at Albany, Albany, NY.

NASA (National Aeronautics and Space Administration). 1997. Cassini Mission, Final Supplemental Environmental Impact Statement. NAS 1.15:111474/SUPPL1, Washington, DC.

NASA (National Aeronautics and Space Administration). 2011. NASA's shuttle and rocket launch schedule. http://www.nasa.gov/missions/highlights/schedule.html

Patel, M. R. 2004. *Spacecraft power systems*. Boca Raton, FL: CRC Press.

Radzicki, M., and R. Taylor, R. 1997. U.S. Department of Energy's Introduction to System Dynamics: A Systems Approach to Understanding Complex Policy Issues, Ver. 1. http://www.systemdynamics.org/DL-IntroSysDyn/inside.htm

Schmidt, M. J., and M. S. Gary. 2002. Combining systems and conjoint analysis for strategic decision making with an automotive high-tech SME. *System Dynamics Review* 18(3):359–379.

Sheldon, F. 2006. Is counter-productive policy creating serious consequences? The case of highway maintenance. *System Dynamics Review* 22(4):371–394.

Tsokos, K. A. 2008. *Physics for the IB diploma*, 5th ed. Cambridge, UK: Cambridge University Press.

Wertz, J. R., and W. J. Larson. 1999. *Space mission analysis and design*, 3rd ed. El Segundo, CA: Microcosm/Kluwer.

# Section II

# Atomic Nanoscale Biotechnology

# 6

# *Light Collection Enhancement Analysis for Digital X-Ray Detector Using $Gd_2O_2S$:Tb and CsI:Tl Phosphors in Nanoscale Treatment*

**Taeho Woo and Taewoo Kim**

**CONTENTS**



## 6.1 Introduction

The clinical mammography examination involves light collection enhancement on the nanoscale. Breast cancer is highly ranked among cancer death rates in American women. It is important to detect cancer cells in the early stages of the disease so that treatment can begin as soon as possible. In the United States (International Agency for Research on Cancer 2008), the five-year survival rate for breast cancer is 85% when the cancer is localized to the breast. In other words, the mortality rate is reduced to 56% when the auxiliary nodes are included. The classical screen/film mammography is considered a reliable diagnostic test but masses and microcalculations can be difficult to image in dense breasts. Therefore, direct digital x-ray image acquisition is necessary.

The active matrix flat-panel imagers (AMFPIs) are being developed for x-ray detection systems. Wronski investigated high-gain avalanche rushing photodetectors (HARP) for avalanche multiplication (Wronski and Rowlands 2008). This study showed that avalanche gains enable x-ray quantum noise limited performance throughout the entire exposure range in radiography and fluoroscopy, respectively. In addition, a charge-coupled device (CCD) is

compared with AMFPI for direct digital radiography (Widmer 2008). Direct digital radiography (DDR) detectors are flat-panel and CCD types. Computed radiography (CR) and DDR provide quality diagnostic images. CR is a mature technology while DDR is an emerging technology.

The detection imagers typically use $Gd_2O_2S$:Tb or CsI:Tl scintillation screens to convert the x-ray into visible photons, which are then collected by an underlying photodetector array for digital radiographic and mammographic applications. The study investigated whether the inclusion of a microlens array between the screen and photodetector may improve light collection when the photodetector has a small optical fill factor. The microlens can treat the nanoscale light collections which could be produced by the micro-thickness screen. The technique for modeling the modulation transfer function (MTF) from measurement obtained for $Gd_2O_2S$:Tb and CsI:Tl scintillation screens has been reported. The measurements were obtained for a number of different mono- and polychromatic x-ray (energy) spectra. The screen MTFs were subsequently transformed into point spread functions (PSFs) and used in a simulation of the proposed imaging system. This imaging system results in a better image with lower radiation exposure to patients.

The purpose of the project is to produce better images in mammography using a microlens array; that is, a good x-ray imager detector as the AMFPI (Antonuk, 1997a, 1997b) photodetector is constructed. In this stage, improved ray-tracing (Shirley 2000, Glassner 1989) and Monte-Carlo simulation are done. The screen, microlens array, and photodetector planes are also considered. Second, the microlens array is designed; the transmittance, focusing, and uniformity are measured; and the predicted and measured light collection efficiencies are compared. Third, the microlens array is matched to AMFPI. Last, the comparisons with and without the microlens are studied for uniform field and phantom images. Figure 6.1 shows the simplified configuration for the microlens.

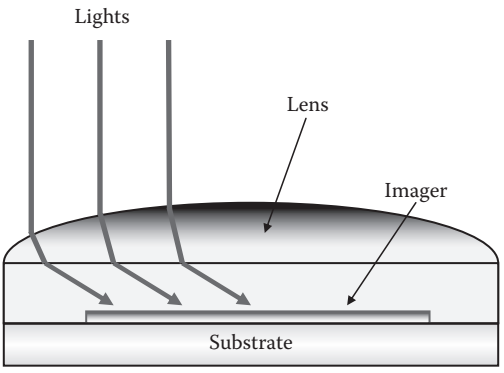


**FIGURE 6.1**
Simplified configuration for microlens.

The simulation of photon detection for the two geometrically defined cases of microlenses attached to photodetectors is investigated in this chapter. The method is examined in Section 6.2, results are provided in Section 6.3, and Section 6.4 includes conclusions.

## 6.2 Method

It is important to enhance the quality of imaging by optical apparatus. The investigation is done to develop an x-ray detector design including microlens arrays that are optimized for the AMFPI photodetector. It is necessary to measure the transmittance, focusing, and uniformity of the microlens arrays (Petrick 2001, 2002). The system configuration for this simulation is in Figure 6.2 where the size of the configuration is in micrometers. Figure 6.3 shows light dispersion by the screens (Hamamatsu 1996). The solid line shows the light dispersion of CsI and the dotted line is the light dispersion of

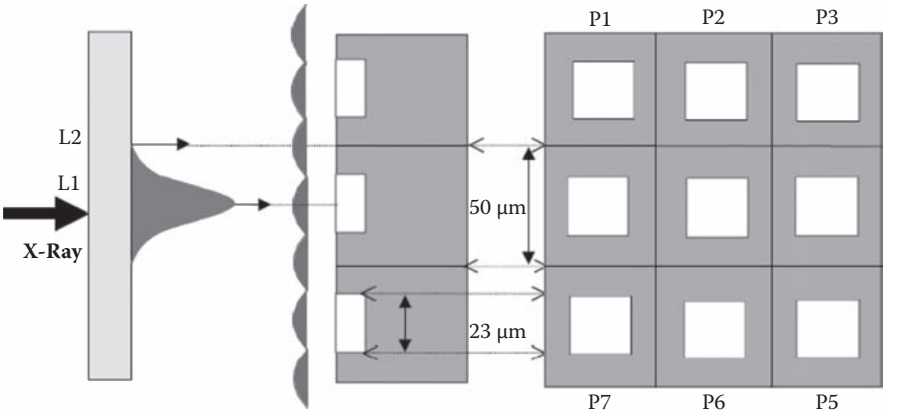


**FIGURE 6.2**
Simplified imager configuration.

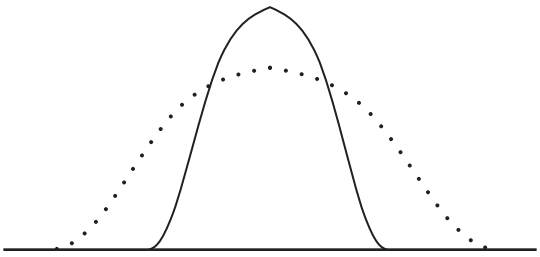

**FIGURE 6.3**
Modeling of light dispersion between CsI (solid line) and $Gd_2O_2S$ (dotted line) phosphors.

**TABLE 6.1**

Phosphor Data List by Exponential Functions

| Energy (kVp) | Thickness (μm; mg/cm²) | FWHM (μm) | MTF (Exponential Function) |
|---|---|---|---|
| *(a) $Gd_2O_2S:Tb$* | | | |
| 25 | 48; 35 | 20.96 | $y$=0.5084 exp(−0.087800χ)+0.5476exp(−0.087755χ) |
| 26 | 46; 34 | 50.54 | $y$=0.5246 exp(−0.196500χ)+0.5331exp(−0.196400χ) |
| 27 | 46; 34 | 42.60 | $y$=0.5954 exp(−0.166400χ)+0.5251exp(−0.166400χ) |
| | 82; 60 | 92.08 | $y$=0.5160 exp(−0.373300χ)+0.4996exp(−0.372800χ) |
| 28 | 40; 29 | 36.81 | $y$=0.5613 exp(−0.153900χ)+0.5337exp(−0.154000χ) |
| 30 | 44; 32 | 27.40 | $y$=0.4926 exp(−0.084820χ)+0.5579exp(−0.084490χ) |
| 90 | 68; 50 | 37.58 | $y$=0.5111 exp(−0.153400χ)+0.5568exp(−0.153700χ) |
| | 68; 50 | 38.31 | $y$=0.5117 exp(−0.157000χ)+0.5212exp(−0.156800χ) |
| | 109; 80 | 51.48 | $y$=0.4813 exp(−0.212198χ)+0.5314exp(−0.212043χ) |
| *(b) CsI:Tl* | | | |
| 20[a] | 150; 68 | 24.98 | $y$=0.0995 exp(−0.652700χ)+0.9001exp(−0.094440χ) |
| 35[a] | 150; 68 | 29.79 | $y$=0.3429 exp(−0.577000χ)+0.6571exp(−0.105000χ) |
| 50[a] | 150; 68 | 30.68 | $y$=0.2790 exp(−0.535900χ)+0.7207exp(−0.096730χ) |
| 30 | 150; 68 | 38.03 | $y$=0.5691 exp(−1.011000χ)+0.4307exp(−0.119900χ) |
| 200 | 147; 47 | 29.64 | $y$=0.4726 exp(−0.121500χ)+0.5069exp(−0.121400χ) |
| | 299; 135 | 41.38 | $y$=0.1424 exp(−65.75000χ)+0.8576exp(−0.143400χ) |

[a] 20, 35, 50 are units of keV.

$Gd_2O_2S$. CsI shows a much narrower shape compared to $Gd_2O_2S$. The *modulation transfer function* (MTF) is obtained by experimental data (Bunch 1997; Cavouras et al. 1998; Jing et al. 1999; Kandarakis et al. 1997a, 1997b; Nagarkar et al. 1996, 1998; Sabol and Boon 1997; Yu et al. 1997). MTFs are formulated using exponential functions, which are shown in Table 6.1. The MTF is changed to a line spread function (LSF) using the inverse Fourier transform (Bracewell 2000) and the LSF is also converted to a PSF using the inverse Abel transform in Figure 6.4. Table 6.2 shows the full width at half maximum (FWHM) of PSF. Using these properties, the light collection efficiency is obtained. In the calculations, the geometries are classified as Lambertian and isotropic methods (Maidment and Yaffe 1995). So, this method simulates how the digital imager configuration collects light. The Lambertian quanta are calculated by

$$E_{Lamb}(\theta,\phi)=\begin{pmatrix} E_o, & 0\le\theta\le\dfrac{\pi}{2} \\ 0, & \text{otherwise} \end{pmatrix} \tag{6.1}$$

| | |
|---|---|
| MTF | $y = a\exp(-bx) + c\exp(-dx)$ |
| ↓ | Inverse Fourier Transform |
| LSF | $y = 2ab/(4\pi^2x^2+b^2) + 2cd/(4\pi^2x^2 + d^2)$ |
| ↓ | Inverse Abel Transform |
| PSF | $f(r^2) = ab/[4\pi^2\{r^2 + \{b/2\pi)^2\}^{3/2}] + cd/[4\pi^2\{r^2+(c/2\pi)^2\}^{3/2}]$ |

**FIGURE 6.4**
Transition for point spread function.

**TABLE 6.2**
FWHM List by PSFs

| Energy (kVp) | Thickness (μm; mg/cm²) | FWHM (μm) |
|---|---|---|
| *(a) $Gd_2O_2S:Tb$* | | |
| 25 | 48; 35 | 21.41 |
| 26 | 46; 34 | 47.93 |
| 27 | 46; 34 | 40.60 |
| | 82; 60 | 91.01 |
| 28 | 40; 29 | 37.56 |
| 30 | 44; 32 | 20.65 |
| 90 | 68; 50 | 37.46 |
| | 68; 50 | 38.28 |
| | 109; 80 | 51.75 |
| *(b) CsI:Tl* | | |
| 20[a] | 150; 68 | 23.09 |
| 35[a] | 150; 68 | 25.99 |
| 50[a] | 150; 68 | 23.85 |
| 30 | 150; 68 | 29.73 |
| 200 | 147; 47 | 29.63 |
| | 299; 135 | 34.98 |

[a] 20, 35, 50 are keV units.

The isotropic case is as follows:

$$E_{I_{so}}(\theta,\phi) = E_1 \cdot sin\theta \tag{6.2}$$

where θ and φ are the meridian and azimuthal angles of the photons.

## 6.3 Results

In the configuration of the system, the microlens diameter is 23 μm. The distance between a screen and the microlens is 50 μm. These are several thousands of nanometers. The light collection efficiency is shown as the percentage of the light collected in the photodetector. Each point *P* stands for the pixel point of the photodetector. The *P9* is the center pixel and there are pixels from *P1* to *P8* around *P9*. Table 6.3 shows each geometrical simulation in the Lambertian and isotropic source assumptions, where the light collection efficiencies for $Gd_2O_2S$ and CsI are shown. The 27-kVp and 82-μm $Gd_2O_2S$ case shows the highest light collection in both Lambertian and isotropic geometries. In the case of CsI, the 20-keV and 150-μm case has the highest light collection efficiency. The energy range is usually between 17 kVp and 25 kVp in clinical situations. It is reasonable that in this step of the experiment the highest efficiency can be standard data by comparisons among data.

**TABLE 6.3**

Light Collection Efficiency (%)

| | | Lambertian Source (%) | | | |
|---|---|---|---|---|---|
| | | L1 | | L2 | |
| Energy (kVp) | Thickness (μm; mg/cm²) | P9 | P1–P8 | P6–P9 | P1–P5 |
| *(a) $Gd_2O_2S:Tb$* | | | | | |
| 25 | 48; 35 | 32.03 | 0.094 | 0.013 | 0.002 |
| 26 | 46; 34 | 14.43 | 0.042 | 0.209 | 0.030 |
| 27 | 46; 34 | 17.07 | 0.049 | 0.174 | 0.025 |
| | 82; 60 | 76.00 | 0.220 | 0.210 | 0.020 |
| 28 | 40; 29 | 18.41 | 0.053 | 0.153 | 0.022 |
| 30 | 44; 32 | 33.50 | 0.097 | 0.001 | 0.000 |
| 90 | 68; 50 | 18.46 | 0.053 | 0.152 | 0.022 |
| | 68; 50 | 18.07 | 0.052 | 0.158 | 0.023 |
| | 109; 80 | 13.36 | 0.039 | 0.220 | 0.031 |
| *(b) CsI:Tl* | | | | | |
| 20[a] | 150; 68 | 76.00 | 0.220 | 0.210 | 0.030 |
| 35[a] | 150; 68 | 67.52 | 0.195 | 0.419 | 0.060 |
| 50[a] | 150; 68 | 73.58 | 0.213 | 0.259 | 0.037 |
| 30 | 150; 68 | 59.25 | 0.171 | 0.749 | 0.107 |
| 200 | 147; 47 | 59.23 | 0.171 | 0.740 | 0.106 |
| | 299; 135 | 50.17 | 0.145 | 1.2111 | 0.173 |

**TABLE 6.3 (*Continued*)**

Light Collection Efficiency (%)

| Energy (kVp) | Thickness (μm; mg/cm²) | Isotropic Source (%) | | | |
|---|---|---|---|---|---|
| | | L1 | | L2 | |
| | | P9 | P1–P8 | P6–P9 | P1–P5 |
| *(a) $Gd_2O_2S:Tb$* | | | | | |
| 25 | 48; 35 | 11.05 | 1.105 | 0.012 | 0.005 |
| 26 | 46; 34 | 4.935 | 0.493 | 0.189 | 0.080 |
| 27 | 46; 34 | 5.839 | 0.584 | 0.158 | 0.066 |
| | 82; 60 | 26.00 | 0.260 | 0.190 | 0.080 |
| 28 | 40; 29 | 6.300 | 0.630 | 0.138 | 0.058 |
| 30 | 44; 32 | 11.46 | 1.146 | 0.001 | 0.000 |
| 90 | 68; 50 | 6.317 | 0.632 | 0.137 | 0.058 |
| | 68; 50 | 6.181 | 0.618 | 0.143 | 0.060 |
| | 109; 80 | 4.572 | 0.457 | 0.199 | 0.083 |
| *(b) CsI:Tl* | | | | | |
| 20[a] | 150; 68 | 26.00 | 0.260 | 0.190 | 0.030 |
| 35[a] | 150; 68 | 23.10 | 2.310 | 0.189 | 0.160 |
| 50[a] | 150; 68 | 25.17 | 2.517 | 0.234 | 0.099 |
| 30 | 150; 68 | 20.19 | 2.019 | 0.678 | 0.285 |
| 200 | 147; 47 | 20.26 | 2.026 | 0.669 | 0.282 |
| | 299; 135 | 17.16 | 1.716 | 1.096 | 0.461 |

[a] 20, 35, and 50 are keV units.

## 6.4 Conclusions

Light collection efficiency may be increased by the microlens optical focusing method. This lens could focus the lights of the nanoscale photon distributions based on the angular distribution of the photons. Basically, the quantum quantity is obtained by the x-ray energy and screen thickness. So, the image blur can be decreased by the photon detection numbers in the photodetector. The optimized light collection efficiency could vary based on the geometry of the breast and several physical values. Energy is an important factor. Dose calibration must consider the safety of the patient's exposure due to the hazard of the radiation. The mammogram examination could be modified by the lower radiation treatment. The screen is manufactured at microscale thickness, which is incorporated in the nanoscale simulations. The molecular structure of the phosphor material is modified for better imaging, which should be investigated by nanoscale analysis. The microlens could be used in other diagnostic x-ray imagers for lung or stomach cancers. Optical imaging manipulation should be widely investigated in x-ray imager systems. The cost of the production of a completed system with AMFPI could be reduced due to advances in micro- and nanoscale manufacturing.

## References

Antonuk, L.E., Y. El-Mohri, J. H. Siewerden, and J. Yorkston. 1997b. Empirical investigation of the signal performance of a high-resolution, indirect detection, active matrix flat-panel imager (AMFPI) for fluoroscopic and radiographic operations, *Medical Physics* 24:512–570.

Bracewell, R. N. 2000. *The Fourier transform and its applications*. Boston: McGraw Hill.

Bunch, P. 1997. (Personal Communication). Company Internal Data, Kodak Company.

Cavouras, D., et al. 1998. An investigation of the imaging characteristics of the $Y_2O_2S$ : Eu phosphor for application in x-ray detectors of digital mammography. *Appl. Radiat. Isot*. 49:931–933.

Glassner, S. 1989. *An introduction to ray tracing*. London: Academic Press.

Hamamatsu, Inc. 1996. FOS (fiber optic plate with scintillator) for digital x-ray imaging. Technical Information. Hamamatsu Photonics S K.K., Electron Tube Center, Japan.

International Agency for Research on Cancer, 2008. World Cancer Report, France.

Jing, Z. et al. 1999. Spatial-frequency-dependent DQE performance of a CsI:Tl-based x-ray detector for digital mammography. *SPIE* 3659:159.

Kandarakis, I., D. Cavouras, G. S. Panayiotakis, and C. D. Nomicos. 1997a. Evaluating x-ray detectors for radiographic applications: A comparison of ZnSCdS:Ag with Gd2O2S:Tb and Y2O2S:Tb screens. *Phys. Med. Biol*. 42:351.

Kandarakis, I., D. Cavouras, G. S. Panayiotakis, D. Triantis, and C. D. Nomicos, 1997b. An experimental method for the determination of spatial frequency-dependent detective quantum efficiency (DQE) of scintillators used in x-ray imaging detectors. *Nuc. Inst. Meas. A* 399:335–342.

Petrick, N., T. H. Woo, H. P. Chan, and B. Sahiner. 2001. Microlens focusing for enhanced light collection in digital x-ray detectors. Paper presented at RSNA (Radiological Society of North America) 2001, 87th Scientific Assembly and Annual Meeting, Chicago, IL, November 25–30.

Petrick, N., T. H. Woo, H. P. Chan, B. Sahiner, and L. M. Hadjiiski. 2002. Evaluation of light collection in digital indirect detection x-ray imagers: Monte Carlo simulations with a more realistic phosphor screen model. Paper presented at the 6th IWDM (International Workshop on Digital Mammography), Bremen, Germany, June 22–25.

Sabol, J., and J. Boon. 1997. Monte Carlo simulation of photon transport within a hybrid grid-detector system for digital mammography. *SPIE* 3032:270.

Shirley, P. 2000. *Realistic ray tracing*. Natick, MA: A. K. Peters.

Maidment, A. D., and M. J. Yaffe. 1995. Analysis of signal propagation in optically coupled detectors for digital mammography: I. Phosphor screens. *Phys. Med. Biol.* 40:877.

Nagarkar, V. V., J. S. Gordon, S. Vasile, P. Gothoskar, and F. Hopkins. 1996. High-resolution x-ray sensor for non-destructive evaluation. *IEEE Trans. on Nuc. Sci.* 43:1559.

Nagarkar, V. V., T. K. Gupta, S. R. Miller, T. Klugerman, M. R. Squillante, and G. Entine. 1998. Structured CsI(Tl) scintillators for x-ray imaging applications. *IEEE Trans. on Nuc. Sci*. 45:492.

Widmer, W. R. 2008. Acquisition hardware for digital imaging. *Vet. Radiol. Ultrasound* 49(1 Suppl 1):S2–8.

Wronski, M. M., and J. A. Rowlands. 2008. Direct-conversion flat-panel imager with avalanche gain: Feasibility investigation for HARP-AMFPI. *Med. Phy.* 35:5207–5218.

Yu, T., J. M. Sabol, J. A. Seibert, and J. M. Boone. 1997. Scintillating fiber optic screens: A comparison of MTF, light conversion efficiency, and emission angle with Gd2O2S:Tb screens. *Med. Phy.* 24:279.

# 7

# *Measurement Profiles of Nanoscale Ion Beam for Optimized Radiation Energy Losses*

**Taeho Woo and Hyosung Cho**

**CONTENTS**



## 7.1 Introduction

The ion beam is used to treat regions of interest in organ material (Fukumura et al. 1998, Iseki et al. 2003, Rebisz-Pomorska et al. 2010). This chapter investigates the behavior of nanoscale ions with respect to their interaction with cancer cells. The optimized dose is classified according to several variables such as beam energy, cell properties, cancer cell depth, and so on. Successful treatment is expected in clinical results. It is important to make the spread out Bragg peak for the therapeutic radiation distribution. Pristine peaks are summed to reveal the optimized broad shape. The purpose of the beam shapes is to fit the target area. It is important to shape to match the dimensions of the tumor, and thus deliver most of the radiation to the targeted tumor mass, not to the surrounding normal tissue. For this purpose, it is necessary to produce several ion beams. Although this is a simple method, the cost of ion beam production will increase. In this chapter, the characteristics of ion beams are classified by ionizations, energy to recoil, and phonons. This chapter discusses a radiation therapy protocol using the Bragg peak where computerized simulations are performed with Stopping Range of Ions in Matter (SRIM) 2008. The results are calculated simply and cheaply using the SRIM 2008 computational code.

The Bragg peak is examined with respect to several variables. Analysis of computational simulations is of importance before construction of a facility due to the size required and the high cost of installation. The SRIM 2008 code

shows the previously mentioned variables for ion beam applications (Ziegler et al. 2008), and an additional study has been done for the ion therapy (Ji et al. 2008). That is to say, it is shown that if a small number of heavy ions are mixed with light ions, the heavy ions can be accelerated to the same velocity as the light ions so that they gain much higher energy because of their large mass. A quantum mechanical scenario is assumed in the beam injections. The charged particle application in radiation therapy has been focused on either neon or carbon ion beams (Fuminori 2001). The first effective proton treatment was done by R. Wilson at the Harvard Cyclotron Laboratory (HCL) (Wilson 1946, 2004). The first ion beam application in medicine was done by Bevalac at the Lawrence Berkeley Laboratory with a neon beam in 1975. The first carbon beam application was performed by the heavy-ion medical accelerator (HIMAC) at Chiba, Japan, in 1994 where the project was proposed in 1979 at the High LET Radiotherapy Division in the U.S.–Japan Cooperative Cancer Research Program at Kyoto, Japan. In this study, two human organs were tested using proton and neon beams. Section 7.2 explains the method of the study. The results for the simulation are shown in Section 7.4 and Section 7.5 describes the conclusions of the study.

## 7.2 Method

Organ material is exposed to heavy mass ions. Ion therapy is usually performed at high doses and as deep in the organ several centimeters. It is necessary to examine how the ions interact with the organ cells. Ion energy is the most important factor in destruction of cancer cells in organ material. The SRIM 2008 code is used to quantify proton interaction with the human organ. The code includes easy and tractable calculations that produce output data concerning stopping power, range, and straggling distributions for any ion at a designed energy and elemental target. Elaborate calculations include objective targets with complex multilayer configurations. The proton beam is widely used in medical therapy, especially in radiation oncology. The organs used in this study are pancreas and thyroid. Table 7.1 shows the organ compounds and the densities.

Several characteristics of the proton are investigated. The well-known Bragg peak is a major effect in ion therapy, and was discovered by Bragg in 1904 (Andrew and Herman 2004). This phenomenon can be used for cancer therapy by which it concentrates the effect of light ion beams on the tumor being treated by only slightly affecting normal tissue. The first patient treatment occurred a decade after Wilson's paper. Robert Wilson, who had been chief of the cyclotron team on the Manhattan project, decided as many other top physicists of that era did that a portion of his future work be directed to the benefit of mankind. He received an appointment at the Department

**TABLE 7.1**

Organ Compound

| | Chemical Compound | Density (g/cm$^3$) |
|---|---|---|
| Pancreas | H-11, C-17, N-2, O-69, P-0.4, S-0.4, Cl-0.2, K-0.2 | 1.04 (±0.05) |
| Thyroid | H-10, C-12, N-2, O-7, Na-0.2, Cl-0.2, K-0.2, I-0.1 | 1.05 (±0.05) |

of Physics at Harvard University and promptly wrote Radiological Use of Fast Protons (Wilson 1946). After that, various particles were used for clinical purposes. Higher mass ions have higher dose values, a fact that was profiled by the Heidelberg Ion-Beam Therapy Center (HIT). In the therapy, the ion beam is sharp and does not conform to the cancer cell shape. Therefore, it is very important to design a treatment plan to cover the entire cancer cell area. The Bragg peak shows the characteristics of the ions of interest for the energy variable (Cukier and McCullough 2001). The position is the depth of the organ tissue. The analysis includes the energy loss per unit length. The angular frequency is shown in Equation (7.1).

$$N(\omega) = \frac{1}{\exp(\hbar\omega / kT) - 1} \tag{7.1}$$

where

$N(\omega)$ = Frequency of phonon.
$k$ = Boltzmann's constant.
$T$ = Temperature.

This implies that the thermal phonon can be made by random energy fluctuations (Krauth 2006). In thermal equilibrium and within the harmonic regime, the probability of finding phonons in a given state with a given angular frequency is shown in Equation (7.1). The energy loss is calculated as a unit of (eV/Å) in this simulation.

## 7.3 Results

The ion beam interaction with the human body is examined within several hundreds of nanometers. Figure 7.1 shows the ion interactions in pancreas tissue. Energy losses decrease as the proton energy increases. The difference

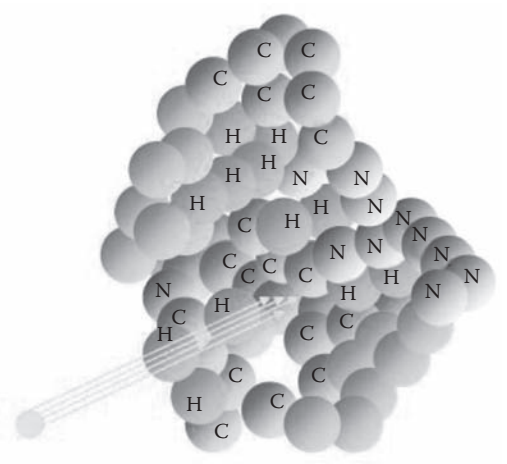


(a)

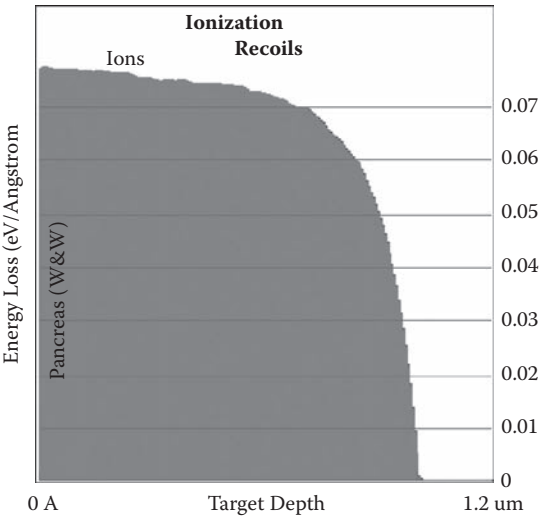


(b)

**FIGURE 7.1**
(a) H+ injections into pancreas molecular structure of carbon (C), hydrogen (H), nitrogen (N), oxygen (unmarked); and (b) energy losses (H+ 100 MeV) in pancreas.

between the highest and lowest values is 0.075 (eV/Å). The energy to recoil increases as the proton energy increases. For phonons, the energy to recoil decreases as the proton energy increases.

The pancreas experiences a larger loss than the thyroid, which is shown in Figure 7.2. In 100 MeV, the difference is 0.0075 (eV/Å) and in 200 MeV, the difference is 0.0210 (eV/Å). The difference in energy loss between the

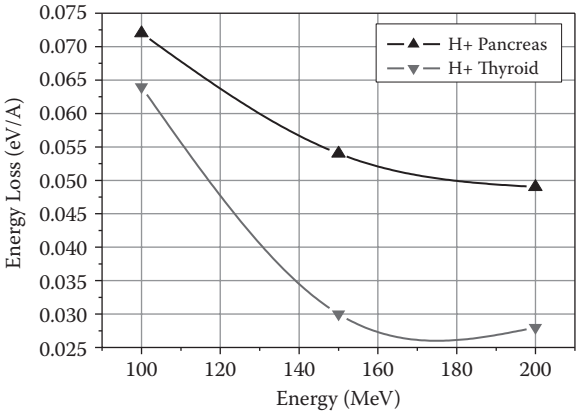


**FIGURE 7.2**
Ionizations in organs (at 600 nm depth).

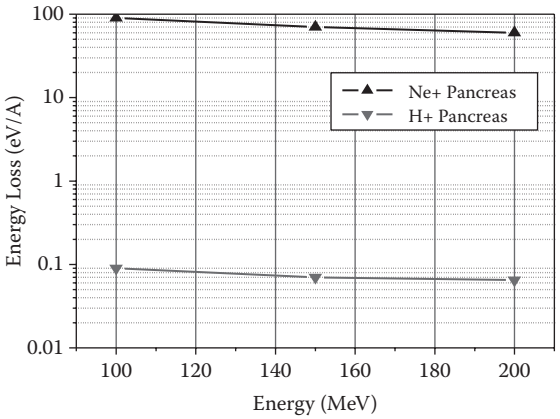


**FIGURE 7.3**
Ionizations in pancreas (at 600 nm depth).

two organs increases about 180% as the energy is doubled, which is seen in Figure 7.3. The neon ion has larger energy losses than the proton, which is related to the higher dose in tumor depth for the heavier ion (Heidelberg Ion-Beam Therapy Center 2007). The energy losses decrease linearly in the pancreas. Figures 7.4 and 7.5 show the energy recoils. In the pancreas, proton energy loss increases while neon ion energy loss decreases, which is seen as the black color in Figures 7.4 and 7.5. The interesting thing is that the energy loss changes around 160 MeV in each figure. This energy is an important point with respect to clinical purpose. The neon ion has the higher energy recoil. The temperature distribution of protons is shown for simulations of the pancreas. The trend is similar to the energy to recoil and the lowest temperature is shown at 150 MeV.

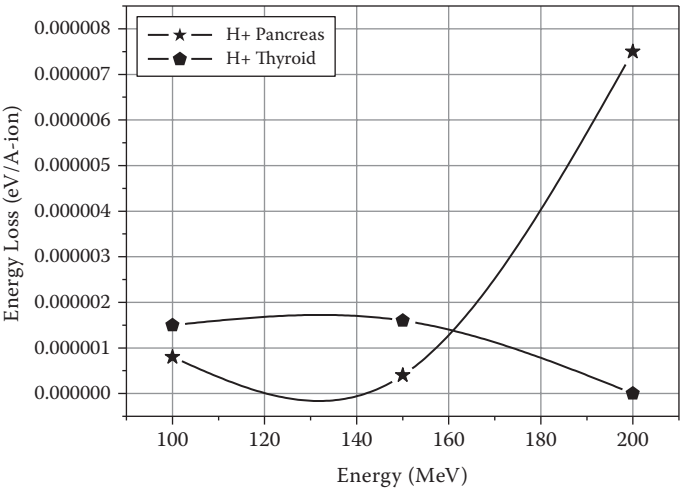


**FIGURE 7.4**
Energy to recoil in organs (H+) (at 600 nm depth).

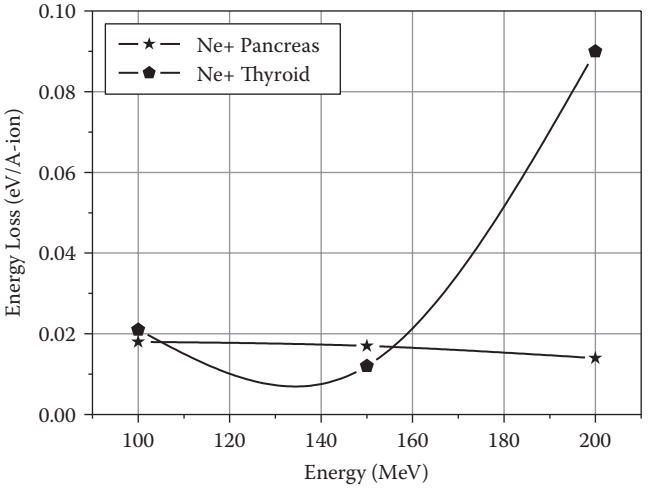


**FIGURE 7.5**
Energy to recoil in organs (Ne+) (at 600 nm depth).

Dose calculation is a major goal in radiation therapy. The members of Task Group No. 20 of the Radiation Therapy Committee of the American Association of Physicists in Medicine (AAPM 1986) have been performing ionimetric and calorimetric intercomparisons as well as other dosimetric measurements using heavy charged particles since 1977. The proposed protocol presents guidelines for dosimetry of therapeutic beams of heavy charged particles based on the experience of this task group. Although there

are insufficient basic data to allow the desired accuracy for dosimetry in all situations, the protocol is intended to serve as a resource for standardization of such dosimetry.

It is useful to determine the absorbed dose based on knowledge of the types of charged particles in heavy charged-particle beams. In the proposed equation, the fluence spectra and the stopping power, *S*, of the absorber material at the point of interest are used. The energy of the particles is denoted by *E* and delta ray equilibrium. The dose in a small mass *m* inside a homogeneous medium is given in Equation (7.2) (Rubach and Bichsel 1982a, 1982b, 1982c),

$$D_m = \sum_{i=1}^{n} \int_0^{\infty} \Phi_i(E)\left(S(E)/\rho\right)_i dE \tag{7.2}$$

where *i* is an index to sum over the different types of contributing particles, (the mass stopping power is the Kerma factor for charged particles). Additionally, a dosimeter can be based on a fluence measurement made in a charged-particle beam. The total fluence can be measured with a Faraday cup (Brown and Tautfest 1956), which is a well-insulated, conductive absorber thick enough to stop all the primaries and charged secondaries in a particle beam, allowing a measurement of the beam current. Using the Faraday cup, the number, *N*, of primary particles of known energy per monitor unit (charge collected on the transmission ionization chamber) is obtained. The Faraday cup can be replaced by a small ionization chamber, which will then collect a charge *Q* per monitor unit at the point of interest. Finally, parameters required for dose calculation are the stopping power of the charged particles of this energy in muscle tissue as well as the effective area of the beam. The dose determination in gray (Gy) is outlined in the Equation (7.3).

$$D_t = \frac{N}{a}\left(S/\rho\right)\left(1.602\times10^{-10}\right) \tag{7.3}$$

where $(S/\rho)$ is the mass stopping power of charged particles of this energy in muscle tissue in units of MeV $cm^2g^{-1}$ and *a* is the effective area of the beam ($cm^2$).

## 7.4 Conclusions

The protocol is constructed using the simulation results in Figure 7.6 where a procedure for a better type of therapy is proposed. Empirical measurements

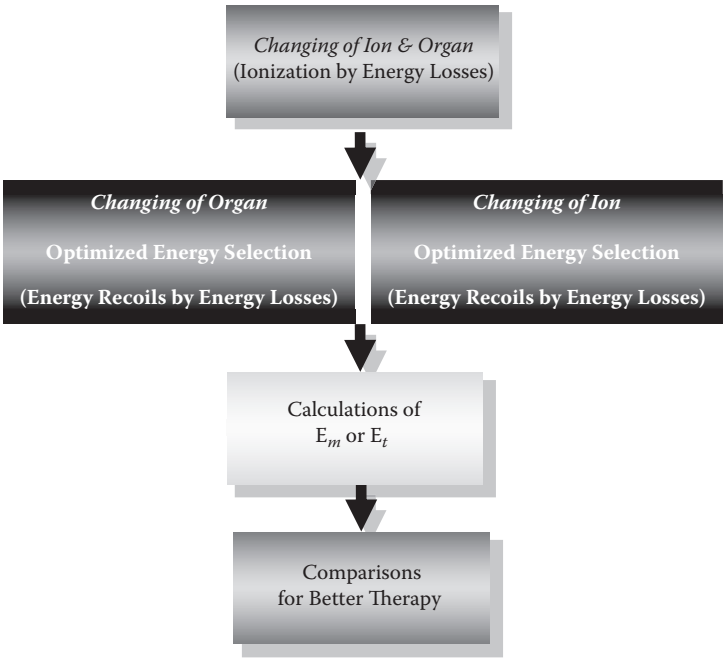


**FIGURE 7.6**
Protocol for ion beam therapy (PIBT).

incorporated with simulations are programmed by this protocol. Therefore, the efficiency of removing cancer cells could be increased. Systematic simulations can avoid the risk of overdosing normal cells. Following the *as low as reasonably achievable* (ALARA) concept of radiation protections, radiation hazards are prevented by this protocol. This new protocol could eliminate the possibility of overdose accidents. In addition, the cost of accelerator operations is reduced because simulation can be done on a small personal computer. Treatment time reduction is also a very important advantage.

To solve the dose distribution of the ion beam, it will be necessary to determine how to manage the ion beam so that it can be shaped appropriately (Kanai et al. 1997, Loncol et al. 1997). Therefore, as we examined in this chapter, heavy ion energy can affect the different Bragg peak distributions. Spreading out of the Bragg peak can be accomplished by varying beam intensity. Probabilistically, like the Monte Carlo simulation of the study where an ion beam is generated as the random sampling for the simulation of the interactions between beam and organ, the higher intensity beam can penetrate into the deep regions of the human body. In a real hospital facility, it will be necessary to make room for therapy planning and the staff's operation space. In addition, the accelerator should be designed for various energies and intensities. The Bragg peak can be varied based on the energy of the ion and the human organ characteristics, so the dose and its related

dose equivalent can be determined based on the injection ion energy and the human organ in question. For future work, it will be necessary to broaden and flatten the Bragg peak using an accelerator, which is called the high acute organ-dependent radiation therapy (HAODRT) system. Furthermore, a 4-dimensional system is under study, which is a 3-dimensional dynamics system. This work is based on the relationship of energy and organ study results where dynamic 4-dimensional simulation is utilized.

## References

AAPM (American Association of Physicists in Medicine). 1986. Protocol for heavy charged-particle therapy beam dosimetry. Task Group No. 20, Physics Radiation Therapy Committee, AAPM Report No. 16.

Andrew, S., and S. Herman. 2004. Commentary: The centenary of the discovery of the Bragg peak. *Radiol. Oncol.* 73:265–268.

Brown, K. L., and G. W. Tautfest. 1956. Faraday-cup monitors for high energy electron beams. *Rev. Sci. Instrum.* 27:696–702.

Cukier, D., and V. McCullough. 2001. *Coping with radiation therapy: A ray of hope*. Los Angeles, CA: Lowell House.

Fukumura, A., Y. Noda, K. Omata, et al. 1998. Simple range measurement of therapeutic ion beams using visible rays generated in a bare plastic scintillator block. *Nucl. Instr. and Meth. A* 416:148.

Fuminori, S. 2001. Progress of heavy ion therapy, http://villaolmo.mib.infn.it/Manuscripts/3_medical_applications/Fuminori_Soga.pdf

Heidelberg Ion-Beam Therapy Center (HIT) brochure. 2007. Heidelberg. Germany. http://www.klinikum.uni-heidelberg.de/fileadmin/medienzentrum/Vorlagen/downloads/Arbeitsproben/070316HIT_BR_SS_Broschuere_engl.pdf

Iseki, Y., H. Mizuno, Y. Futami, et al. 2003. Positron camera for range verification of heavy-ion radiotherapy. *Nucl. Instr. and Meth. A* 515:840.

Ji, L., B. Shen, X. Zhang, et al. 2008. Generating monoenergetic heavy-ion bunches with laser-induced electrostatic shocks. *Phys. Rev. Lett.* 101:164802.

Kanai, T., Y. Furusawa, K. Fukutsu, et al. 1997. Irradiation of mixed beam and design of spread-out Bragg peak for heavy-ion radiotherapy. *Radiation Research* 147:78–85.

Krauth, W. 2006. *Statistical mechanics: Algorithms and computations*, 231–232. Oxford, UK: Oxford University Press.

Loncol, T., V. Cosgrove, J. Denis, et al. 1997. Radiobiological effectiveness of radiation beams with broad LET spectra: Microdosimetric analysis using biological weighting functions. *Radiat. Protect. Dosim.* 52:347–352.

Rebisz-Pomorska, M., M. Ciobanu, M. Kis, et al. 2010. Diamond detectors for the monitoring of carbon-ion therapy beams. *Nucl. Instr. and Meth. A* 620:534.

Rubach, A., and H. Bichsel. 1982a. Neutron dosimetry with spherical ionization chambers I. Theory of the dose conversion factors r and Wn. *Phys. Med. Biol.* 27:893–904.

Rubach, A., and H. Bichsel. 1982b. Neutron dosimetry with spherical ionization chambers III. Calculated results of tissue-equivalent chambers. *Phys. Med. Biol.* 27:1231–1243.

Rubach, A., and H. Bichsel. 1982c. Neutron dosimetry with spherical ionization chambers IV. Neutron sensitivities for $C/CO_2$ and tissue-equivalent chambers. *Phys. Med. Biol.* 27:455–1463.

Wilson, R. 1946. Radiological use of fast protons. *Radiology* 47:487–491.

Wilson, R. 2004. *A brief history of the Harvard University cyclotrons*, 9. Cambridge, MA: Harvard University Press.

Ziegler, J. F., J. P. Biersack, and U. Littmark. 2008. *The stopping and range of ions in solids*, 2nd ed. New York: Pergamon Press.

# 8

# *Brachytherapy for Nanoscale Cancer Therapy Using Radioisotopes*

**Taeho Woo**

**CONTENTS**



## 8.1 Introduction

There are four kinds of brachytherapy: high-dose-rate (HDR), medium-dose-rate (MDR), low-dose-rate (LDR), and pulse-dose-rate (PDR) methods. HDR brachytherapy protocol has been developed for nanoscale treatment (Korean Food and Drug Administration [KFDA] 2004). The object of this project is the establishment of safety and accuracy standards for the HDR treatment system, which includes the HDR afterloader, source, and radiotherapy treatment planning (RTP). There are many functional and structural features, such as the structure of a source, source dwelling method, safety interlock feature, and dose calculation accuracy, which are unique for each model. It is necessary for the different features of the HDR treatment system to be evaluated by a standardized criterion in order to be approved for patient treatment (AAPM [American Association of Physicists in Medicine] 1994, 1995, 1997; IAEA [International Atomic Energy Agency] 2000;, Khan 2003; Van Dyk 1999). Table 8.1 shows the acceptable physical application sites of brachytherapy with respect to patient sex. Table 8.2 lists the sampled radioisotopes in clinical usage. It is important to accurately calculate dosage for patient therapy in clinical applications. The automatic calculator is developed using commercial software. It is quite exact in RTP. The clinical result is matched with the calculations by comparison.

Hrycushko et al. (2011) studied brachytherapy in lumpectomy focal treatment. Postoperative radiotherapy has commonly been used for early-stage

**TABLE 8.1**

Brachytherapy Treatment Sites

| Physical Site | Men | Women |
|---|---|---|
| Brain, Eye, Tongue, Oropharynx | Yes | Yes |
| Trachea, Bronchi, Lung | Yes | Yes |
| Oesophagus, Bile Ducts, Anus, Rectum | Yes | Yes |
| Bladder, Urethra | Yes | Yes |
| Skin | Yes | Yes |
| Prostate, Penis | Yes | No |
| Breast | No | Yes |
| Uterus, Cervix, Vagina, Vulva | No | Yes |

**TABLE 8.2**

Radioisotopes Used in Brachytherapy

| Radioisotope | Radiation | Energy (MeV) |
|---|---|---|
| Cesium-137 | Gamma ray | 0.662 |
| Cobalt-60 | Gamma ray | 1.17, 1.33 |
| Iridium-192 | Gamma ray | 0.38 |
| Iodine-125 | X-ray | 0.0274, 0.0314, 0.0355 |
| Palladium-103 | X-ray | 0.021 |
| Ruthenium-106 | Beta particles | 3.54 |

breast cancer to treat residual disease after surgery. The primary objective of this work was to characterize, through dosimetric and radiobiological modeling, a novel focal brachytherapy technique that uses direct intracavitary infusion of β-emitting radionuclides ($^{186}$Re/$^{188}$Re) carried by lipid nanoparticles (liposomes). The porphyrins in targeted molecular brachytherapy have been investigated by Yao (2008). In a new therapy that aims to concentrate and immobilize therapeutic radionuclides in nanoscale assemblies within solid tumors, a soluble precipitable reagent (SPR) is administered as the radionuclide carrier and is converted to nondiffusible precipitate by an enzyme located in tumor tissues. In addition, the uncertainties in measuring or estimating brachytherapy dose distributions are addressed using Monte Carlo methods with discussion of the components intrinsic to the overall dosimetric assessment (DeWerd et al. 2011). The report addresses uncertainties pertaining to brachytherapy source dosimetry. The International Organization for Standardization (ISO) *Guide to the Expression of Uncertainty in Measurement* (GUM) and the National Institute of Standards and Technology (NIST) Technical Note 1297 are used as reference standards for uncertainty formalism (DeWerd et al. 2011).

## 8.2 Method and Results

Mathematical therapy planning is performed. Radiation therapy is done with the Nucletron Microelectronic Classic and RTP is performed by Nucletron's Plato (Nucletron B. V., Veenendaal, the Netherlands). The exposure time is 1 minute in the zero point of the body coordinate. In the study, absorption calculations are performed for eight treatment points, from $p_1$ to $p_8$ as $p_0$ (0, 2 cm, 0), $p_1$ (–2 cm, 2 cm, 0), $p_2$ (2 cm, –2 cm, 0), $p_3$ (0, 2 cm, 2 cm), $p_4$ (0, 2 cm, 0), $p_5$ (0, 5 cm, 0), $p_6$ (2 cm, 4 cm, 0), $p_7$ (–2 cm, 4 cm, 0), and $p_8$ (0, 4 cm, 2 cm).

The dosimeters are calculated in the designed geometry. First of all, one needs to choose a point source or cylindrical source in order to determine the geometry factor. According to the Technical Guide (TG) 41, the point source is described as $1/r^2$ and the line source as $\beta/(L \times r \times \sin\theta)$. Equation (8.1) shows the calculation of dosage in brachytherapy. Figure 8.1 shows the line source case. The calculated doses are compared to the RTP doses in Table 8.3.

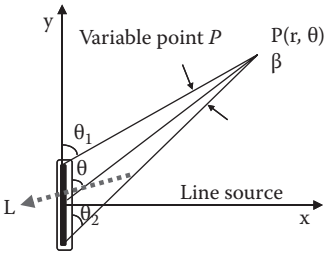


**FIGURE 8.1**
Diagram of the line source case.

**TABLE 8.3**

Calculated Doses versus RTP Doses

| Var. | *r* | θ | *g(r)* | *φan* | *Cal. D (r, θ)* | *RTP D(r,θ)* | *Dif. (%)* |
|---|---|---|---|---|---|---|---|
| $p_0$ | 1.9990 | 0.0000 | 1.0105 | 0.6450 | 79.2162 | 92.4 | –14.27 |
| $p_1$ | 2.8277 | 45.0371 | 1.0149 | 0.9607 | 59.2186 | 59.3 | –0.14 |
| $p_2$ | 2.8277 | 44.9629 | 1.0149 | 0.9607 | 59.2185 | 56.7 | 4.33 |
| $p_3$ | 2.8277 | 45.0372 | 1.0149 | 0.9606 | 59.2185 | 59.0 | 0.37 |
| $p_4$ | 1.9990 | 0.0000 | 1.0105 | 0.6450 | 79.2162 | 88.4 | –10.39 |
| $p_5$ | 4.9990 | 0.0000 | 0.9956 | 0.6960 | 13.4665 | 14.6 | –7.76 |
| $p_6$ | 4.4721 | 26.5843 | 1.0047 | 0.8947 | 21.8361 | 22.1 | –1.19 |
| $p_7$ | 4.4721 | 26.5843 | 1.0047 | 0.8947 | 21.8361 | 22.2 | –1.64 |
| $p_8$ | 4.4721 | 26.5843 | 1.0047 | 0.8947 | 21.8361 | 22.1 | –1.19 |

$$D(r,\theta)=\frac{\Lambda \cdot S_K \cdot g(r) \cdot \phi_{an} \cdot 60}{r^2} \tag{8.1}$$

where

| Variable | Meaning |
|---|---|
| $r$ | Distance between source and detection (cm). |
| $\theta$ | Angle of detection point from y axis. |
| $D(r, \theta)$ | Absorption dose rate in detection point. |
| $\Lambda$ | Dose rate constant (1.12 cGy/h U). |
| $S_K$. | Air-kerma strength (7.2274 cGy cm$^2$/sec). |
| $1/r^2$ | Geometry factor, point source approximation. |
| $g(r)$ | Radial dose function. |
| $\varphi_{an}$ | Average anisotropy factor (x axis point = 1.0). |

## 8.3 Conclusions

This study addresses the establishment of method and accuracy standards for an HDR brachytherapy treatment system. There are many possibilities for application in human organs. The important points are how to construct the reasonable radiation dose and therapy planning in the hospital. Brachytherapy is an example of nanoscopic technology in radiation applications.

## References

American Association of Physicists in Medicine (AAPM). 1994. *Comprehensive QA for radiation oncology*. Report of Task Group No. 40. College Park, MD: AAPM.

American Association of Physicists in Medicine (AAPM). 1995. *Dosimetry of interstitial brachytherapy sources*. Report of Task Group No. 43. College Park, MD: AAPM.

American Association of Physicists in Medicine (AAPM). 1997. *Code of practice for brachytherapy physics*. Report of Task Group No. 56. College Park, MD: AAPM.

DeWerd, L. A., G. S. Ibbott, A. S. Meigooni, et al. 2011. A dosimetric uncertainty analysis for photon-emitting brachytherapy sources. *Medical Physics* 38:1–21.

Hrycushko, B. A., A. N. Gutierrez, B. Goins, et al. 2011. Radiobiological characterization of post-lumpectomy focal brachytherapy with lipid nanoparticle-carried radionuclides. *Phys. Med. Biol.* 56:703.

IAEA (International Atomic Energy Agency). 2000. *Lessons learned from accidental exposures in radiotherapy*. Safety Reports Series No. 17. Vienna: IAEA.

Khan, 2003. *The physics of radiotherapy*. 3rd ed. Philadelphia, PA: Lippincott Williams & Wilkins.

Korea Food and Drug Administration (KFDA). 2004. The development of quality assurance standards for the remote controlled afterloading brachytherapy systems and radiation source.

Van Dyk, J. 1999. *The modern technology of radiation oncology*. Madison, WI: Medical Physics Publishing.

Yao, Z., K. E. Borbas, and J. S. Lindsey. 2008. Soluble precipitable porphyrins for use in targeted molecular brachytherapy. *New J. Chem.* 32:436–451.

# Section III

# Atomic Nanoscale Material Management

# 9

# *Analysis for Nanotechnology Financial Progression in the Energy Industry Using Systems Thinking Decision Making*

**Taeho Woo and Yunil Kim**

**CONTENTS**



## 9.1 Introduction

New technology applied in the nuclear industry is one of most important advances of the twenty-first century. Nanotechnology (NT), information technology (IT), and biotechnology (BT) have interdisciplinary applications in nuclear technology. Investigations in the nuclear industry as well as academic fields are useful in managing these new technology fields, and applications using these interdisciplinary technologies will enhance power production in nuclear power plants (NPPs).

Historically, NT was initiated in the 1990s as the National Nanotechnology Initiative (NNI), which has promoted applications in many areas of science and technology. The object of the NNI is to improve efficiency in a variety of fields. In the area of NPPs, NT application to nuclear technology has been introduced. This new trend highlights a possible solution for the current stagnation in NPP construction. Dr. Albert Einstein calculated the size of a single sugar molecular from experimental data on the diffusion of sugar in water, which showed that each molecule measures about one nanometer in diameter (Stix 2001). Richard Feynman mentioned there were plenty of rooms at the bottom of the matter around 1960s (Toumey 2005). Nanoscale research was initiated nationally in the United States in the 1990s. The NNI is a government effort and therefore depends on tax dollars for its operation.

Funding for the NNI as a National Science and Technology Council (NSTC) program was approved by Congress in the 1999 budget (WTEC 1999, 2007, 2008, 2009, 2010). The major goals of the NNI (NNCO 2009) are to advance world-class NT research programs and to develop educational resources, a skilled workforce, and the supporting infrastructure tools.

Professor J. Forrester at the Massachusetts Institute of Technology (MIT) created system dynamics (SD) for analysis of the nonlinear characteristics of complex dynamic social and economic systems; this is called also *systems thinking*. In this chapter, SD is used to quantify the assessment of the NT case. There are some publications for the organizations by the transitions of the time (Forrester 1961, 1969, 1971). Decision-making studies were also performed.

To increase understanding, a smaller model based on selected dynamics generated by the original model and containing only a subset of the feedback loops in the original model was developed (Eberlein 1989). Linking feedback loops and system behavior is part of the foundation of SD, yet the lack of formal tools has so far has prevented a systematic application of the concept, except for very simple systems (Kampmann 1996). The SD approach is combined with a statistical forecasting model—a combination that proved to be valuable for the analysis and management of airline business cycles (Liehr 2001). Marcelloni and Vecchio (2010) propose an approach to perform lossy compression on a single node based on a differential pulse code modulation scheme with quantization of the differences between consecutive samples.

Ronald et al. (2007) examined the global classifications of NT in the literature where applications address the infrastructure and taxonomy of specific nonmedical and medical applications. In addition, Nikulainen and Palmberg (2010) showed that university researchers are more active in nanotechnologies that are endowed with motivations and face challenges that are different from other disciplines (Nikulainen and Palmberg 2010). Puurunen and Vasara (2007) investigated an example where NT's possible applications in the paper industry, especially in emissions reduction and dematerialization, had attracted only limited attention. Azadeh et al. (2008) performed an energy analysis involving ergonomic performance in a gas refinery. Another energy analysis was done to evaluate energy capacity for the nodes of wireless sensor networks (Marcelloni and Vecchio 2010).

Section 9.2 explains the method used in the study. The calculation for the modeling is shown in Section 9.3. Section 9.4 describes the results of the study, and some conclusions are presented in Section 9.5.

## 9.2 Method

It is important to examine NT with reliable simulation. The characteristics of NT are shown in Figure 9.1. The treatment property and the scale property are combined for the ionic force and the molecular atom in the NT; namely,

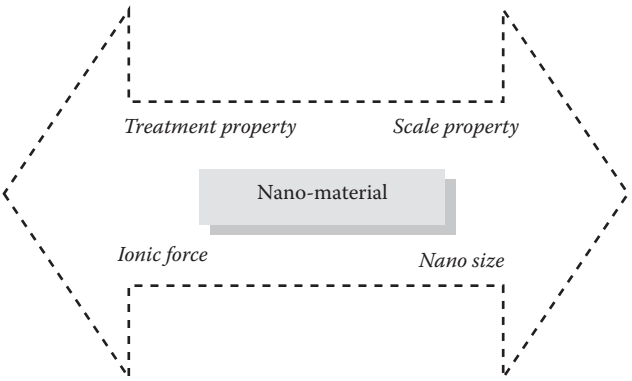


**FIGURE 9.1**
Characteristics of nanotechnology (NT).

**TABLE 9.1**
Comparisons between Feedback and Accumulation

| Classification | Accumulation | Feedback |
|---|---|---|
| Application | Many kinds | All kinds |
| Concentration | Yes | No |
| Event characteristics | Yes | Yes |
| Event flow | Forward and backward | Forward and backward |
| Magnitude | Yes | No |
| Quantification | Yes | No |
| Time step | No | Yes |

the property of ions has attractive and repulsive forces. Otherwise, the molecular property is related to the size of any substance. The performance of NT, therefore, could be expressed as the manipulation of material charges and sizes (nanosize) of molecules. The properties of NT are usually investigated in the general industrial field, with the academic approach and the marketing. Basically, SD can be expressed in terms of feedback and accumulation in the event flow, which is often used in the assessment of new technology fields like NT, because progress in technology is characterized by nonlinear feedback and asset-added accumulation. There are comparisons between feedback and accumulation for SD in Table 9.1. These characteristics are very important in dynamic assessment, especially when attempting to quantify success. Using the SD method, simulations are performed for both analytic estimations and quantification. SD is used to investigate particular problems taking into account the technological implications of a variety of factors. Furthermore, SD can assist in dynamic decision making in complex matters. The Vensim package used for simulation was developed by Ventana Systems, Inc.

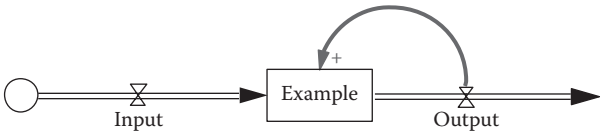


**FIGURE 9.2**
Stock flow (asset accumulation) and feedback.

System dynamics can be described as a powerful computer simulation modeling technique for understanding, framing, and discussing complex issues and problems (Radzicki and Taylor 1997). SD helps managers to improve their understanding of industrial processes, and is currently used in many kinds of policy analysis and design. SD takes into account basic building blocks that can be used to construct models of how and why complex real-world systems behave the way they do during a specified time period. The main objective is to leverage this added understanding to design and implement more effective policies. The important thing is to understand the dynamic behavior of a system, its key physical and information stocks, flows, and feedback structures. Some properties of SD are as follows:

1. Nonlinearity: There are many SD modeling processes that apply common sense to dynamic problems. The SD operator should always understand model behaviors that do not make sense linearly. Such behaviors usually indicate a nonlinearity of the events. This is seen as single and double arrow lines in the model. The arrows show the event flow without any restriction.
2. Stock flow: SD modeling can be used to examine the dynamic behavior of stock accumulation. Many dynamic behaviors could be happening when flows accumulate in stocks, which are seen as input and output for flows in Figure 9.2. This is like a bathtub where a flow can be thought of as a faucet and pipe assembly that fills or drains the stock. This is considered the simplest dynamic system in the stock flow structure. In the SD model, both informational and noninformational objects can move through flows and accumulate in stocks.
3. Feedback: The feedback algorithm can simulate stocks and flows in real-world systems. Several feedback loops are often joined together by nonlinear couplings where any object can cause counterintuitive behavior. This is seen as a loop in Figure 9.2. The plus sign indicates an addition to the example of the feedback value, output. If a minus sign is shown, the feedback value, output, is subtracted from the example.
4. Time paths: Dynamic behavior of systems is expressed in time steps, where the operator tries to identify the patterns of behavior exhibited by various system variables, and then builds a model with

the characteristics of those patterns. SD modeling can be used as a laboratory for testing policies aimed at altering a system's behavior in desired ways shown as the single and double arrow lines in the model. The lines indicate event and time flows.

In SD modeling, there are special expressions for these characteristics. In the Vensim code, the technical methods are indicated by single and double arrow lines as follows:

1. Single arrow line: This line indicates the flow of the event. The line represents the sequence of the scenarios as well as the dynamic behavior. Therefore, the direction of line gives the event flow and event feedback.
2. Double arrow line: The dynamic behavior of the principle of accumulation is considered in SD modeling. Any dynamic behavior can be expressed when flows accumulate stocks, as seen in Figure 9.2. The feedback loops are often modeled with nonlinear couplings, where any object can show counterintuitive behavior, which is seen as the loop in Figure 9.2.

## 9.3 Calculation

The academic and industrial fields are connected in Figure 9.3, and NT applications in the nuclear industry are investigated. Eventually, one can estimate the future trend of the governmental budget. The main modeling for atomic nanotechnology is shown in Figure 9.4, where the three aspects of technology, manpower, and marketing are combined. These three aspects are connected by academic promotion and industrial promotion.

Academic promotion involves research and education factors (Figure 9.5). The subfactors include skill, license, educational material, and faculty numbers. Each factor is quantified using a Monte Carlo simulation of random sampling (Table 9.2) except the license case. For example, when the random value for a skill is below 0.2, the value is 0 and, in the other case, it is 1. This is defined as the *importance value*, which is determined at the discretion of the operator. The importance value is obtained by random sampling and given a value of 0, 1, or 2 in Table 9.2. For the license case, the modeling is seen in Figure 9.6. The event flows from input to output and feedback from output. In the new technology, the value is cumulative based on the difference between input and output, which have plus or minus signs, because the license is a legal factor. This is expressed in the event flow diagram as a double arrow line.

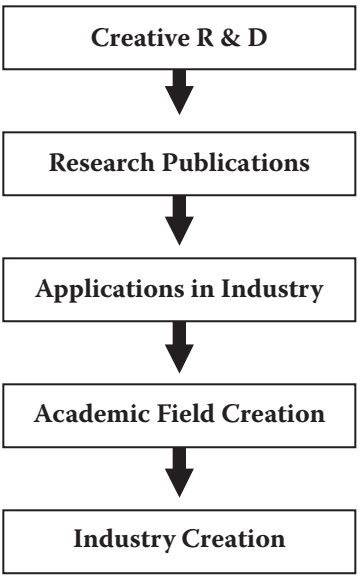


**FIGURE 9.3**
Merging of the academic and industrial fields.

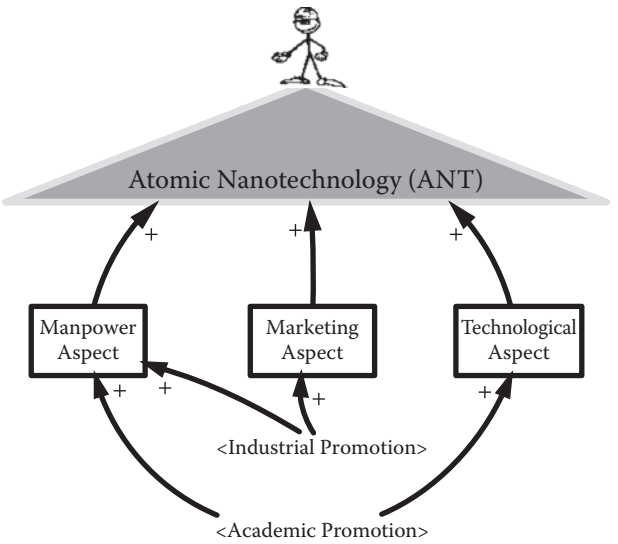


**FIGURE 9.4**
Main modeling of atomic nanotechnology.

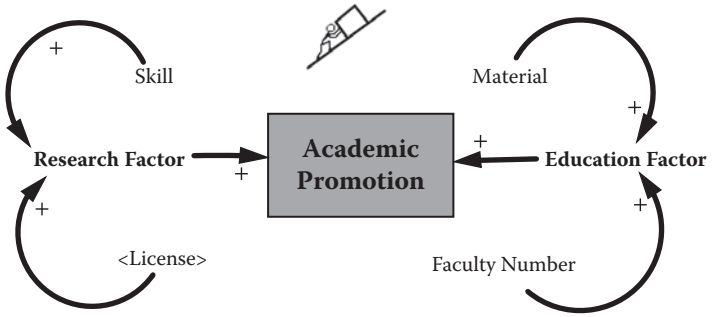


**FIGURE 9.5**
Modeling of academic promotion.

**TABLE 9.2**

Importance Values of All Elements

| Element | | | Value |
|---|---|---|---|
| Academic Promotion | Education | Faculty Number | (random < 0.1, 0, 1) |
| | | Material | (random < 0.5, 0, 1) |
| | Research | License | New Technology |
| | | Skill | (random < 0.2, 0, 1) |
| Industrial Promotion | Company Factor | Construction Ability | (random < 0.1, 0, 1) |
| | | Income | (random < 0.2, 0, 2) |
| | Economic Factor | GDP | (random < 0.2, 0, 1) |
| | | Price | Price Decision |
| | Government Factor | Leadership | (random < 0.3, 0, 2) |
| | | Tax | (random < 0.2, 0, 1) |

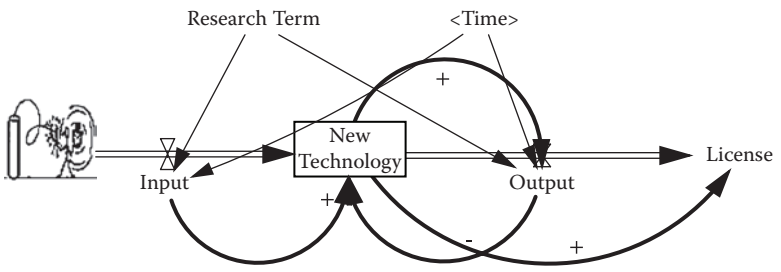


**FIGURE 9.6**
Modeling of license.

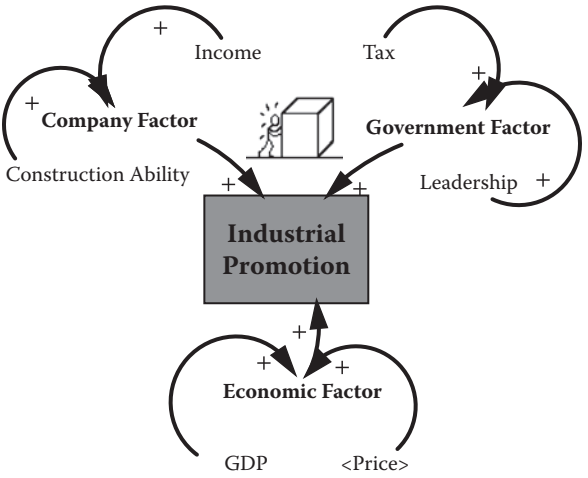


**FIGURE 9.7**
Modeling of industrial promotion.

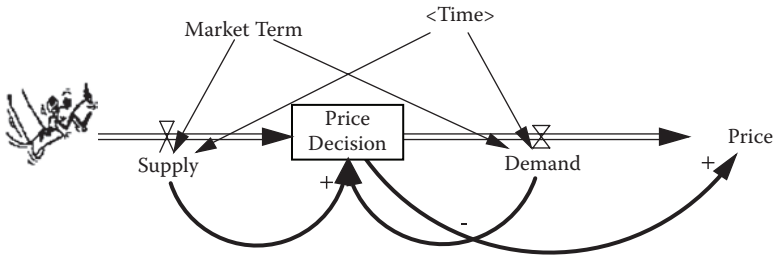


**FIGURE 9.8**
Modeling price.

Industrial promotion has three factors: the company factor, economic factor, and government factor (Figure 9.7) and follows a procedure similar to academic promotion. The subfactors include income, construction ability, GDP, price, tax, and leadership. Each factor is quantified using a Monte Carlo simulation of random sampling (Table 9.2) except the price case. That is to say, in case of income, when the random value is lower than 0.2, the value is 0 and, in the other case, it is 1. This is the importance value, which is determined at the discretion of the operator. The importance value is obtained by random sampling and a given value of 0, 1, or 2 in Table 9.2. For the price case, the modeling is seen in Figure 9.8. The event flows from supply to demand and feedback from demand. In the price decision, the value is cumulative based on the difference between supply and demand, which have plus or minus signs, because the results of price should be accumulated based on its marketing principle which, like competition, is based on the perceptions of producers and consumers. This is expressed in the event flow diagram as a double arrow line.

## 9.4 Results

Figure 9.9 includes five graphs showing the simulation results. Figure 9.9(a) shows the results for atomic nanotechnology, which is calculated by the summation of the technological aspect, manpower aspect, and marketing aspect, where the value increases with increasing slope. Figure 9.9(b) shows the results for academic promotion, where the value increases nonlinearly. Figure 9.9(c) shows the results for industrial promotion, where the value increases with decreasing slope. Figure 9.9(d) shows the results for the license

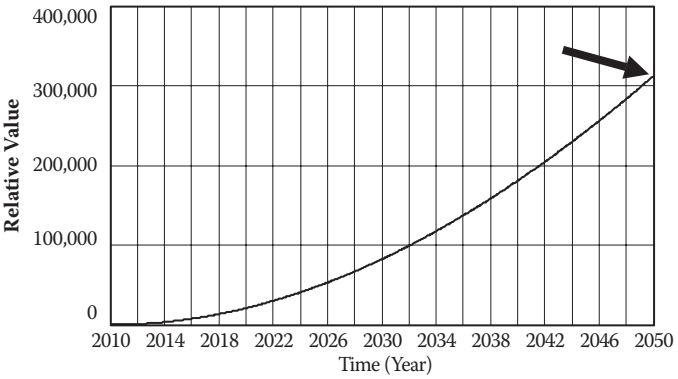


(a)

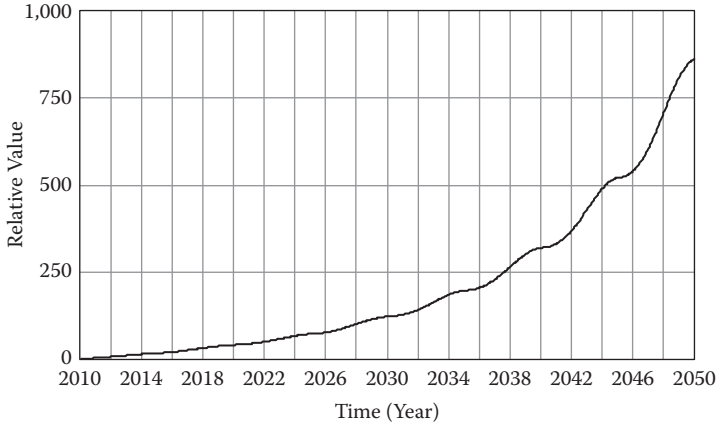


(b)

**FIGURE 9.9**
Quantification of (a) atomic nanotechnology, (b) industrial promotion, (c) academic promotion, (d) license, and (e) price.

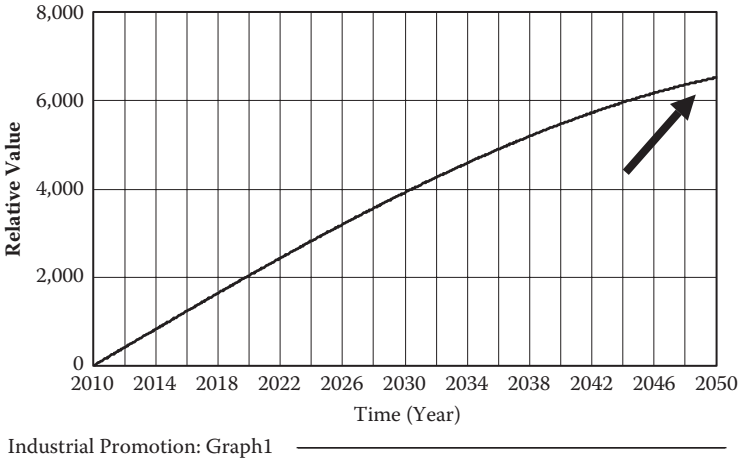


(c)

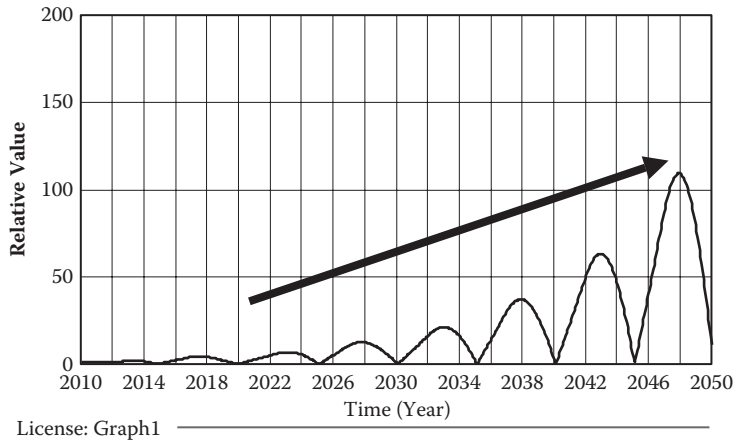


(d)

**FIGURE 9.9** ***(Continued)***

factor, a sinusoidal graph with increasing values, which is obtained for a five-year research cycle. The value cycle increases as time goes on because the NT research trend is matured in the new academic field. Figure 9.9(e) shows the results for price, which decreases with increasing slope. This means that price decreases with growth in the industry. The maximum value of Figure 9.9(a) is 312,209 in 2050. This is the total value of the NT field. So, the size of the academic and economic areas is 312,209 times the initial value in 2010.

One can estimate the financial value using the previous calculations. The value is considered for the nuclear industry. If this model is applied to the United States, the budget of the Department of Energy (DOE) could be used as an example. The estimated value of the DOE budget in 2010 is calculated

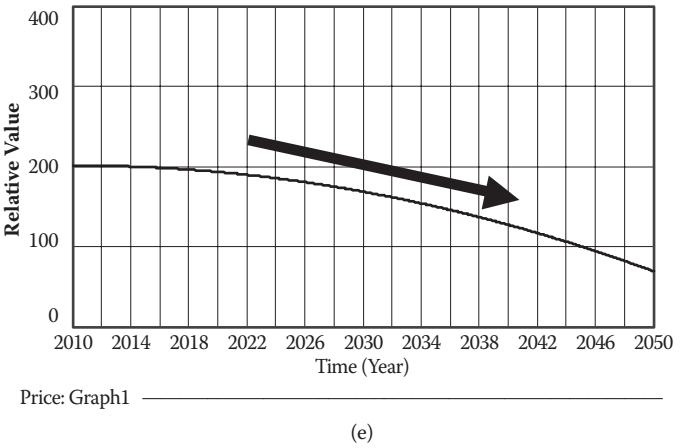


**FIGURE 9.9** ***(Continued)***

using Table 9.3 (NSTC [National Science and Technology Council] 2007, 2008, 2009, 2010), which shows the nanotechnology budget values for several U.S. government departments. Therefore, the calculated value in 2050 is $116,329,073.6 million ($372.6 million × 312,209). This was calculated using the 2010 DOE estimated nanotechnology budget value of $372.6 million.

## 9.5 Conclusions

The quantitative simulation for the new industrial field was projected for 2010 to 2050. The core factors are introduced by the academic and industrial promotions. Following the importance values, the top event of the NT is quantified. The success of the new industrial field was shown as the combination of several factors. The model can be summarized as follows:

A dynamical simulation has been performed in the new industrial field.

The characteristics of NT and the trend of the new economic field were used to determine a budget value using SD.

Nonlinear investigation using SD was effective in analyzing future event scenarios.

The time feedback algorithm, SD, was applied to the industrial decision-making case, which was incorporated with the academic field.

Feedback and cumulative algorithms are used to simulate the economic principles of license and price.

Very tractable quantification was obtained using a computer package.

**TABLE 9.3**

Comparisons of Nanotechnology Budgets

| | U.S. Government Nanotechnology Budgets (in millions) | | | | | |
|---|---|---|---|---|---|---|
| **Organization** | **2006** | **2007** | **2008** | **2009** | **2010 (Estimated)** | **2011 (Proposed)** |
| Department of Energy | $213.0 | $236.0 | $245.0 | $332.6 | $372.6 | $423.9 |
| National Science Foundation | 359.7 | 389.0 | 409.0 | 408.6 | 417.7 | 401.3 |
| Department of Defense | 423.9 | 450.0 | 460.0 | 459.0 | 436.4 | 348.5 |
| National Institutes of Health | 191.6 | 215.0 | 305.0 | 342.8 | 360.6 | 382.4 |
| Department of Commerce | 77.9 | 88.0 | 86.0 | 93.4 | 114.4 | 108.0 |
| **TOTAL** | **1,351.2** | **1,425.0** | **1,554.0** | **1,701.5** | **1,718.7** | **1,761.7** |

A number of other significant future works are possible. SD could be applied in the field of biotechnology, and could be of use to biological scientists, medical doctors, and pharmaceutical companies. Future predictions can be based on the feedback available from past events. Accumulation of events means that the important characteristics will be considered, because they are reflections of past scenarios. For example, accumulation of capital can contribute significantly to an industry, while accumulation of the debt can be fatal. Therefore, capital assessments are crucial to success.

## References

Azadeh, A., I. M. Fam, M. Khoshnoud, M., and M. Nikafrouz. 2008. Design and implementation of a fuzzy expert system for performance assessment of an integrated health, safety, environment (HSE) and ergonomics system: The case of a gas refinery. *Inf. Sci.* 178:4280–4300.

Eberlein, R. L. 1989. Simplification and understanding of models. *System Dynamics Review* 5:51–68.

Forrester, J. W. 1961. *Industrial dynamics*. Cambridge, MA: Productivity Press.

Forrester, J. W. 1969. *Urban dynamics*. Waltham, MA: Pegasus Communications.

Forrester, J. W. 1971. *World dynamics*. Cambridge, MA: Wright-Allen Press.

Kampmann, C. E. 1996. Feedback loop gains and system behavior. Proceedings of the 1996 International System Dynamics Conference, Albany, NY. Cambridge, MA: System Dynamics Society.

Liehr, M., et al. 2001. Cycles in the sky: Understanding and managing business cycles in the airline market. *System Dynamics Review* 17:311–332.

Marcelloni, F., and M. Vecchio. 2010. Enabling energy-efficient and lossy-aware data compression in wireless sensor networks by multi-objective evolutionary optimization. *Inf. Sci.* 180:1924–1941.

National Nanotechnology Coordination Office (NNCO). 2009. Website of the NNI. http://nano.gov

National Science and Technology Council (NSTC). 2007. National Nanotechnology Initiative, Research and Development Leading to a Revolution in Technology and Industry, Washington, D.C.

National Science and Technology Council (NSTC). 2008. National Nanotechnology Initiative, Research and Development Leading to a Revolution in Technology and Industry, Washington, D.C.

National Science and Technology Council (NSTC). 2009. National Nanotechnology Initiative, Research and Development Leading to a Revolution in Technology and Industry, Washington, D.C.

National Science and Technology Council (NSTC). 2010. National Nanotechnology Initiative, Research and Development Leading to a Revolution in Technology and Industry, Washington, D.C.

Nikulainen, T., and C. Palmberg. 2010. Transferring science-based technologies to industry: Does nanotechnology make a difference? *Technovation* 30:3–11.

Puurunen, K., and P. Vasara. 2007. Opportunities for utilizing nanotechnology in reaching near-zero emissions in the paper industry. *Journal of Cleaner Production* 15:1287–1294.

Radzicki, M., and R. Taylor, 1997. U.S. Department of Energy's Introduction to System Dynamics, A Systems Approach to Understanding Complex Policy 1. http://www.systemdynamics.org/DL-IntroSysDyn/intro.htm

Ronald, N.K., et al. 2007. Global nanotechnology research literature overview. *Technological Forecasting and Social Change* 74:1733–1747.

Stix, G. 2001. Little big science. *Scientific American* 285, http://www.ruf.rice.edu/~rau/phys600/stix.htm

Toumey, C. 2005. Apostolic succession. *Engineering & Science* 1/2:16–23.

WTEC (World Technology Evaluation Center). 1999, 2007, 2008, 2009, 2010. Nanotechnology Research Directions: IWGN Workshop Report Vision for Nanotechnology Research and Development in the Next Decade, WTEC, Loyola College in Maryland.

# 10

# *Safeguard Assessment of Nanoscale Nuclear Material in Nuclear Power Plant Operations Using the Analytic Hierarchy Process and Production Function*

**Taeho Woo**

**CONTENTS**



## 10.1 Introduction

Nuclear power plant (NPP) safeguards are vital because of possible security failures. Nanoscale nuclear material could be used for nonpeaceful purposes by terrorists or nations, for political or financial reasons. These nanoscale nuclear materials are nuclear wastes, nanofluids, nanotechnology applied power cells, nuclear material in space, substances in radiology and oncology, and so on. In the case of NPPs, dangerous attacks as a result of terror or sabotage can happen without warning. The possibility of terrorist attack should be estimated using random number sampling and numerical quantification. It is suggested that the safeguards make use of the regulations of the related systems. The perception is that pending nuclear disarmament, world security is better served with fewer rather than more nuclear weapons and nuclear weapon states (IAEA [International Atomic Energy Agency] 2004). In addition, safeguards have been studied in several industrial areas (Johnson 2010; Yun et al. 2009; Zhong et al. 2006).

Nuclear power plants are used for the modeling of this study. The NPPs in operation in the Republic of South Korea since 1978 are listed in Table 10.1 (KHNP [Korea Hydro and Nuclear Power] 2009). The first group includes

**TABLE 10.1**

Operating NPPs in the Republic of South Korea (2010)

| Name | | Power | |
|---|---|---|---|
| **Site** | **Number** | **($MW_e$)** | **Rx Number** |
| Kori | 1 | 586 | 1 |
| | 2 | 650 | 2 |
| | 3 | 950 | 4 |
| | 4 | 950 | 4 |
| Wolsong | 1 | 679 | 2 |
| | 2 | 700 | 3 |
| | 3 | 700 | 3 |
| | 4 | 700 | 3 |
| Younggwang | 1 | 950 | 4 |
| | 2 | 950 | 4 |
| | 3 | 1000 | 5 |
| | 4 | 1000 | 5 |
| | 5 | 1000 | 5 |
| | 6 | 1000 | 5 |
| Ulchin | 1 | 950 | 4 |
| | 2 | 950 | 4 |
| | 3 | 1000 | 5 |
| | 4 | 1000 | 5 |
| | 5 | 1000 | 5 |
| | 6 | 1000 | 5 |

NPPs with 586 megawatt electrical ($MW_e$) power. The second group includes NPPs with 650 $MW_e$ power, although this group also includes 650 and 679 $MW_e$. The first NPP was Kori Unit 1 in 1978. These groups include the five classifications of power generation, which are also factors in the modeling of this chapter. Modeling of secure operations involves comparisons among these five plant types.

Monte Carlo random sampling used with respect to the basic nuclear material flow quantifications. The Analytic Hierarchy Process (AHP) is used when considering safeguards in NPPs. The AHP was created for military analysis, though it is not restricted to military problems. Pairwise comparisons are applied for decision making, which involves matrix-oriented calculations that allow multiple comparisons in simultaneous analyses of unclear and ambiguous matters such as unexpected terror attacks on NPP facilities. Cagno and colleagues worked on a simulation approach based on the AHP to assess the probability of winning in a competitive bidding process where competing bids are evaluated on multiple criteria, assuming the point of view of the contractor (Cagno et al. 2001). Wang and et al. combined the improved AHP and the entropy information methods with the use of linear

combination weighting (Wang et al. 2008). This optimal weighting method takes into account both the subjectivity of the decision maker and the objectivity of numerical data to obtain a comprehensive assessment result. Suh and Han studied a method that adds the first stage, organizational investigation, to traditional risk analysis (Suh and Han 2003). The process utilizes various methodologies such as paired comparison, asset-function assignment tables, and asset-dependency diagrams.

In another modeling, the Cobb–Douglas function is modified to take into account quality of life in the simulation. This is a kind of production function where the nuclear refueling period is emphasized with respect to power production losses. This was done using game theory in security in which stochastic modeling is applied to the reward and cost concept instead of a production function (Sallhammar et al. 2006). Other applications are related to extending life after radiation exposure (Thomas and Jones 2009; Jones et al. 2006). The modeling is discussed in Section 10.2. Section 10.3 presents the results, and conclusions are covered in Section 10.4.

## 10.2 Modeling

Nuclear material is the focus of secure processing in NPPs. Safeguards were applied to all nuclear materials in all nations that had not acquired nuclear weapons and to keep rigorous records of such material. A general configuration of safeguards was shown by the flows of nuclear fuels in NPPs (IAEA 1980, 1981). The literature shows that safeguard monitoring events are analyzed with respect to low enrichment and spent fuels, which are shown in the report of IAEA (IAEA 1980). Another critical report of the IAEA concerns the strategy modeling of diversion of materials to a different storage venue (IAEA 1999), which is shown in Figure 10.1. The report shows the concealments of dummy substitutions which are connected to safeguard measures. The safeguard measures include core discharge monitoring (CDM) and nondestructive assay (NDA). Therefore, the safeguard is related to nuclear fuel monitoring, which was studied by the network effect method of the zero-sum quantification (Woo and Lee 2011). The safeguard measures are shown in Figure 10.1.

With respect to economics, as the monitoring sequence increases, the relative surplus value also increases. Table 10.2 lists the basic nuclear material safeguard conditions. For example, the table shows an alphabetical rating (from A to E) of five types of fuel monitoring conditions, which are assigned at the discretion of the operator. That is to say, the random samplings have different meanings and standard deviations, which are decided based on the power of the reactor and subjective judgment. In this study, three kinds of random samplings are used, with a mean of 0.5 and standard deviations of 0.341, 0.477, and 0.499.

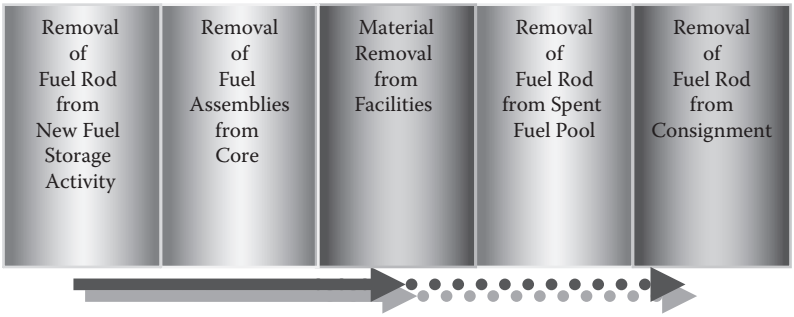


**FIGURE 10.1**
Safeguard measures described by monitoring (safeguard monitoring direction; spent fuel [dotted line], low enrichment fuel [solid line)].

**TABLE 10.2**

Nuclear Material Safeguard Conditions

| Name | Condition |
|---|---|
| A | Removal of fuel rod from new fuel storage activity |
| B | Removal of fuel assemblies from core |
| C | Material removal from facilities |
| D | Removal of fuel rod from spent fuel pool |
| E | Removal of fuel rod from consignment |

The AHP was created by Saaty (1980). The Saaty method is widely used for modeling of social and economic matters. Saaty used this process in applications ranging from the choice of a school for his son to the planning of transportation systems for the Sudan. The basic principle is described by a relevant example (Coyle 2004). Your company is considering the purchase of a new piece of equipment of a certain type, and four factors will govern its choice: expense, *E*; operability, *O*; reliability, *R*; and adaptability for other uses, or flexibility, *F*. The manufacturers of that equipment have offered three options, *X*, *Y*, and *Z*. The engineers of the company have looked at these options and decided that *X* is cheap and easy to operate, but is not very reliable and could not easily be adapted to other uses. Option *Y* is somewhat more expensive, is reasonably easy to operate, and is very reliable, but not very adaptable. Finally, *Z* is very expensive, not easy to operate, is a little less reliable than *Y*, but is claimed by the manufacturer to have a wide range of alternative uses. The object of the analysis is to determine how *X*, *Y*, and *Z* will satisfy the firm's requirements to differing extents, and determine which option best meets the firm's needs.

It is difficult to control nuclear materials, which are characteristically enclosed in containers. So it is reasonable to quantify the basic event by random sampling using the Monte Carlo method, although the quantification

**TABLE 10.3**

Saaty's Scale for Comparisons*

| Number | Meaning |
|---|---|
| 1 | Two elements are equally important |
| 3 | One element is slightly more important than another |
| 5 | One element is strongly more important than another |
| 7 | One element is very strongly more important than another |
| 9 | One element is extremely more important than another |
| 2, 4, 6, 8 | Intermediate values |

* Modified from Saaty, T. L. 1980. *The Analytic Hierarchy Process*. New York: McGraw Hill.

of AHP is usually obtained by the survey of an expert group. In addition, dynamic quantification requires repeated numerical assessments during the life cycle. Random number generation can be used for these repeated numbers. The Saaty comparison rating scale is shown in Table 10.3.

The Saaty scale is used in the numerical rating for fuel monitoring. The consistency (λ) calculation is obtained using the following weighting multiplication. Each element of $a_{ii}$ is shown in the matrix in Equation (10.1).

$$\text{Weighting multiplication} = \begin{bmatrix} a_{11}a_{11}a_{11}a_{11}a_{11} \\ a_{21}a_{22}a_{23}a_{24}a_{25} \\ a_{31}a_{32}a_{33}a_{34}a_{35} \\ a_{41}a_{42}a_{43}a_{44}a_{45} \\ a_{51}a_{52}a_{53}a_{54}a_{55} \end{bmatrix} \begin{bmatrix} W_1 \\ W_2 \\ W_3 \\ W_4 \\ W_5 \end{bmatrix} \tag{10.1}$$

$$\text{Consistency } (\lambda) = \frac{\text{Weighting Mult.}}{\text{Weighting}} \tag{10.2}$$

The *C.I.* (consistency index) and *C.R.* (consistency ratio) are obtained for the weighting value and consistency. The random index in Table 10.4 is used for the *C.R.* where the *C.R.* should be 0.1 for the consistency of hierarchy

**TABLE 10.4**

Random Index for Modeling

| Size | 1 | 2 | 3 | 4 | 5 | 6 | 7 | 8 | 9 | 10 |
|---|---|---|---|---|---|---|---|---|---|---|
| RI | 0 | 0 | 0.58 | 0.9 | **1.12** | 1.24 | 1.32 | 1.41 | 1.45 | 1.49 |

distributions (Holder 1990; Drake 1998). So, using the maximum value of λ, *C.I.* and *C.R.* are obtained as follows:

$$C.I. = \frac{\lambda_{\max} - n}{n-1} \tag{10.3}$$

$$C.R. = \frac{C.I.}{\text{Random Consistency Index}} \tag{10.4}$$

The Vensim simulation code is used for developing, analyzing, and packaging high-quality dynamic models (Vensim 2009). Models are constructed graphically or in a text editor. Features include dynamic functions, subscripting (arrays), Monte Carlo sensitivity analysis, optimization, data handling, application interfaces, and more (Vensim 2009).

For the application of economic theories, the production function has been applied to a life quality index that is a function of life expediency, average income, and safety expenditures. This is based on the Cobb–Douglas function (Thomas et al. 2006). The production function was developed by K. Wicksell and the Cobb–Douglas function is used in the field of economics. The nuclear production function (NPF) is applied in the nuclear industry in safeguard situations (Cobb and Douglas 1928). These equations are described as follows:

$$P = (1 - R)S \tag{10.5}$$

$$O_1 = \alpha_1 X^{\beta} P^{\gamma} \tag{10.6}$$

$$O_2 = O_1^{1/\gamma} = \alpha_1^{1/\gamma} X^{\beta/\gamma} P = \alpha_2 X^q P = \alpha_2 X^q \left(1 - R\right) S \tag{10.7}$$

where

$O$ is the operating product (*kW*).
$X$ is the operating product rate (*kW/s*).
$K$ is the original operating product (*kW/s*).
$P$ is the working period(s).
$S$ is the secure spending time(s).
$R$ is a random number from 0.0 to 0.9.
$\alpha$ is the constant number in the NPF based on the Cobb–Douglas formulation.
$\beta$ is the constant number in the NPF based on the Cobb–Douglas formulation.
$\gamma$ is the constant number in the NPF based on the Cobb–Douglas formulation.

$$X = KR \tag{10.8}$$

$$O_2 = \alpha_2 (KR)^q (1-R) S = \alpha_2 K^q S \left( R^q - R^{q+1} \right) \tag{10.9}$$

For the substitution as follows:

$$t = \left( R^q - R^{q+1} \right) \tag{10.10}$$

$$O_2 = \alpha_2 K^q \cdot S \cdot t \tag{10.11}$$

$$dt = \left( qR^{q-1} - (q+1) R^q \right) dR \tag{10.12}$$

For the derivative:

$$\begin{aligned} \frac{dQ_2}{dS} = 0 &= \frac{dQ_2}{dt} \cdot \frac{dt}{dR} \\ &= \alpha_2 K^q \cdot S \cdot \left( qR^{q-1} - (q+1) R^q \right) \\ &= \alpha_2 K^q \cdot S \cdot R^{q-1} \left( q - (q+1) R \right) \end{aligned} \tag{10.13}$$

Therefore,

$$\left( q - (q+1) R \right) = 0 \tag{10.14}$$

$$q = (q+1) R \tag{10.15}$$

$$q = \frac{R}{1-R} \tag{10.16}$$

using $\frac{1}{1-x} = 1 + x + x^2 + x^3 + \cdots$, for $|x| \langle 1$

Therefore

$$O_2 = \alpha_2 (KR)^q (1-R) S = \alpha_2 K^q S \left( R^q - R^{q+1} \right) = Z \cdot \left( \frac{\text{Lifetime}}{\text{Refueling period}} \right) \tag{10.17}$$

where

$Z$ is the total power in the period of interest.
Lifetime is the total operation period, 60 years.
Refueling period is the refueling period, every 18 months.

$$\frac{\alpha_2 K^q S\left(R^q - R^{q+1}\right)}{\left(\frac{\text{Lifetime}}{\text{Refueling period}}\right)} = Z \tag{10.18}$$

If $Z_1$ and $Z_2$ are proposed,

$$Z_1 = \frac{\alpha_2 K_1{}^q S_1\left(R_1{}^q - R_1{}^{q+1}\right)}{\left(\frac{\text{Lifetime}}{\text{Refueling period}}\right)},\ Z_2 = \frac{\alpha_2 K_2{}^q S_2\left(R_2{}^q - R_2{}^{q+1}\right)}{\left(\frac{\text{Lifetime}}{\text{Refueling period}}\right)} \tag{10.19}$$

where $\alpha_2$ are constants. The $S$ value is the secure period, which is the operation period except the refueling period. Therefore, the $Z$ value is how the secure operation is affected by the refueling period. A timeline of operation with nuclear fuel values shows that the refueling period is the least secure time because the security is in a negative situation. It is quantized by the random number, which is shown as follows:

$$S = \frac{60\times 12 - \frac{60\times 12}{18}}{60\times 12} = 1 - \frac{1}{18} \approx 0.944 \tag{10.20}$$

$$\frac{Z_1}{Z_2} = \frac{\alpha_2 K_1{}^q S_1\left(R_1{}^q - R_1{}^{q+1}\right)}{\alpha_2 K_2{}^q S_2\left(R_2{}^q - R_2{}^{q+1}\right)} = \frac{K_1{}^q S_1\left(R_1{}^q - R_1{}^{q+1}\right)}{K_2{}^q S_2\left(R_2{}^q - R_2{}^{q+1}\right)} \tag{10.21}$$

The NPF is defined in Equation (10.21). This is performed repeatedly as the five types of reactors are examined. It is applied for rational values for the two power plants that are to be compared. The Vensim code is used for modeling.

## 10.3 Results

The overview of AHP for safeguard conditions is shown in Figure 10.2. The comparisons of safeguard conditions and the five associated reactors are connected by hierarchy processes in the figure. The results of AHP are obtained by the maximum pair values with multiplications that are decided by reactor type number for maximum values. The maximum values are calculated by the matrices in Tables 10.5 through 10.9. The underlined numbers

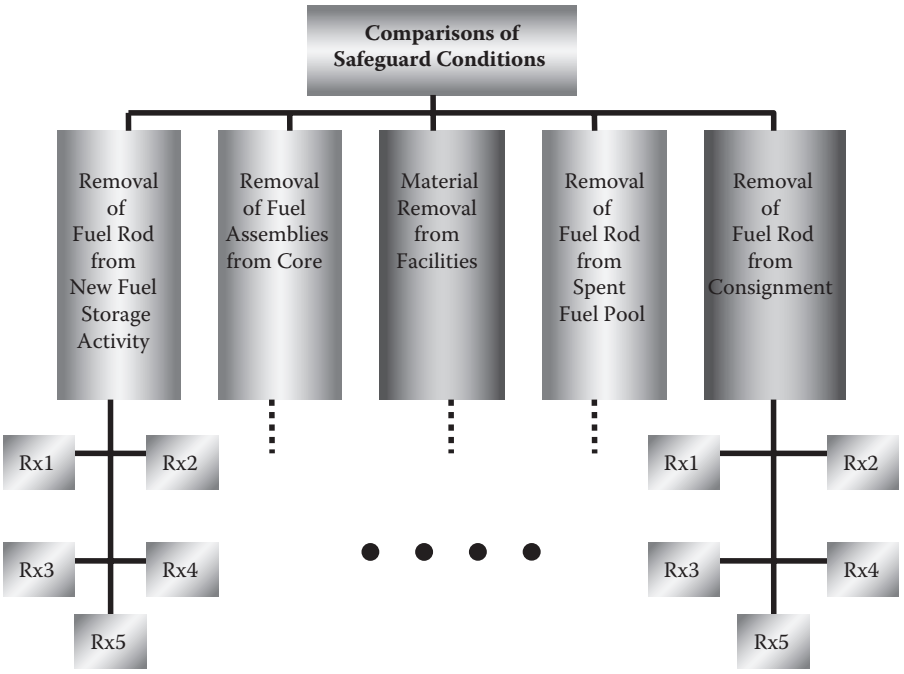


**FIGURE 10.2**
Overview for AHP of safeguard conditions.

are generated by the random sampling, which has different means and standard deviations that are determined based on the power of the reactor and subjective judgment. The diagonal line is obtained by the inverse number as seen in the tables. Table 10.5 is the matrix of the comparison for case A. Five reactors are compared. For example, reactor 1 (Rx# 1) is compared with Rx# 2 as a random number 8 (the underlined number in the cell where the columns for Rx#1 and Rx#2 meet). The diagonal position is written as 1/8. The others are similar to this case. The five columns are repeated from Rx#1 to Rx#5, which are normalized as 1.0. The farthest column to the right is a summation of the five columns as a normalization of the total of 1.0.

This is the first of the 60 runs where the quantification is done one time per year. Table 10.10 shows the weighting and the corresponding values. In the first row, the values are, from left to right, the values from Tables 10.5 through 10.9. The weighting values are produced by matrix calculations. For example, the first blank is found for Rx#1, which is in Equation (10.22). The circled values in Table 10.10 are the maximum and minimum values.

$$0.506 \times 0.0012 + 0.442 \times 0.0041 + 0.516 \times 0.0051 + 0.493 \times 0.0091 + 0.489 \times 0.0041 = 0.011542 \tag{10.22}$$

**TABLE 10.5**

Matrix Table of Comparisons for A (1st Run)

| Rx# | 1 | 2 | 3 | 4 | 5 | 1 | 2 | 3 | 4 | 5 | Relative Rate |
|---|---|---|---|---|---|---|---|---|---|---|---|
| 1 | 1 | 8 | 9 | 7 | 8 | 0.664908 | 0.852972 | 0.493526 | 0.278607 | 0.242424 | 0.506 |
| 2 | 1/8 | 1 | 8 | 9 | 7 | 0.083113 | 0.106622 | 0.43869 | 0.358209 | 0.212121 | 0.24 |
| 3 | 1/9 | 1/8 | 1 | 8 | 9 | 0.073879 | 0.013328 | 0.054836 | 0.318408 | 0.272727 | 0.147 |
| 4 | 1/7 | 1/9 | 1/8 | 1 | 8 | 0.094987 | 0.011847 | 0.006855 | 0.039801 | 0.242424 | 0.079 |
| 5 | 1/8 | 1/7 | 1/9 | 1/8 | 1 | 0.083113 | 0.015232 | 0.006093 | 0.004975 | 0.030303 | 0.028 |
| Total | 1.503968 | 9.378968 | 18.23611 | 25.125 | 33 | 1 | 1 | 1 | 1 | 1 | 1 |

**TABLE 10.6**

Matrix Table of Comparisons for B (1st Run)

| Rx# | 1 | 2 | 3 | 4 | 5 | 1 | 2 | 3 | 4 | 5 | Relative Rate |
|---|---|---|---|---|---|---|---|---|---|---|---|
| 1 | 1 | 7 | 7 | 5 | 1 | 0.402299 | 0.749235 | 0.636364 | 0.353535 | 0.066667 | 0.442 |
| 2 | 1/7 | 1 | 1 | 7 | 5 | 0.057471 | 0.107034 | 0.090909 | 0.494949 | 0.333333 | 0.217 |
| 3 | 1/7 | 1 | 1 | 1 | 1 | 0.057471 | 0.107034 | 0.090909 | 0.070707 | 0.066667 | 0.079 |
| 4 | 1/5 | 1/7 | 1 | 1 | 7 | 0.08046 | 0.015291 | 0.090909 | 0.070707 | 0.466667 | 0.145 |
| 5 | 1 | 1/5 | 1 | 1/7 | 1 | 0.402299 | 0.021407 | 0.090909 | 0.010101 | 0.066667 | 0.118 |
| Total | 2.485714 | 9.342857 | 11 | 14.14286 | 15 | 1 | 1 | 1 | 1 | 1 | 1 |

**TABLE 10.7**

Matrix Table of Comparisons for C (1st Run)

| Rx# | 1 | 2 | 3 | 4 | 5 | 1 | 2 | 3 | 4 | 5 | Relative Rate |
|---|---|---|---|---|---|---|---|---|---|---|---|
| 1 | 1 | 8 | 9 | 7 | 8 | 0.664908 | 0.772118 | 0.464849 | 0.331579 | 0.347826 | 0.516 |
| 2 | 1/8 | 1 | 9 | 4 | 1 | 0.083113 | 0.096515 | 0.464849 | 0.189474 | 0.043478 | 0.175 |
| 3 | 1/9 | 1/9 | 1 | 9 | 4 | 0.073879 | 0.010724 | 0.05165 | 0.426316 | 0.173913 | 0.147 |
| 4 | 1/7 | 1/4 | 1/9 | 1 | 9 | 0.094987 | 0.024129 | 0.005739 | 0.047368 | 0.391304 | 0.113 |
| 5 | 1.8 | 1 | 1/4 | 1/9 | 1 | 0.083113 | 0.096515 | 0.012912 | 0.005263 | 0.043478 | 0.048 |
| Total | 1.503968 | 10.36111 | 19.36111 | 21.11111 | 23 | 1 | 1 | 1 | 1 | 1 | 1 |

**TABLE 10.8**

Matrix Table of Comparisons for D (1st Run)

| Rx# | 1 | 2 | 3 | 4 | 5 | 1 | 2 | 3 | 4 | 5 | Relative Rate |
|---|---|---|---|---|---|---|---|---|---|---|---|
| 1 | 1 | 9 | 7 | 8 | 7 | 0.657106 | 0.867138 | 0.405704 | 0.318584 | 0.21875 | 0.493 |
| 2 | 1/9 | 1 | 9 | 7 | 8 | 0.073012 | 0.096349 | 0.521619 | 0.278761 | 0.25 | 0.244 |
| 3 | 1/7 | 1/9 | 1 | 9 | 7 | 0.093872 | 0.010705 | 0.057958 | 0.358407 | 0.21875 | 0.148 |
| 4 | 1/8 | 1/7 | 1/9 | 1 | 9 | 0.082138 | 0.013764 | 0.00644 | 0.039823 | 0.28125 | 0.085 |
| 5 | 1/7 | 1/8 | 1/7 | 1/7 | 1 | 0.093872 | 0.012044 | 0.00828 | 0.004425 | 0.03125 | 0.03 |
| Total | 1.521825 | 10.37897 | 17.25397 | 25.11111 | 32 | 1 | 1 | 1 | 1 | 1 | 1 |

**TABLE 10.9**

Matrix Table of Comparisons for E (1st Run)

| Rx# | 1 | 2 | 3 | 4 | 5 | 1 | 2 | 3 | 4 | 5 | Relative Rate |
|---|---|---|---|---|---|---|---|---|---|---|---|
| 1 | 1 | 4 | 8 | 8 | 4 | 0.571429 | 0.717489 | 0.598131 | 0.376471 | 0.181818 | 0.489 |
| 2 | 1/4 | 1 | 4 | 8 | 5 | 0.142857 | 0.179372 | 0.299065 | 0.376471 | 0.227273 | 0.245 |
| 3 | 1/8 | 1/4 | 1 | 4 | 8 | 0.071429 | 0.044843 | 0.074766 | 0.188235 | 0.363636 | 0.149 |
| 4 | 1/8 | 1/8 | 1/4 | 1 | 4 | 0.071429 | 0.022422 | 0.018692 | 0.047059 | 0.181818 | 0.068 |
| 5 | 1/4 | 1/5 | 1/8 | 1/4 | 1 | 0.142857 | 0.035874 | 0.009346 | 0.011765 | 0.045455 | 0.049 |
| Total | 1.75 | 5.575 | 13.375 | 21.25 | 22 | 1 | 1 | 1 | 1 | 1 | 1 |

**TABLE 10.10**

Matrix Table of Comparisons (1st Run)

| Rx# | A | B | C | D | E | Weighting | Value |
|---|---|---|---|---|---|---|---|
| 1 | 0.506 | 0.442 | 0.516 | 0.493 | 0.489 | 0.5103 | 0.468425 |
| 2 | 0.24 | 0.217 | 0.175 | 0.244 | 0.245 | 0.3012 | 0.219221 |
| 3 | 0.147 | 0.079 | 0.147 | 0.148 | 0.149 | 0.1348 | 0.182302 |
| 4 | 0.079 | 0.145 | 0.113 | 0.085 | 0.068 | 0.0386 | 0.182302 |
| 5 | 0.028 | 0.118 | 0.048 | 0.03 | 0.049 | 0.0151 | 0.079731 |

**TABLE 10.11**

Pairwise Comparison of Safeguard Measures by Monitoring (1st Run)

| | A | B | C | D | E |
|---|---|---|---|---|---|
| **A** | 1 | 8 | 8 | 6 | 8 |
| **B** | 1/8 | 1 | 8 | 8 | 6 |
| **C** | 1/8 | 1/8 | 1 | 8 | 8 |
| **D** | 1/6 | 1/8 | 1/8 | 1 | 8 |
| **E** | 1/8 | 1/6 | 1/8 | 1/8 | 1 |

**TABLE 10.12**

Consistency (λ) Values

| | A | B | C | D | E | Weighting | Weighting Multiple | Consistency (λ) |
|---|---|---|---|---|---|---|---|---|
| **A** | 1 | 8 | 8 | 6 | 8 | 0.5103 | 4.35105 | 8.52717 |
| **B** | 1/8 | 1 | 8 | 8 | 6 | 0.3012 | 1.84300 | 6.11912 |
| **C** | 1/8 | 1/8 | 1 | 8 | 8 | 0.1348 | 0.66646 | 4.94506 |
| **D** | 1/6 | 1/8 | 1/8 | 1 | 8 | 0.0386 | 0.29979 | 7.77221 |
| **E** | 1/8 | 1/6 | 1/8 | 1/8 | 1 | 0.0151 | 0.15086 | 9.91825 |

The pairwise comparison of safeguard measures by monitoring (1st Run) in Table 10.11 is used to find the *C.I.* (consistency index), *C.R.* (consistency ratio), and consistency (λ) calculations. The underlined numbers are results of random sampling, which has different means and standard deviations decided by the operator. The number of a diagonal line is the inverse number as seen in Table 10.11. In Table 10.12, the matrix calculation is the product of the five columns of the five reactors and the weighting column, which gives the weighting multiplication values. The next column includes consistency values, which are obtained by Equation (10.2). Table 10.12 shows the maximum consistency ($\lambda_{max}$), which represents the highest consistency (λ) values. The *C.I.* and *C.R.* are found using consistency (λ). The *C.R.* in Equation (10.24) shows a less consistent number in the first run because the value is

higher than 0.1. The simulation in this chapter shows the *C.R.* presented in a dynamic manner. The important thing is that the results show the reliability of the value.

$$C.I. = \frac{\lambda_{\max} - n}{n-1} = \frac{7.45636 - 5}{5-1} = 0.614091 \tag{10.23}$$

$$C.R. = \frac{C.I.}{\text{Random Consistency Index}} = \frac{0.614091}{1.12} = 0.548295 \tag{10.24}$$

Total *C.I.* and *C.R.* are found in Figure 10.3. The dotted circles show the minimum value of the *C.R.*; the consistency has the highest values in years 14 and 26 as the lowest values of the *C.I.* and *C.R.* The results are shown as the maximum pair values with multiplications in Figure 10.4(a), accompanied by the reactor number for maximum pair values in Figure 10.4(b). The range of secure operation is between 0.486635 in year 20 and 0.327661 in year 53 during the life cycle of 60 years. The highest value in the range of secure power operation is about 1.4852 times higher than that of the lowest value in this study. The highest and lowest values are seen as dotted circles in the figure, which are values of Rx#1.

The value of the Cobb–Douglas function is described by NPF values in Figure 10.5. The maximum value is 0.642836 and the minimum value is 0.0932656; both cases are for Rx#5. Therefore, the highest value for secure power operation is 6.8925 times higher than the lowest value in this study where the safeguard assessment is quantified mathematically for the NPPs. Figure 10.5 shows the lowest and highest values, where the dotted lines show the trend of NPF values. Using APH and NPF, the nuclear safeguard protocol (NSP) in Figure 10.6 is proposed for the nuclear industry in Korea.

## 10.4 Conclusions

The AHP method incorporated with the NPF has been studied for the secure operation of NPPs. Nuclear fuel behavior is investigated with respect to nanoscale nuclear fuel behavior. As time goes on, the maximum pair values with multiplications in AHP tend to change. It is reasonable to use the Monte Carlo method of random sampling in the relative outputs due to the many uncertainties in safeguard matters. In the AHP method, the oscillations of the values increase; the values of NPF in the Cobb–Douglas function increase steadily. Although the reactors in AHP are changeable by the five types, to control the multifactor comparisons of nuclear fuel flows, the reactors in NPF are just Rx# 3, 4, and 5, which are seen in the dotted circles in Figure 10.5.

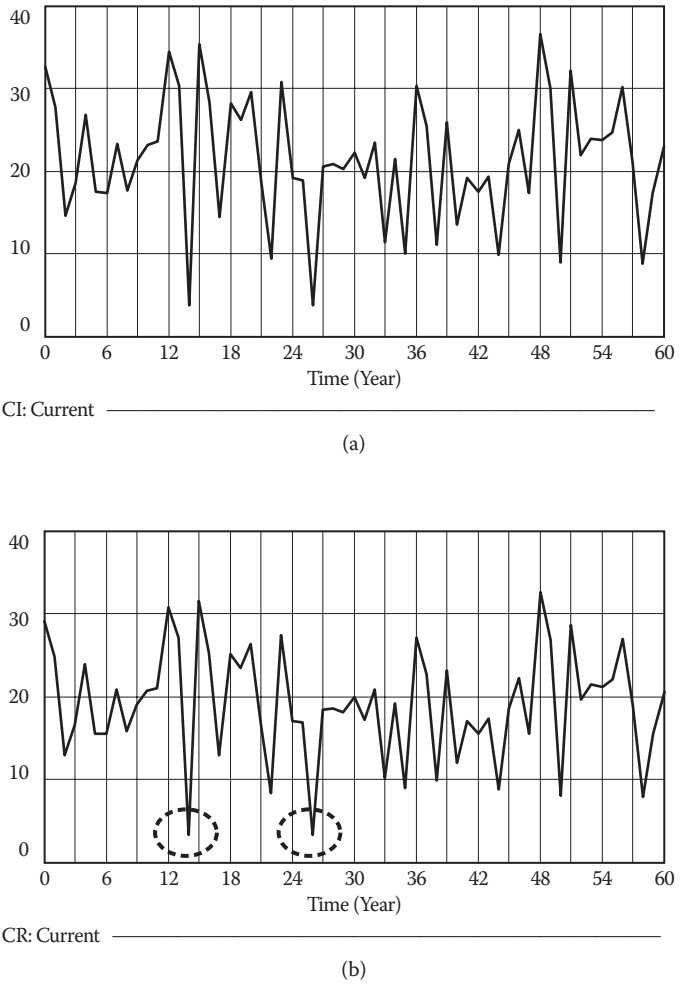


**FIGURE 10.3**
Indexes: (a) C.I. and (b) C.R.

This is a very interesting finding of the study. In the AHP, the values are compared over many characteristics of nuclear material flow. However, in the NPF, the power of the reactor and refueling are considered. Both results show that the highest values are increasing. This means that the security of the reactor is increasing, which is positive for reactor operations. One of the critical purposes of the study is to determine a better security method over a reactor's lifetime. The NPFs are compared simultaneously with respect to NPP safeguards. In the NPF, the algorithm of this work is similar that used in economic matters such as the relationship between gross domestic product (GDP) and personal GDP per capita. Hence, it is necessary to find the

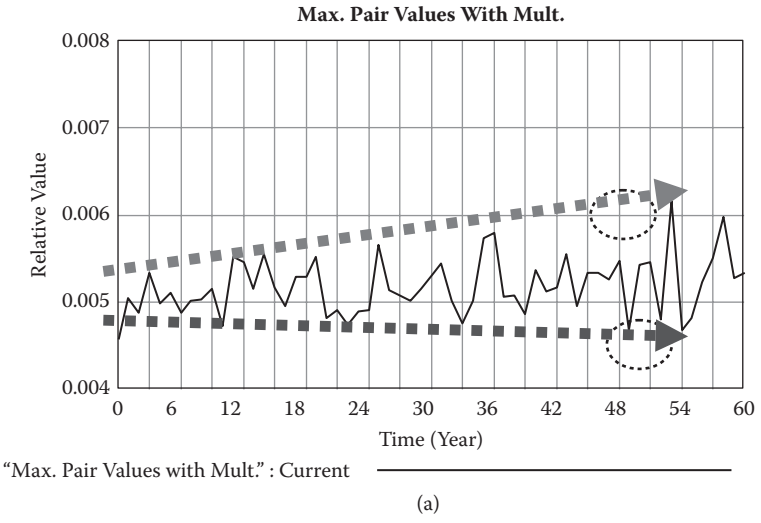


(a)

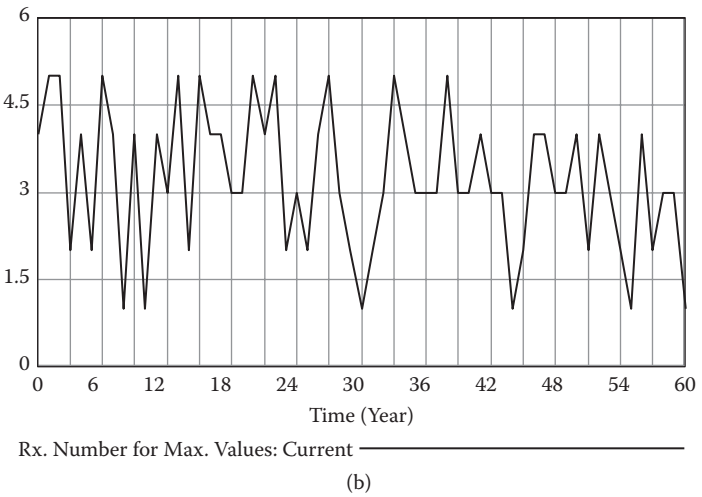


(b)

**FIGURE 10.4**
Maximum value comparison: (a) maximum pair values with multiplications, (b) Rx number for maximum pair values.

NPFs of all plants. The summary of the two methods is shown in Table 10.13. These different methods complement each other and help to create an NSP for NPPs of interest. Using these two methods could result in higher reliable values. This comparison is necessary to quantify security, because there are many uncertainties in economic, political, and social matters. Important points of this study are as follows:

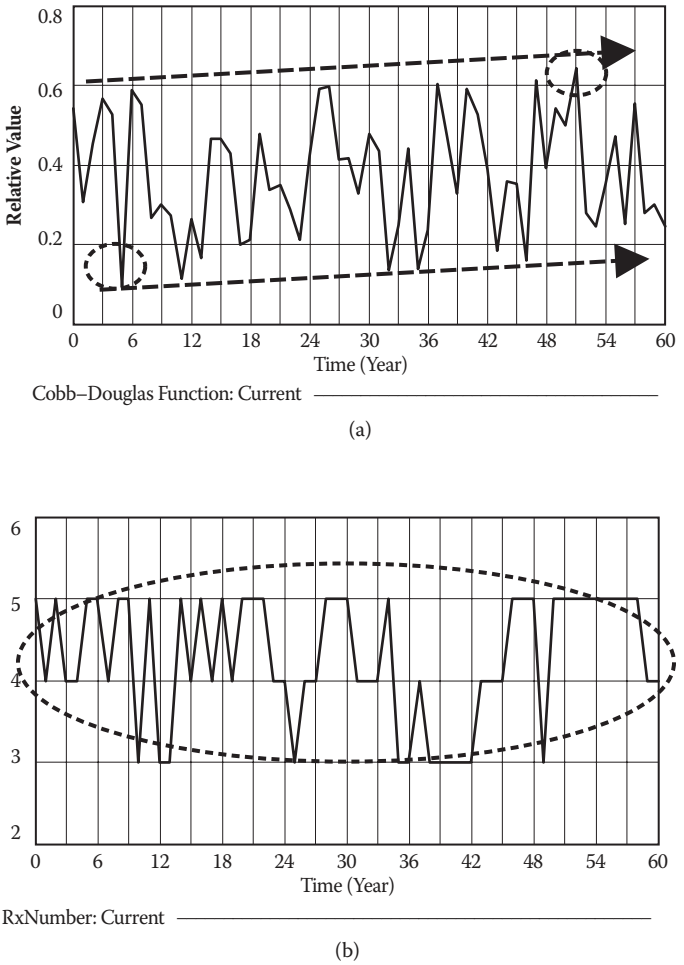


**FIGURE 10.5**
Value comparisons: (a) production function value by Cobb–Douglas function, (b) reactor number for production function value by Cobb–Douglas function.

- Quantification of the safeguard estimates is performed to enhance operation safety.
- Maximum pair values with multiplications are obtained by AHP for more secure situations.
- Dynamic simulations performed by using an energy policy for safeguard assessments are analyzed.
- Comparisons using NSP are useful for enhancing security.
- Better operation skill is developed using AHP and NPF.

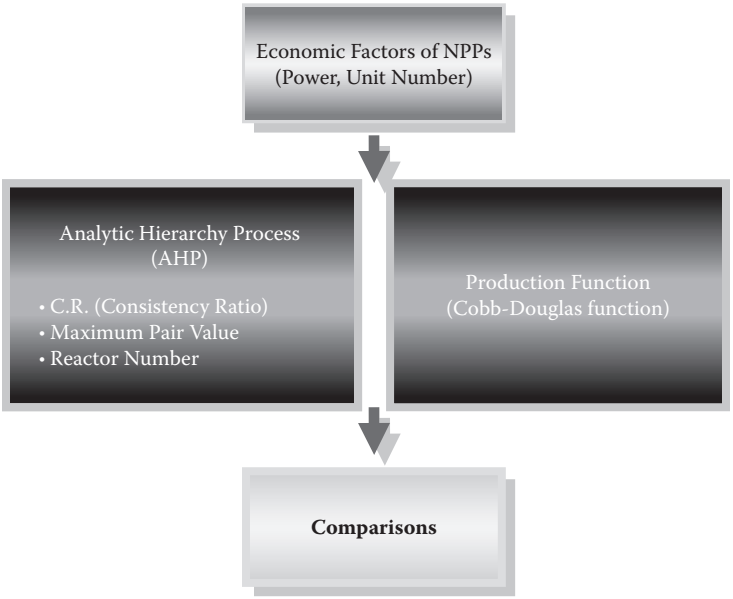


**FIGURE 10.6**
Nuclear Safeguard Protocol (NSP).

**TABLE 10.13**
Comparison of AHP and NPF

| | **AHP** | **NPF** |
|---|---|---|
| Factor | Multifactor comparisons | Power, life, and refueling time |
| Basic element | Random sampling | Random sampling |
| Data reliability | Consistency evaluation | — |
| Result | Maximum pair values are oscillating | Cobb–Douglas function values are steadily increasing |
| Estimation | Multifactors are considered simultaneously | Economic factors are considered |

The expenses for safeguard enhancements have increased as a result of actual and potential terrorist incidents. It is, however, possible to save funds by simulating cases using the above study. In addition, the NSF can be applied in other industries such as the airline or chemical industry, for better estimations. However, large-budget industries need quantified regulations to better safeguard operations, and terror incidents could be prevented by the technological estimation of the AHP and NPF methods. Finally, security management in the nuclear industry could be modeled using this study.

## References

Cagno, E., F. Caron, and A. Perego. 2001. Multi-criteria assessment of the probability of winning in the competitive bidding process. *International Journal of Project Management* 19:313–324.

Cobb, C. W., and P. H. Douglas. 1928. A theory of production. *American Economic Review* 18:139–165.

Coyle, G.. 2004. *The Analytic Hierarchy Process*, Upper Saddle River, NJ: Pearson Education Ltd.

Drake, P. R. 1998. Using the Analytic Hierarchy Process in engineering education. *International Journal of Engineering Education* 14:191–196.

Holder. R. D. 1990. Some comment on the Analytic Hierarchy Process. *Journal of the Operational Research Society* 41:1073–1076.

IAEA (International Atomic Energy Agency). 1980. *IAEA safeguards: Guidelines for states' systems of accounting for and control of nuclear materials*. IAEA Safeguards Information Series No. 2. Vienna: IAEA.

IAEA (International Atomic Energy Agency). 1981. *IAEA safeguards: An introduction*. IAEA Safeguards Information Series No. 3. Vienna: IAEA.

IAEA (International Atomic Energy Agency). 1999. *Design measures to facilitate implementation of safeguards at future water cooled nuclear power plants*. Technical Reports Series No. 392. Vienna: IAEA.

IAEA (International Atomic Energy Agency). 2004. *Guidelines and format for preparation and submission of declarations pursuant to articles 2 and 3 of the model protocol additional to safeguards agreements*. IAEA Services Series No. 11. Vienna: IAEA.

Johnson, R. W., 2010. Beyond-compliance uses of HAZOP/LOPA studies. *Journal of Loss Prevention in the Process Industries* 23:727–733.

Jones R. D., P. J. Thoma, and D.W. Stupples. 2006. Numerical techniques for speeding up the calculation of the life extension brought about by removing a prolonged radiation exposure. *Process Safety and Environmental Protections* 85:269–276.

KHNP (Korea Hydro and Nuclear Power). 2009. *A government report for nuclear power generation*. Korea Hydro & Nuclear Power Co. Ltd.

Sallhammar, K., B. E. Helvik, and S. J. Knapskog. 2006. On stochastic modeling for integrated security and dependability evaluation. *Journal of Networks* 1:31–42.

Saaty, T. L. 1980. *The Analytic Hierarchy Process.* New York: McGraw Hill International.

Suh, B., and I. Han. 2003. The IS risk analysis based on a business model. *Information & Management* 41:149–158.

Thomas, P. J., and R. D. Jones. 2009. Numerical techniques for speeding up the calculation of the life extension brought about by removing a prolonged radiation exposure. *Process Safety and Environmental Protections* 87:161–174.

Thomas, P. J., D. W. Stupples, and M. A. Alghaffar. 2006. The extent of regulatory consensus on health and safety expenditure, Part 1: Development of the J-value technique and evaluation of regulators' recommendations. *Process Safety and Environmental Protections* 84:329–336.

Vensim. 2009. Vensim Simulation Software.

Wang, J. J., Y. Y. Jing, C. F. Zhang, X. T. Zhang, and G. H. Shi. 2008. Integrated evaluation of distributed triple-generation systems using improved grey incidence approach. *Energy* 33:1427–1437.

Woo, T., and U. Lee. 2011. Safeguard management for operation security in nuclear power plants (NPPs). *Annals of Nuclear Energy* 38(2–3):167–174.

Yun, G.., W. J. Rogers, and M. S. Mannan. 2009. Risk assessment of LNG importation terminals using the Bayesian–LOPA methodology. *Journal of Loss Prevention in the Process Industries* 22:91–96.

Zhong M., T. Liu, Y. Deng, et al. 2006. Safety evaluation: Important safeguard of work safety for enterprises in China. *Journal of Loss Prevention in the Process Industries* 19:762–768.

# 11

# *Investigation of Safeguards Management for Operation Security of Nanoscale Nuclear Material in Nuclear Power Plants Using Game Theory*

**Taeho Woo**

**CONTENTS**



## 11.1 Introduction

After the terror attack on the World Trade Center in the United States, safeguards in industrial facilities have become more important. The nuclear industry in particular has been interested in developing a better method for safe operations involving nanoscale nuclear material. Increasing the power using the power uprate method has been used in nuclear power plants (NPPs). Currently, the demand for electricity has been offset by increasing power rates in conventional NPPs. New construction of a power plant is very costly. As an alternative, power uprate of existing NPPs has been used frequently. Power uprate means the increase of the maximum power level at which a commercial nuclear power plant may operate.

Safeguard management with respect to power uprates has been done with a nonlinear algorithm that considers neutronics and thermohydraulics of nuclear reactions as the characteristics of interest. In the United States, there are 55 units in stretch power uprate (SPU), 34 units in measurement uncertainty recapture (MUR), and 12 units in extended power uprate (EPU) (Lee et al. 2004). Power uprates are based on the magnitude of the power increase and the uprate methods (U.S. NRC [U.S. Nuclear Regulatory Commission] 2003). MUR power uprates result in power level increases that are less than 2 percent and are achieved by implementing enhanced techniques for calculating reactor power. SPU uprates involve power level increases of up to 7 percent, and do not generally involve major plant modifications. The power level increases in EPUs are greater than those for SPUs and usually require significant modifications to major plant equipment.

A utility will usually refuel a reactor with slightly more enriched uranium fuel or a higher percentage of new fuel to increase the reactor's power (U.S. NRC 2008). Safety factors involve many NPP components such as pipes, valves, pumps, heat exchangers, electrical transformers, and generators, because increased nuclear power causes changes in the stream and water flow. Consequently, approval from the U.S. Nuclear Regulatory Commission (NRC) is required prior to any changes in a facility's operating licenses and technical specifications, which specify the maximum power level (U.S. NRC 2003). These operating licenses and technical specifications are governed by Title 10 of the Code of Federal Regulations, Part 50.

There are several studies in the literature regarding nuclear safeguards. Matsuoki and coauthors calculated the degree of assurance that nuclear explosive devices would not be manufactured with nuclear materials from a NPP using a simple logic tree and fuzzy linguistic variables (Matsuoka et al. 2002). The work centered on low-enrichment uranium and spent fuel. However, there is a limitation involved in considering terrorist possibilities based on the uranium concentration rate. Rothschild suggested dual safeguard systems (Rothschild 2007). Using the exact evaluation of a single safeguard system, it is expanded as a dual safeguard system using the Monte Carlo algorithm. A dynamic simulation is performed incorporating time steps. Tagami proposed a model of safeguards for *N*-fold multiple barriers with a simple formula (Tagami 1966). The release of fission products is quantified with radioactive diffusion equations. The exponential function is a major component of radioactive release. Some operating NPPs were used in this model.

For these types of investigation, analytic and dynamic methods are performed. Figure 11.1 shows an overview of modeling for the configuration of safe power operation. The dynamic method is done by the quantities of the dynamical scenarios. Section 11.2 explains several factors for modeling. The time-based method for modeling is given in Section 11.3. Section 11.4 shows results of the study and conclusions are offered in Section 11.5.

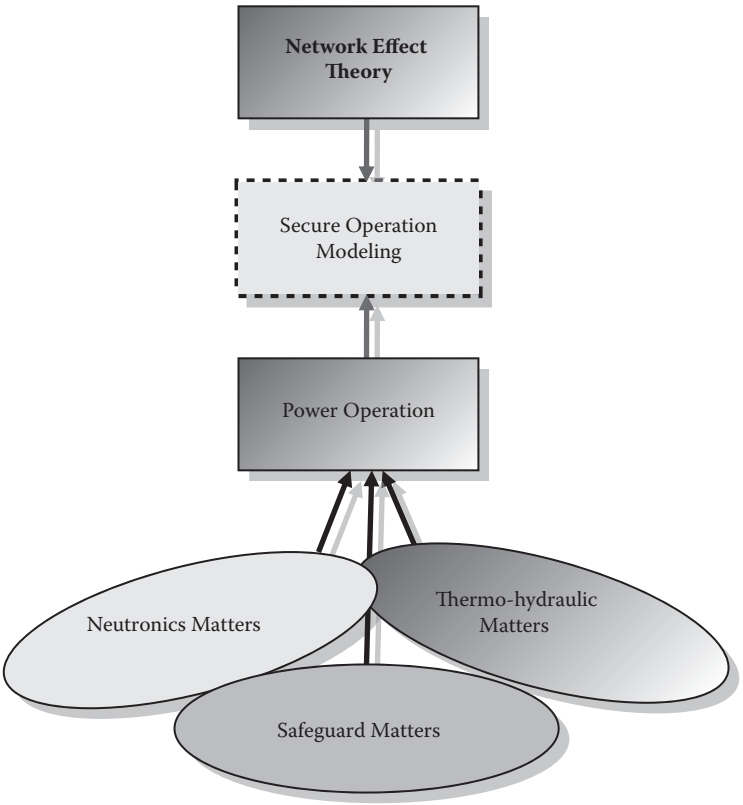


**FIGURE 11.1**
Overview of modeling.

## 11.2 Factors for Modeling

### 11.2.1 Safeguard Measures Factor (SMF)

Safeguards have been analyzed by the meaning of the regulations. In the late 1950s and the 1960s, as nations started to trade in nuclear plants and fuel, safeguard regulations began. The next phase was a growing perception that, "pending nuclear disarmament, world security is better served with fewer rather than more nuclear weapons and nuclear weapon states" (IAEA [International Atomic Energy Agency] 2004). The method was to apply safeguards on all nuclear material in the countries that had not acquired nuclear weapons, and to keep rigorous accounts of such material. Figure 11.2

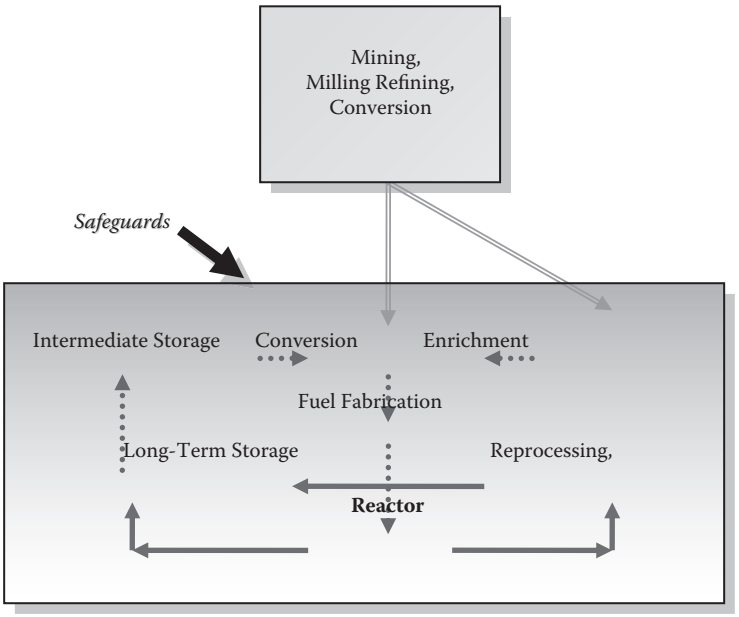


**FIGURE 11.2**
Configuration of safeguards in the nuclear fuel cycle. Solid line: spent fuel; dotted line: low-enrichment fuel; double line: yellow cake and natural uranium. Adapted from IAEA (International Atomic Energy Agency). 1981. *IAEA safeguards: An introduction*, IAEA Safeguards Information Series No. 3. Vienna: IAEA.

illustrates the flow of nuclear fuels that must be considered in configuring safeguards for NPPs, which is based on a report of the IAEA (IAEA 1981). The elements of safeguard monitoring are shown in Figure 11.3, which is also modified from a report of the IAEA (IAEA 1981). The simplified safeguard configuration for a power uprate focuses on the flows of spent fuel and low-enrichment fuel in Figures 11.2 and 11.3. Safeguard monitoring is based on the diversion strategy model. Figure 11.4 illustrates the diversion strategy model, which is also based on a report of the IAEA (IAEA 1999). Each step is related to the concealment of dummy substitutions, which are related to the safeguard measures. This is quantified as the safeguard measures factor (SMF). The safeguard measures are composed of core discharge monitoring (CDM) and nondestructive assay (NDA).

Power uprates are related to nuclear fuels, and safeguard monitoring is important for NPPs. In addition, the nuclear fuel concentration is also of importance with respect to safeguards. The power increase is a higher load to the turbine that generates the electricity. The containment must be able to withstand the increased power load, which could impact the reactor and lead to an accident.

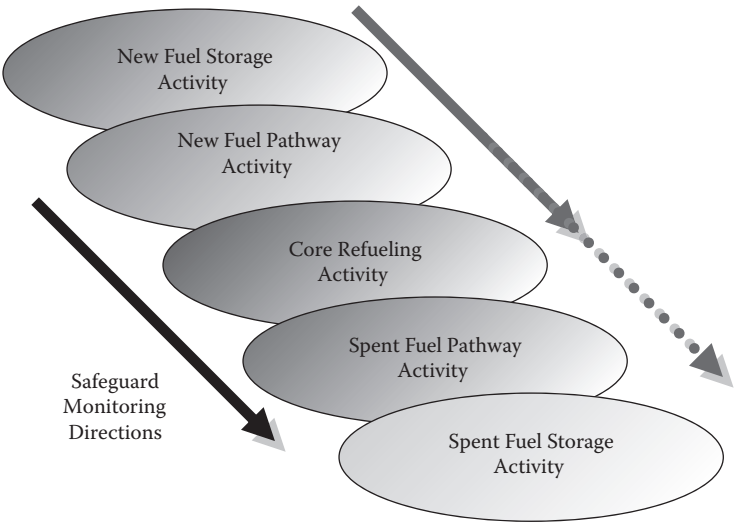


**FIGURE 11.3**
Elements of safeguard monitoring. Dotted line: spent fuel; solid line: low-enrichment fuel. Adapted from IAEA (International Atomic Energy Agency). 1981. *IAEA safeguards: An introduction*, IAEA Safeguards Information Series No. 3. Vienna: IAEA.

### 11.2.2 Power Uprates Factor (PUF)

Table 11.1 shows the number of power uprate approvals in the United States (U.S. NRC 2008). Table 11.2 shows some selected the power uprates in the United States from 1977 to 2011 along with the year in which the approval was granted (U.S. NRC 2008). Table 11.3 shows the expectations for power uprates approvals in the United States as of 2008 (U.S. NRC 2008). The dynamic preparation of the event scenarios is characterized by linear connections. The power uprates factor (PUF) is used for the quantification of each NPP (PUF is seen in Table 11.6). This is based on the relative values of the uprate percent power. The random numbers are generated by the Vensim code system. Vensim is used for developing, analyzing, and packaging high-quality dynamic models (Vensim 2009). Models are constructed graphically or in a text editor. Features include dynamic functions, subscripting (arrays), Monte Carlo sensitivity analysis, optimization, data handling, application interfaces, and more (Vensim 2009).

There are two kinds of random numbers—the (a) mean = 0.5, standard deviation = 1 σ and (b) mean = 0.5, standard deviation = 2 σ. The random numbers are uniformly distributed. The secure distribution has a narrower shape than the nonsecure distribution, which means that *nonsecure* is a much more uncertain situation than the larger standard deviation. Figure 11.5 shows the random number generator, which selects random numbers as 0.0

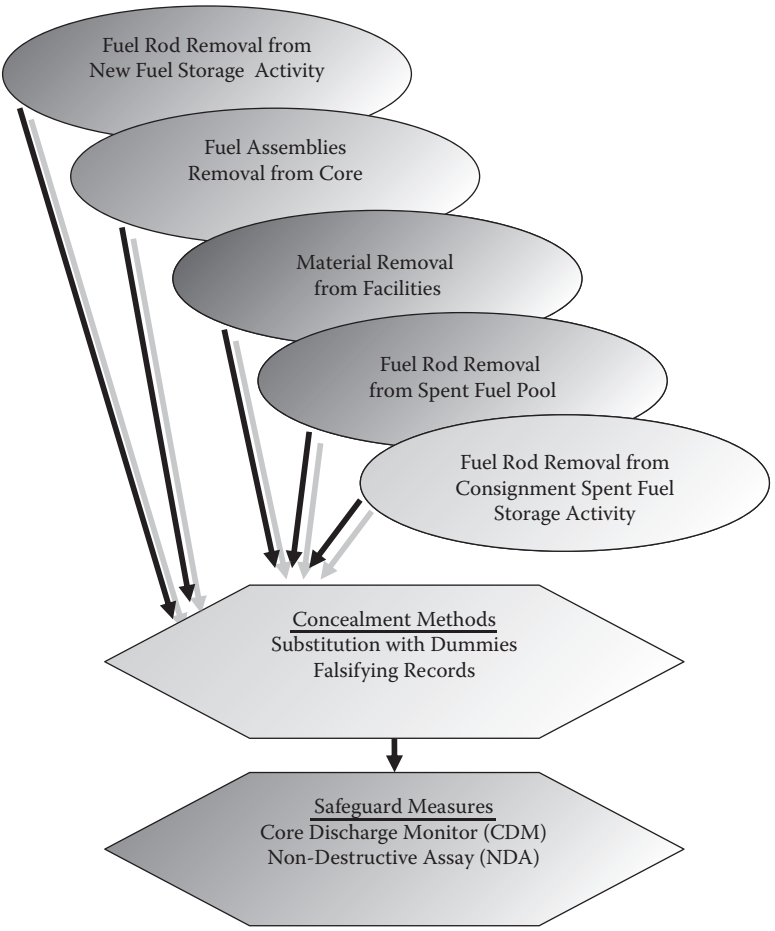


**FIGURE 11.4**
Safeguard measures factor (SMF) by monitoring. (Adapted from IAEA (International Atomic Energy Agency). 1999. *Design measures to facilitate implementation of safeguards at future water cooled nuclear power plants*, Technical Reports Series, Vienna: IAEA.)

**TABLE 11.1**

Power Uprate Approvals in the United States

| Name | Units |
|---|---|
| Stretch power uprate (SPU) | 55 |
| Measurement uncertainty recapture (MUR) | 34 |
| Extended power uprate (EPU) | 12 |

*Source:* Data from U.S. NRC (Nuclear Regulatory Commission). 2008. *Power uprates for nuclear plants, backgrounder*. Washington, DC: Office of Nuclear Reactor Regulation.

**TABLE 11.2**

Selected Power Uprates in the United States

| Number | Plants | % Uprates | $MW_{th}$ | Approved Year | Type |
|---|---|---|---|---|---|
| 1 | Calvert Cliffs 1 | 5.5 | 140 | 1977 | S |
| 2 | Monticello | 6.3 | 105 | 1998 | E |
| 3 | Comanche Peak 2 | 1 | 34 | 1999 | MUR |
| 4 | ANO-2 | 7.5 | 211 | 2002 | E |
| 5 | Match 1 | 1.5 | 41 | 2003 | MUR |
| 6 | Susquehanna 1 | 13 | 463 | 2008 | E |

*Note:* Type: S = Stretch; MUR = measurement uncertainty recapture; E = Extended.
*Source:* Data from U.S. NRC (Nuclear Regulatory Commission). 2008. Power uprates for nuclear plants, backgrounder. Washington, DC: Office of Nuclear Reactor Regulation.

**TABLE 11.3**

Power Uprate Expectations in the United States

| Fiscal Year | Stretch Power Uprates | Measurement Uncertainty Recapture Uprates | Extended Power Uprates | Total Uprates Expected | Thermal Power ($MW_{th}$) |
|---|---|---|---|---|---|
| 2008 | 0 | 2 | 2 | 4 | 804 |
| 2009 | 0 | 5 | 6 | 11 | 1,966 |
| 2010 | 0 | 0 | 6 | 6 | 1,368 |
| 2011 | 0 | 0 | 2 | 2 | 895 |
| 2012 | 0 | 0 | 1 | 1 | 221 |
| Total | **0** | **7** | **17** | **24** | **5,254** |

*Source:* Data from U.S. NRC (Nuclear Regulatory Commission). 2008. Power uprates for nuclear plants, backgrounder. Washington, DC: Office of Nuclear Reactor Regulation.

from 0.001 to 1 based on the power uprate. This is used for the power uprates measures (PUMs) expressed as a percent power uprate.

Therefore, in Figure 11.5, each dot is increasing linearly up to a 10% power uprate, because the maximum power uprate for most NPPs is 10% for the examples in Table 11.6. For the translation of the figure into a graph of the distribution function of power uprates in Table 11.6, the random number selector is 0.4 in Calvert Cliffs 1, because the uprate is 5.5%, which is a value between 5.0 and 5.9.

### 11.2.3 Refueling Factor (RF)

Security of an NPP is extremely important during a refueling period because there are unexpected fuel losses, so this period is considered to be an operational uncertainty. The refueling cycle is assumed as 18 months. The quantifications

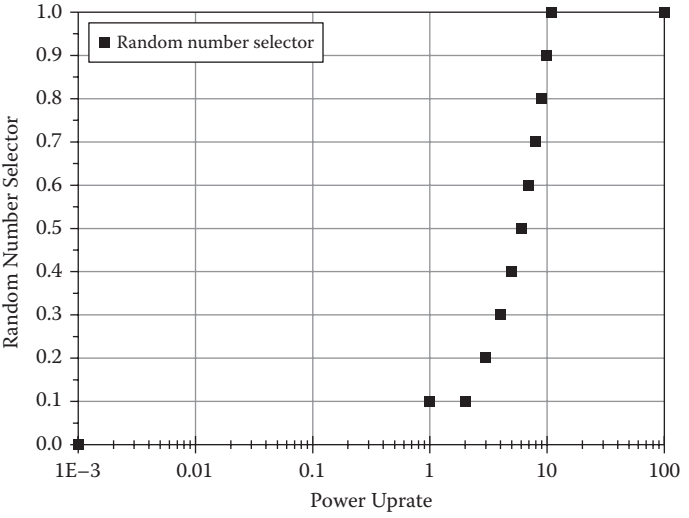


**FIGURE 11.5**
Random number selector.

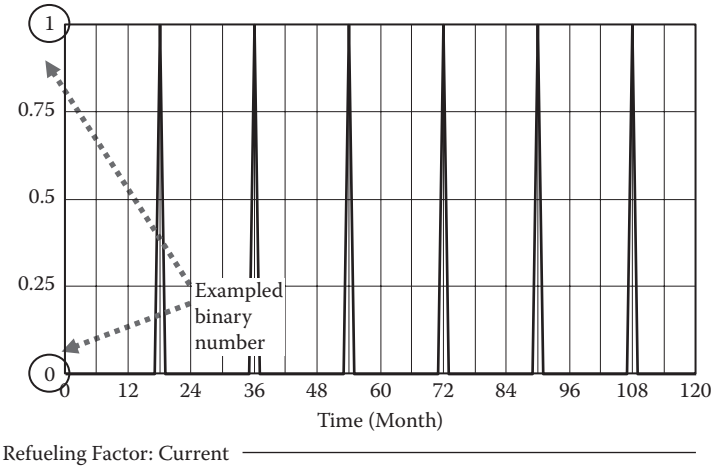


**FIGURE 11.6**
Refueling factor (RF) by refueling.

are done using the binary numbers 0 and 1. That is, this is quantized as a value 1 during the one-month refueling period in every 18 months (see Figure 11.6). This value is converted to 0 for the refueling factor (RF), so the random sampling is done as 0.0 in the power production calculation. This means that the possibility of successful operation is very poor when refueling is performed because of the possibility of fuel theft and other issues. Hence, the effect of this value on the operation success is going to be negative.

## 11.3 Dynamic Method

### 11.3.1 Network Effect

When using a nonlinear algorithm, a network effect is introduced where one user's actions with respect to the good or service can affect the product's value to other users. Network effects arise when a user wants compatibility with other users so that he can interact or trade with them; this creates economies of scope among different users' purchases (Farrell and Kelmperer 2007). The value of a product increases as more people use it due to the network effect. One classic example is the telephone. The telephone is more valuable to each owner as more people have telephones. Since a user may purchase a phone without intending to create value for other users, this creates a positive externality. The most important issue in the network effect is how users connect to each other. The Monte Carlo method can be used to predict a mutual event scenario like the telephone connection. Random number sampling is used to determine the value of the event that is designed and used in this chapter's model.

Network effect can be viewed using game theory. This is expressed by the matrix form in Table 11.4. One can create an example involving safeguards. There are two cases, A and B, for which there are two situations, secure and nonsecure. The summations or subtractions of each element are calculated. The value of the matrix is zero for a zero-sum game (Samuel 2004). In another kind of game theory, a cooperative game is defined for a group players (Bilbao 2000). If one chooses a pair $(N,k)$ where $N$ is the set of players. The characteristic function is as follows:

$$k:2^N \to H$$

This also meets $k(\varnothing)=0$.

Historically, network effects were a central theme in the arguments of T. Vail, the first postpatent president of Bell Telephone, in gaining a monopoly on U.S. telephone services. In 1908, there were many local and regional telephone exchanges, most of which were eventually merged into the Bell System. In 1917, the economics of network effects were reported by N. Lytkins. Network effects were more recently popularized by R. Metcalfe (*Forbes* 2007), who insisted that customers needed Ethernet cards, one kind of network adapter that supports the Ethernet standard for high-speed network connections via

**TABLE 11.4**

Matrix of Game Theory

| Classification | Secure A | Secure B |
|---|---|---|
| Nonsecure A | Secure A–Nonsecure A | Secure B–Nonsecure A |
| Nonsecure B | Secure A–Nonsecure B | Secure B–Nonsecure B |

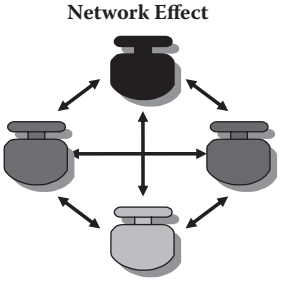


**FIGURE 11.7**
Network effect model.

cables, to grow above a certain critical mass if the company were to reap the benefits of their network in selling the product. He said that the cost of cards was directly proportional to the number of cards installed, but the value of the network was proportional to the square of the number of users. This can be expressed mathematically as having a cost of $N$ and a value of $N^2$.

In other words, the connections in a network of a number of nodes $N$ can be written mathematically as the triangular number of $N(N - 1)/2$. This is proportional to $N^2$ asymptotically. R. Beckstrom presented a mathematical model for describing networks by a state of positive network effect at BlackHat and Defcon in 2009. This also presented the inverse network effect with an economic model for defining it (*Forbes* 2009). J. Schachter created an online system (website) that included a list of links that he found valuable. When site visitors began submitting related sites, he said that even if no other user joined, the system would still be valuable to him (Schachter 2006).

The network effect in this study is based in game theory. Hence, the theoretical background is explained (Fernandez 1998, Miller 2003, Rasmusen 2006). Interactions of cases like the secure and the nonsecure safeguard cases are shown by the connecting lines in Figure 11.7. The nodes and links are the interaction case numbers. As previously stated, it is $N^2$. However, the case in this study is $N \times 2$, because the interaction numbers are just the secure and the nonsecure cases. This is shown in Figure 11.8.

### 11.3.2 Model Calculation

Figure 11.9 shows the event networks for secure power operations in NPPs. There are the three major submodels for power uprates of NPPs—neutronics matters, thermohydraulic matters, and safeguard matters—all of which affect secure power operations. Neutronics refers to neutron behavior analysis where energy and dynamics of neutrons are quantified. Neutronics is critical for NPPs because nuclear energy is produced by nuclear fuel. Therefore, the neutronics matters include fuel temperature, fuel uncertainty, power production, and nuclear data files. These factors are important elements that affect the energy of nuclear fuel. Each factor is quantified using the Monte

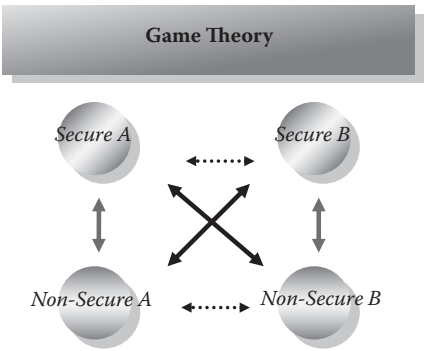


**FIGURE 11.8**
Configuration for the basic events of game theory. Straight lines: interactions; dotted lines: possible interactions.

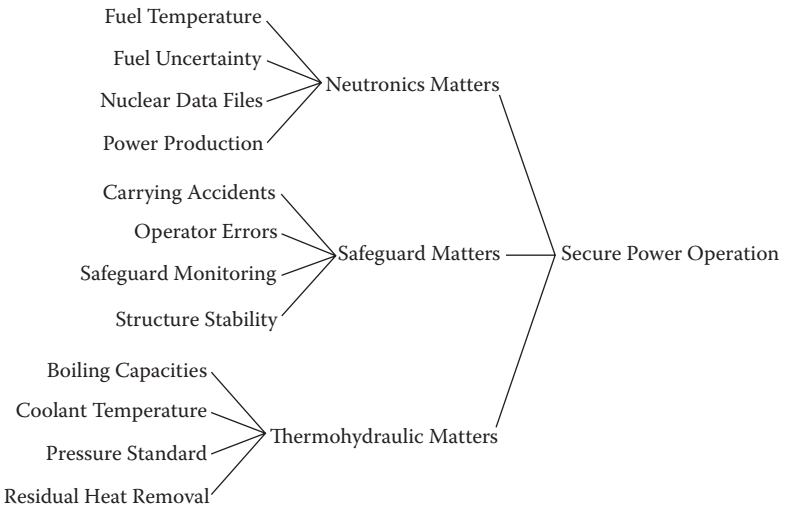


**FIGURE 11.9**
Event networks of secure power operation in NPPs.

Carlo simulation of random sampling in Table 11.5. For example, in the case of fuel temperature, the random number is decided by the random number selector, which is obtained by the PUF in selected NPPs in Figure 11.5. That is, the random number is selected as 0 from 0.001 to 1 of the power uprate in Figure 11.5. The random number is generated as a uniform number between 0 and 1. There are elective PUFs in Table 11.6, which are decided by the random number selector. The model for this study is the Monticello NPP with a 6.3% power uprate. Therefore, the fuel temperature indicates how safe operation is affected by the nuclear fuel concentration change as a result of a power uprate. In addition, when the random value for fuel uncertainty and

**TABLE 11.5**

Values of Basic Elements

| Classification | | Plausible Value |
|---|---|---|
| Neutronics Matters | Fuel Temperature | Power Uprate Factor (PUF) |
| | Fuel Uncertainty | Random # Factor < 0.5 [0, 1] |
| | Power Operations | Random # < Refueling Factor (RF) [0, 1] |
| | Nuclear Data Files | Random # Factor < 0.5 [0, 1] |
| Thermohydraulic Matters | Coolant Temperature | Random # Factor < 0.3 [0, 2] |
| | Pressure Standard | Random # Factor < 0.8 [0, 1] |
| | Residual Heat Removal | Random # Factor < 0.3 [0, 1] |
| | Boiling Capacities | Random # Factor < 0.5 [0, 1] |
| Safeguard Matters | Fuel Concentration | Random#<Safeguard Measures Factor (SMF) [0, 2] |
| | Structure Stability | Random # Factor < 0.5 [0, 1] |
| | Carrying Accidents | Random # Factor < 0.5 [0, 1] |
| | Operator Errors | Random # Factor < 0.5 [0, 1] |

**TABLE 11.6**

Power Uprate Factor (PUF) in Selected NPPs

| Number | Plants | % Uprates | $MW_{th}$ | Plausible Value |
|---|---|---|---|---|
| 1 | Calvert Cliffs 1 | 5.5 | 140 | Random # < 0.4 [0, 1] |
| 2 | Monticello | 6.3 | 105 | Random # < 0.5 [0, 1] |
| 3 | Comanche Peak 2 | 1 | 34 | Random # < 0.1 [0, 1] |
| 4 | ANO-2 | 7.5 | 211 | Random # < 0.6 [0, 1] |
| 5 | Match 1 | 1.5 | 41 | Random # < 0.1 [0, 1] |
| 6 | Susquehanna 1 | 13 | 463 | Random # < 1.0 [0, 1] |

nuclear data files is lower than 0.5, the value is 0; when it is above 0.5 the value is 1. The value, 0.5, is based on the manager's judgment. The manager's judgment is affected by human psychology. This is defined as the process of drawing conclusions to understand how people solve problems and make decisions (Leighton 2004). Most experimentation on deduction has been carried out on hypothetical thought, in particular, examining how people reason about conditionals (Evans et al. 1993). Operators in experiments use one of two rules of inference. In the *modus ponens* inference, reasoning proceeds as follows:

If A, then B.

A.

Therefore, B.

In the *modus tollens* inference, reasoning is as follows:

If A, then B.
Not B.
Therefore, not A.

About half of the operators decide "not A," and the remainder decide that nothing follows. Operators' choices are based on psychological factors that are incorporated within the operators' judgments. Therefore, psychological decision making is deeply related to the operator's judgment. The values in this study are a result of psychological decision making by the operator.

A plausible value is obtained by random sampling of the interval between 0 and 1. The random number is generated by the subtraction of the nonsecure random number from the secure random number, which reflects the summation or subtraction in the zero-sum method of game theory or the network effect. This means that the secure situation is measured by the subtraction of the nonsecure situation in a random process. The new random number is called a *random # factor*. Fuel uncertainty includes several factors, with the exception of fuel handling at a site. Nuclear data files indicate how secure operations are affected by reasonable nuclear data, such as experiment and experience data, which could be related to accident analysis. In cases of power production, when the random value is lower than the refueling factor, the value is 0; when the random value is higher than the refueling factor, the value is 1. Therefore, the random number is 0.0 when the refueling is done. This means that the secure operation is very risky. Power production indicates how safe operation is affected by the refueling period. The modeling is seen in Figure 11.9.

Thermohydraulic matters involve coolant behavior analysis where the energy of nuclear fuel is transferred to the heat energy of the coolant. This coolant causes the turbine to move and generate electricity. Thermohydraulic matters have four factors: coolant temperature, pressure standard, residual heat removal, and boiling capabilities (see Figure 11.9). These factors are important elements of the heat energy of the coolant. Each factor is quantified using a Monte Carlo simulation of random sampling (see Table 11.5). For coolant temperature, when the random value is lower than 0.3, the value is 0; when the random value is higher than 0.3, the value is 2. The 0.3 value is based on the operator's judgment. A plausible value is obtained by the interval of the random sampling and the given value of 0, 1, or 2 in Table 11.5. For coolant temperature, pressure standard, residual heat removal, and boiling capabilities, safe operations are affected by reactor power, reactor stability, emergency cooling, and severe accident, respectively. The random number is generated by subtracting the nonsecure random number from the secure random number, which is the summation or subtraction in the zero-sum method of game theory or the network effect. The new random number is called a random # factor.

**TABLE 11.7**

Concealment Methods for Safeguard Monitoring

| Content | Plausible Value |
|---|---|
| Fuel rod removal from new fuel storage | Random # < 0.9 [0, 1] |
| Fuel assemblies removal from core | Random # < 0.7 [0, 1] |
| Material facilities removal | Random # < 0.5 [0, 1] |
| Fuel rod removal from spent fuel pool | Random # < 0.3 [0, 1] |
| Fuel rod removal from consignment | Random # < 0.1 [0, 1] |

Figure 11.9 shows the safeguard aspect of modeling, which has four factors: safeguard monitoring, structure stability, carrying accidents, and operator errors. Safeguard monitoring is quantified using the safeguard measures factor (SMF) in this study. Each factor is quantified as a Monte Carlo simulation of random sampling (Table 11.7). The random number is generated as a uniform value between 0 and 1. In case of fuel rod removal from new fuel storage, when the random value is lower than 0.5, the value is 0; when the random value is higher than 0.5, the value is 1. In safeguards monitoring, fuel monitoring is simulated as in Figures 11.2, 11.3, and 11.4. Each factor in Figure 11.3 is quantified as a Monte Carlo simulation of random sampling. That is, the random number is quantified as seen in Table 11.7. The multiplication of all elements is done using the concealment method. This value is used as the safeguard measures factor (SMF) in Table 11.5. Other cases are handled in a similar manner. For structure stability, when the random value is lower than 0.5, the value is 0; when the random value is higher than 0.5, the value is 1. For structure stability, carrying accidents, and operator errors, safe operation is affected by reactor building, fuel carrying accidents, and human errors, respectively. The random number is generated by subtracting the nonsecure random number from the secure random number, which is the summation or subtraction in the zero-sum method of game theory or the network effect. The new random number is called a random # factor.

## 11.4 Results

Figure 11.10 summarizes the connections among the various factors. Figure 11.11 includes four graphs of the simulation results, which were created in the Vensim code system. Figure 11.11(a) shows quantification of neutronics matters, where 4.0 is the most secure value. Figure 11.11(b) is the quantification of thermohydraulic matters, where 5.0 is the most secure value. Quantification of safeguard matters is shown in Figure 11.11(c), where 4.0 is the most secure value. Figure 11.11(d) shows secure power operation where the value is shown as an oscillation. The risk for secure power operation

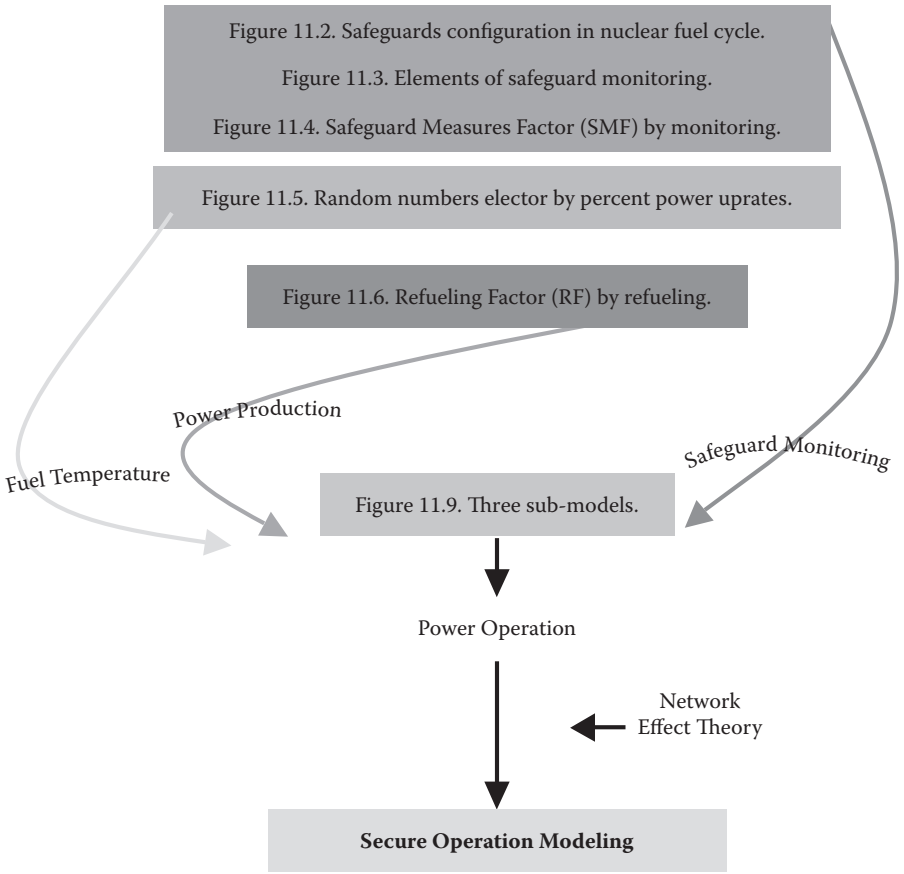


**FIGURE 11.10**
Summary of connections.

is much more unstable; it is the summation of neutronics matters, thermo-hydraulic matters, and safeguard matters as a function of the time interval (months). The maximum value of Figure 11.11(d) is 12.0 in month 3 and the minimum value is 1.0 in months 18 and 54. This illustrates the secure power operation situation. The success of power uprates increases to a value that is 12 times higher than the lowest value.

The vertical axis indicates the relative values of the quantifications. Comparisons between the values of interest are used for the results of the simulations. Using the results, the operator can prepare for possible terrorist attacks. For example, using Figure 11.11(d), the operator should beware of terror incidents when the values are lowest, such as the value of 1.0 in months 18 and 54. In addition, this study provides dynamic simulations, so it is possible to make much more accurate real-time measurements by changing the time interval from months (of this study) to hours or minutes.

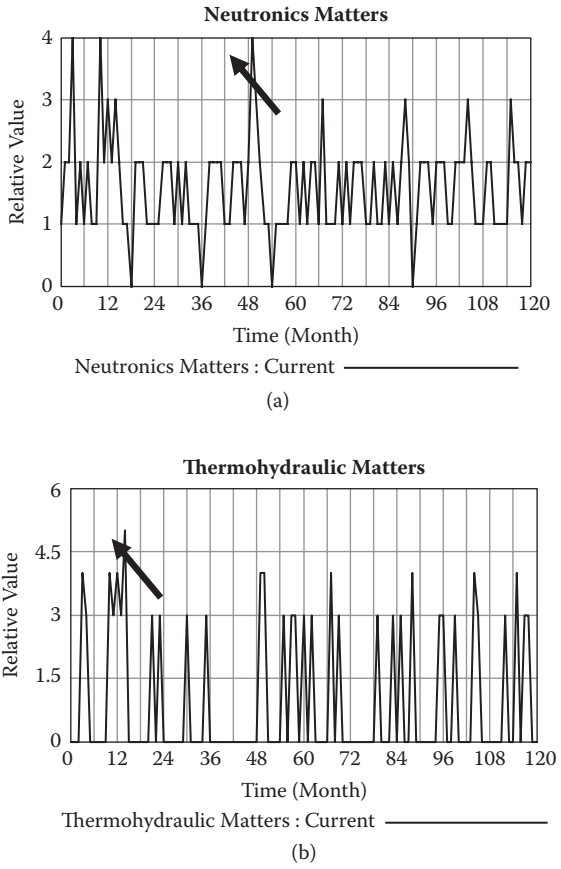


**FIGURE 11.11**
Quantification of models: (a) neutronics matters, (b) thermohydraulic matters, (c) safeguard matters, (d) secure power operation in NPPs.

## 11.5 Conclusions

Safeguard operations are successfully modeled using the dynamic method, based on nanoscale nuclear fuel material. Each event is quantified as random number generations, because it is impossible to predict the exact time of the terror event. Network effect is used to model power uprate safeguards, where the zero-sum effect is used for several event quantifications. The life of an NPP is assumed to be 10 years, so the period is 120 months. The main issue in the model is simulation of the neutronics matters and thermohydraulic matters. Safeguard matters are also investigated. The plausible values are defined for the numerical values of basic events. Using the simulation, here are some conclusions:

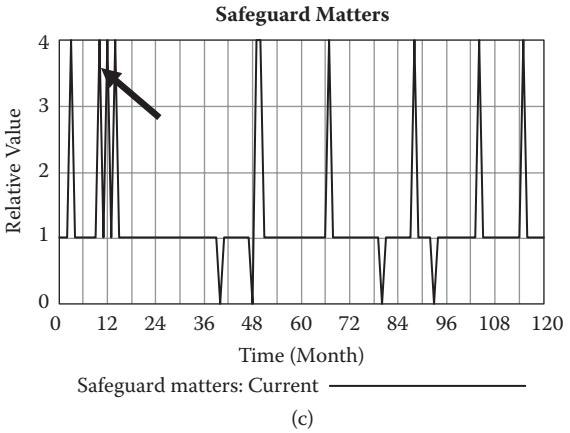


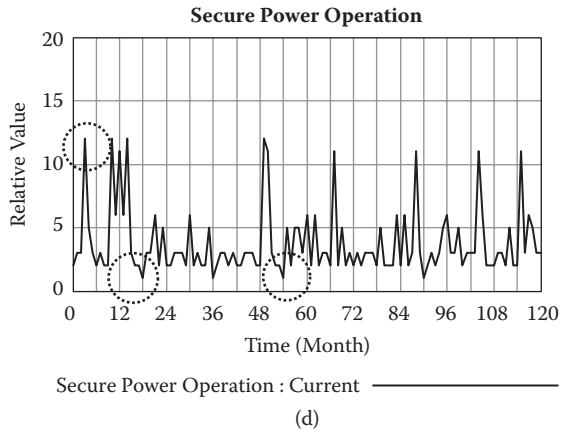


**FIGURE 11.11** ***(Continued)***

- Dynamic simulation has been performed using the characteristics of power uprates.
- Successful nonlinear investigations were done using network theory.
- Particular properties of reasonable relations have quantifications of power uprates in NPPs.
- A management algorithm is applied to the complex decision-making case where the dynamic scenario is addressed.
- For safeguard matters, a network effect algorithm is used for interpretation of risk management.

There is much potential for future works. The risk quantification could be expressed by the network effect of the event flows for natural accidents.

The safety assessment could be quantified by time intervals for earthquakes or traffic accidents. Furthermore, human error could be simulated by network effect simulations. A nonlinear algorithm concerning human factors like emotion and fatigue of operators is an interested topic. Using fuzzy set theory for the modeling, the reliability of the network effect is increased, so several kinds of analyses could use modeling of the network effect. This study can be used for security safeguard assessment in any kind of nanoscale nuclear material, such as nanoscale nuclear waste forms, nanoscopic power cells, nanofluids, atomic material in space, substances in medical imaging and radiation oncology, and so on.

## References

Bilbao, J. 2000. *Cooperative games on combinatorial structures*. Boston: Kluwer Academic.

Buley, T. 2009, July 31. How to value your networks. *Forbes*.

Evans, J., S. Newstead, and R. M. J. Byrne. 1993. *Human reasoning: The psychology of deduction.* Hove, UK: Psychology Press.

Farrell, J., and P. Kelmperer. 2007. Coordination and Lock-In: Competition with switching costs and network effects. In *Handbook of Industrial Organization, Volume 3*, ed. M. Armstrong and R. Porter, 1967–2072.

Fernandez, L F., and H. S. Bierman. 1998. *Game theory with economic applications*. Reading, MA: Addison-Wesley.

*Forbes.* 2007. It's All In Your Head, Forbes, LLC.

*Forbes.* 2009. How to Value Your Networks, Forbes, LLC.

IAEA (International Atomic Energy Agency). 1981. *IAEA safeguards: An introduction*, IAEA Safeguards Information Series No. 3. Vienna: IAEA.

IAEA (International Atomic Energy Agency). 1999. *Design measures to facilitate implementation of safeguards at future water cooled nuclear power plants*, Technical Reports Series No. 392. Vienna: IAEA.

IAEA (International Atomic Energy Agency). 2004. *Guidelines and format for preparation and submission of declarations pursuant to articles 2 and 3 of the model protocol additional to safeguards agreements*, IAEA Services Series No. 11. Vienna: IAEA.

Lee, J. Y., C. S. Lee, and J. L. Kim. 2004. Status of power uprate technology for operating nuclear power plants. In *Proceedings of Korea Society for Energy Engineering Fall Meeting*, 329–334. Kangwon Land, Kangwondo.

Leighton, J. P. 2004. Defining and describing reason. In *The nature of reasoning*. Cambridge, UK: Cambridge University Press.

Matsuoka, H., Y. Nishiwaki, A. Ryjov, and A. Belenki. 2002. An evaluation method on the integrated safeguards based on fuzzy theory. *Information Sciences* 142:131–150.

Metcalfe, R. M. 2007, May 7. It's all in your head. *Forbes*.

Miller, J. H. 2003. *Game theory at work: How to use game theory to outthink and outmaneuver your competition.* New York: McGraw Hill.

Rasmusen, E. 2006. *Games and information: An introduction to game theory,* 4th ed. Malden, MA: Wiley-Blackwell.

Rothschild, M. 2007. Update hazard rate equations for dual safeguard systems. *Journal of Hazardous Materials* 142:741–746.

Schachter, J. 2006. Young innovators under 35: Joshua Schachter. *Technology Review* 32, http://www.technologyreview.com/TR35/Profile.aspx?TRID=432

Tagami,T. 1966. Considerations on fission product release suppression factors of engineered safeguards for nuclear power plants. *Nuclear Engineering and Design* 4:214–223.

U.S. NRC (Nuclear Regulatory Commission). 1954. Title 10, Code of Federal Regulations, Part 50-Domestic Licensing of Production and Utilization Facilities.

U.S. NRC (Nuclear Regulatory Commission). 2003. *Review standard for extended power uprates*. Washington, DC: Office of Nuclear Reactor Regulation.

U.S. NRC (Nuclear Regulatory Commission). 2008. *Power uprates for nuclear plants, backgrounder*. Washington, DC: Office of Nuclear Reactor Regulation.

Vensim. 2009. Vensim Simulation Software, Ventana Systems, Inc.

# 12

# *Conclusions*

Using statistical and experimental methods, the economic and safety studies were performed by the application of nanoscale technology in the nuclear industry. This book shows a wide range of the information aspects in nuclear power plant NPPs. The main objective of the chapters was to discuss highly advanced performance in the commercial use of atomic power. Critical matters such as nuclear waste or terror-related safeguards are investigated using mathematical methods, which could give us an opportunity for objective decision making. This is expected to enhance the reliability of nanoscale technology in the nuclear industry.

In this book, three areas were investigated by simulation-based experiments in power engineering, biotechnology, and management. Although these fields developed separately, following twenty-first-century technology as an interdisciplinary approach, nanotechnology is applied to the nuclear industry. Hence, this approach is a challenge for the better performance of power production as well as reliable safety in atomic research and development areas.

This book is a basic approach in the vast nuclear market where new profits will be created by many synergistic effects such as combining computer simulation technology and nuclear science. Many relevant papers have been published in the nuclear industry. The current situation, however, suffers from an antinuclear trend in the construction of NPPs. This technology could overcome the limitations of public apprehension because it is a clean and reliable means of enhancing power production. It is expected that future books will be published on NPPs covering economic and safety improvements.

Electrical Engineering

# Atomic Nanoscale Technology in the Nuclear Industry

Developments at the nanoscale are leading to new possibilities and challenges for nuclear applications in areas ranging from medicine to international commerce to atomic power production and associated waste treatment. Progress in nanotech is helping the nuclear industry slash the cost of energy production. It also continues to improve application reliability and safety measures, which remain a critical concern, especially since the reactor disasters in Japan.

Exploring the broad new landscape of nuclear function, **Atomic Nanoscale Technology in the Nuclear Industry** details the breakthroughs in nanoscale applications and methodologies that are revolutionizing power production, biotechnology, and material science.

**Developments in atomic nanoscale technology have given us the ability to**

- Use ion beams to investigate and optimize radiation energy losses at the nanoscopic level
- Assess nanoscopic safety circumstances involved in a reactor failure
- Analyze characteristics of nuclear spacecraft operating in the nanogravity of deep space
- Evaluate light-collection enhancement for digital X-ray detection
- Apply brachytherapy using radioisotopes for cancer therapy
- Treat nuclear waste at the nanoscopic level
- Use systems-thinking decision making to analyze the financial progress of nanotech in the energy industry
- Assess safety (and safety management methods) for nuclear nanomaterials used in plant operations

Representing a first step in multi-combinatorial research, this text incorporates advanced studies that use Monte Carlo and solid-state measurement (including radiation detection) methods. These studies demonstrate the potential to upgrade methods of radiation protection and nuclear reactor operation, which includes safety, waste disposal, etc. The author also addresses how we can use nanotechnology to deal with industrial concerns and enhance nuclear medicine techniques. He highlights several nanomaterial systems and devices to illustrate developments in this area.

***About the Author***

**Taeho Woo** launched the specialized field of *atomic multinology* (interdisciplinary research of nuclear technology), which combines the application of information technology, biotechnology, and nanotechnology in the nuclear industry.

K13811

CRC Press
Taylor & Francis Group
an **informa** business
www.taylorandfrancisgroup.com

6000 Broken Sound Parkway, NW
Suite 300, Boca Raton, FL 33487
711 Third Avenue
New York, NY 10017
2 Park Square, Milton Park
Abingdon, Oxon OX14 4RN, UK

ISBN: 978-1-4398-8108-8
90000
9 781439 881088

www.crcpress.com